Beachwatch

Netherlands Geographical Studies 366

Beachwatch

The effect of daily morphodynamics on seasonal beach evolution

Susanne Quartel

Utrecht 2007

Royal Dutch Geographical Society /
Faculty of Geosciences, Utrecht University

This publication functioned as a Ph.D. thesis, which was defended in public 4 December 2007 at Utrecht University, The Netherlands.

Promotor
Prof. dr. P. Hoekstra, Utrecht University

Co-promotor
Dr. B.G. Ruessink, Utrecht University
Dr. E.A. Addink, Utrecht University

Examination committee
Prof. dr. R.A. Holman, Oregon State University (United States)
Dr. A. Kroon, University of Copenhagen (Denmark)
Prof. dr. F.D. van der Meer, ITC Enschede
Prof. dr. ir. M.J.F. Stive, Delft University of Technology
Prof. dr. ir. H.J. de Vriend, WL|Delft Hydraulics / Delft University of Technology

ISBN 978-90-6809-408-4

Printed in the Netherlands by Labor Grafimedia b.v. - Utrecht.

Contents

Figures

Tables

'Dat is aan de rand van Nederland
Dat is aan ons onvolprezen strand.'
Boudewijn de Groot, 1964

1 Introduction

1.1 General problem definition

The societal importance of sandy beaches reaches further than its allurement for sunbathers and beach strollers. Sandy beaches are also relevant with respect to nature conservation and, more crucial, protection of the inland against flooding. They constitute a dynamic interface between the sea and the land, and continuously change in width, volume and appearance in response to stochastically changing wave conditions and tides. The beach appearance comprises interesting morphologic patterns with characteristic spatial scales, but these patterns and their accompanying forcing wave conditions are still hardly understood. Coastal morphodynamic processes relate to the variations in beach width, volume and appearance and cover a broad range of time scales varying from seconds (e.g. swash-backwash) up to tens of decades (e.g. climate-induced sea-level change). Uncertainty exist on how the shorter timescale variations lead to the longer time scale variations.

This timescale aspect triggers the interest of the coastal manager (e.g. De Vriend, 1991; Hamm et al., 2002). The natural defense function of the beach pertains to the scope of climatic change discussions in which coastal managers debate whether the coastline can aggrade to keep up with the expected sea-level rise or whether the beach can cope with an increase in storm frequency and intensity. In these discussions, beach behaviour needs to be known over long-term timescales starting at the seasonal scale. However, the knowledge on the coastal morphodynamic processes is mainly obtained on shorter timescales (hours to days) and the available knowledge on long-term morphodynamic processes are limited in temporal and spatial resolution.

The broad range in time scale of the coastal morphodynamic processes correlate positively to their spatial scale. Besides, the morphodynamic processes possess a hierarchical structure and always consist of smaller, lower level processes, but at the same time are part of a larger, higher level process. The suggestion is easily made that the longer-term beach morphodynamics is the cumulative effect of shorter-term morphodynamic processes (physical reductionism; Descartes, 1637). However, simply summing up all short-term processes will not lead to longer-term beach morphodynamics due to interaction and nonlinearity of many morphodynamic processes (Cowell et al., 1995; De Vriend, 1997). Besides, when the scale of interest is large, the importance of the small-scale processes is constrained and they function as noise on

these large-scale processes (see De Vriend, 1997). The scale limit at which a process operates as noise or starts contributing to the large scale process is unclear though.

Long-term morphodynamics of a beach system is generally seen as a trend, whereas shorter-term processes are seen as fluctuations superimposed on the present trend (e.g. Stive et al., 2002). Short-term processes such as storms may have a large impact due to large-volume, instantaneous erosion of beach sediment, but beaches tend to recover during subsequent calm conditions. On a decadal timescale, the extreme storm events may be responsible for changes in the trend of beach behaviour (Morton et al., 1995) and an increase of storminess may cause a trend of beach erosion (Fenster & Dolan, 1993). Whereas a storm removes sand from the beach, successive post-storm (calm) conditions bring sediments ashore. The alternation of calm and storm conditions, and the frequency and intensity of major storm events varies over the seasons. This leads to an infinite series of possible day-to-day beach changes, which generally incorporate a seasonal signal.

Previous studies describe quite profoundly the seasonal variations of swell-dominated beaches. These swell-dominated beaches show an alternation of accretion and erosion in beach volume in phase with seasons, which identifies a winter and a summer profile of the beach (e.g. Shepard, 1950; Winant et al., 1975; Aubrey, 1979). Here, the seasonal volumetric changes relate inversely with the wave conditions, which exhibit extreme seasonal variations. However, the seasonal variations of the wave climate is less pronounced at many other beaches. And in contrast with the seasonal variations of swell-dominated beaches, seasonal variations of storm-dominated beaches received little scientific attention. Therefore, little is known on the temporal variability of seasonal beach variations associated with accretion and erosion, and how these relate with the prevailing wave conditions. Besides, storm-dominated beaches are frequently associated with permanent subtidal bar systems in the nearshore, which cause local wave breaking and therefore influence the wave field approaching the beach. The effect of these permanent bar systems on beach behaviour is also not well understood. The beach and nearshore behaviour are generally examined separately and beach behaviour received little attention compared to nearshore behaviour.

The morphology of microtidal (i.e. tidal range < 2 m) beaches are generally quite variable, whereas the morphology of meso- to macrotidal (i.e. tidal range > 2 m) beaches appear more static (e.g. Wijnberg & Kroon, 2002; Masselink et al., 2006). The large morphologic variability provides the opportunity to easily recognize the daily (i.e. day-to-day) morphologic changes on microtidal beaches. Previous studies on daily beach behaviour are generally biased in the cross-shore direction and based on measurements over a time span of a few weeks resulting in limited spatial and temporal resolution (see Kroon, 1994). Besides these studies focus on the event-scale of daily behaviour with little comparison of different seasons and interseasonal variability. Therefore, the central aim of this thesis is to understand the contribution of daily morphologic changes to seasonal beach evolution along a microtidal, storm-dominated coast.

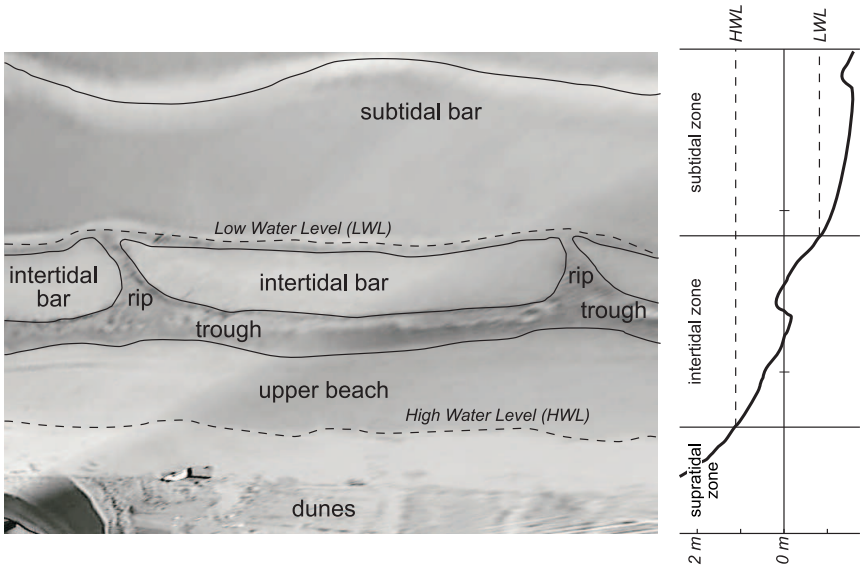

Figure 1.1 Schematic intertidal beach morphology draped over an Argus image with a cross-shore profile in the right panel

1.2 Sandy beach morphodynamics

Beaches are defined as an accumulation of unconsolidated sediment extending from the mean low-tide line to some physiographic change such as a sea cliff or dune field (Komar, 1998). The unconsolidated sandy material of the intertidal beach, i.e. the area between the mean low- and high water level, is generally organized in shore-parallel bodies of sand (bars) and accompanying depressions (troughs; Figure 1.1). Rip channels are cross-shore or obliquely oriented depressions in the alongshore direction of the intertidal bar. The intertidal bar, trough and rip channels as a whole (i.e. bar system) characterize the morphology of the intertidal, storm-dominated beaches.

1.2.1 Intertidal bar systems

Intertidal bars on microtidal, storm-dominated beaches are elongated features along the coastline with a distinct landward-facing slip face, also referred to as slip-face ridges (see Wijnberg & Kroon, 2002; Masselink et al., 2006). The landward-located trough drains water during falling tide. The height-difference between the crest of the bar and accompanying trough varies between decimeters to over one meter, whereas the cross-shore length of a bar or a trough is in the order of tens of meters (Wijnberg & Kroon, 2002).

The sequential cross-shore behaviour of intertidal bars on a daily time scale shows a cyclic pattern during persistent calm (low energy) conditions. The cyclic behaviour consists of: (I) generation near the low tide water line; (II) landward migration of $O(1$ m/day); and (III) disappearance due to merging of the bar at the high water mark to create a berm (Doeglas, 1955; Hayes & Boothroyd, 1969; Wijnberg & Kroon, 2002).

This cyclic migration of an intertidal bar system comprises the primary mechanism of net landward sediment transport. Successive bar merging supplies new sediment to the upper part of the beach to ultimately compensate the sediment losses due to a storm. This suggests the cross-shore bar migration to be an important aspect for seasonal beach patterns. Characteristics of the cyclic pattern as duration and migration rates vary with different coastal settings. For example, the duration ranges from days to weeks (Hayes & Boothroyd, 1969; Owens & Frobel, 1977). Besides, cross-shore bar behaviour was never examined on seasonal variability.

The behaviour of the trough originates from the bar behaviour during phase I and II, although it is not known to what extent the behaviour of these two features are coherent. The merging bar compresses the trough which will consequently loose its drainage function and disappear during phase III. Besides disappearance due to merging, the bar - trough system may also disappear as a consequence of beach erosion during storms. The bar - trough systems reappears within days near the low-water line (Doeglas, 1955) leading to a semi-permanent character of bar-trough systems. The wave conditions inducing the disappearance by merging as well as by erosion are broadly specified as low- and high-energetic, respectively, but are not well specified (Wijnberg & Kroon, 2002).

Rip channels (Figure 1.1) intercept the intertidal bars through which the drainage water flows from the trough to the sea. Rip channels exhibit a quasi-rhythmic alongshore pattern and lead to a curved shape of the bar system (e.g. Figure 1.1). Little is known about the temporal evolution of intertidal rip channels, although more information is available on subtidal rip channels. The alongshore migration of the intertidal rip channels probably ranges in the order of 1 - 10 m/day and can be approached as the the alongshore migration of a bar system (Anthony et al., 2005; Van Houwelingen et al., 2006). Characteristics of subtidal rip channels, as spacing and migration rates, can often be coupled to offshore wave energy (Short, 1985; Short & Brander, 1999), although this relation remains uncertain (Ranasinghe et al., 1999; Lafon et al., 2005).

1.2.2 Relation with the subtidal zone

Morphologic changes of the beach are generally a response to variations in forcing wave conditions. The presence of subtidal bar systems affects beach behaviour, because it influences the wave field approaching the beach (Section 1.1). Previous studies described the possible influence of the subtidal bars on the beach as morphologic coupling, that is a similarity in quasi-rhythmic pattern of two different bar systems. However, frequently no direct spatial relation is found between two bar systems (e.g. Sonu, 1973; Van Enckevort & Ruessink, 2003a). This lack of relation was suggested to be due to the dominance of processes within the inner bar systems over coupling processes between the outer and inner bar systems. Ruessink et al. (2007) showed how two subtidal bars were initially uncoupled, but became coupled in response to the onshore migrating, increasingly non-uniform outer bar. To what extent and in what sense the intertidal bar system behaviour is forced by the subtidal morphology is unknown.

1.2.3 Application of remote sensing

To study daily beach morphology during different seasons, successive beach observations with high temporal resolution are needed for an ongoing period of at least one year. Remote sensing provides the possibility to obtain spatial data with high temporal resolution. Besides remote sensed data delivers continuous coverage of the beach surface with varying spatial resolution. Due to the detailed, continuous coverage of the surface, remote sensing is cost-efficient. Interpretation of the spatial data, however, is always needed, because the data consists of spectral observations and thus delivers indirect information of the surface (Lillesand & Kiefer, 1994). Various remote sensing techniques are applied for coastal monitoring including techniques with multi- to hyperspectral imagery and LIDAR (e.g. Lafon et al., 2005; Deronde et al., 2006; Van Houwelingen et al., 2006).

The Argus video program is such a shore-based remote sensing technique, initiated and developed by the Coastal Imaging Lab, Oregon State University (USA). The system incorporates an unmanned, automated video station at interesting coastal sites (Holman et al., 1993) and typically comprises five video cameras with different orientation. This results in a 180 $^\circ$ view over a several kilometers long stretch of coast. The data is collected hourly during daylight and results in three image types: snapshots, ten-minute time-exposure (timex) images and variance images. The snapshot shows individual breaking waves and the wave activity of the nearshore zone. Timex images expose the wave dissipation patterns that reveal the positions of submerged bar crests, rip channels and water line. The variance images separate the steady areas from the dynamic areas in the image. An extensive description of the Argus system can be found in Holman & Stanley (2007).

Beach research using Argus imagery focusses on water line detection models (e.g. Turner et al., 2000; Aarninkhof et al., 2003; Kingston, 2003). If a water line is detected at a certain moment, a coupling to offshore measured water level can be made and a contour line of the beach is known. Applying the water line detection method on subsequent Argus images from one tidal cycle, several elevation contours are obtained resulting in estimates of beach topography and sediment budgets. However, these results are limited in vertical scale and accuracy $O(10^1$ cm) (Plant et al., 2007). Besides water line detection provides elevation data, but does not supply the intertidal morphology. Low-tide Argus images display the intertidal morphology and often confuse waterline detection methods (Aarninkhof et al., 2003). Therefore, a new methodology is needed to delineate and extract the morphologic features as objects rather than as lines. With respect to monitoring of the nearshore zone, Argus video imagery is widely used for subtidal bar behavior research (e.g. Lippmann & Holman, 1990; Van Enckevort & Ruessink, 2003a). Waves break over the subtidal bar and produce a white band on the timex image. The breaking position gives a good indication about the underlying bathymetry. Thus with the Argus video system, both the intertidal and subtidal morphology can simultaneously be monitored on a daily timescale.

1.3 Research objectives

The central objective of this thesis is to understand the contribution of daily morphologic changes on seasonal beach evolution at a microtidal, storm-dominated coast. The daily morphologic changes of the beach comprise the cross-shore and alongshore migration of the intertidal bar system. Low-tide Argus video images display this intertidal bar system, which means that differences in the spectral (RGB) information lead to the discrimination of the morphologic features. But a new methodology needs to be developed to classify these spectral differences and extract the intertidal morphology from these images. The daily cross-shore changes are associated to the cross-shore migration of the bar and the trough. Previous studies suggest the cross-shore sequential behaviour of the bar and trough on a microtidal beach to be cyclic. Little attention has been paid to differences between bar and trough behaviour, and to the seasonal aspects of this sequential behaviour. The alongshore behaviour of the intertidal rip channels is supposed to reflect the daily alongshore changes, but knowledge lacks on the intertidal rip channels characteristics. The alongshore distribution and behaviour of the intertidal rip channels may correlate to the subtidal rip channels, revealing the presence or absence of morphologic coupling between the beach and the subtidal morphology. Seasonal beach variations are generally associated to volumetric changes of the beach, which are induced by seasonal variability of the wave conditions. But a lack of knowledge exists on the seasonal patterns in sediment budgets for storm-dominated beaches exists. Furthermore, seasonal patterns may emerge from successive daily changes for a one-year period. Consequently, an overview of all daily and seasonal beach changes is eventually needed to achieve the central aim of this thesis. Therefore, five research objectives are formulated:

Objective 1. Develop a methodology to extract intertidal morphologic features from video imagery in a (semi-)automated manner using object-oriented image analysis

- How can the morphologic entities be distinguished in video images?
- Which spectral characteristics are coupled to these morphologic entities?
- How accurate can beach morphology be classified from the video images?

Objective 2. Determine the sequential cross-shore behaviour of an intertidal bar - trough system, and examine the conditions that regulate or interrupt this sequential pattern

- What are the characteristics of the sequential behaviour of the bar - trough system?
- Are the bar and trough behaving in a identical way or do they differ from each other?
- Which conditions determine the transition of the bar - trough system from one stage to the next?

Objective 3. Investigate daily spatial and temporal variability of intertidal rip channels and examine whether these rip channels are coupled to subtidal alongshore variability

- What are the amount, spacing and migration rates of intertidal rip channels?
- How are these characteristics related to offshore wave heights and proxies of the alongshore current?
- Does the subtidal bar morphology and the accompanying rip channels influence intertidal rip channel behaviour?

Objective 4. Distinguish a seasonal pattern in sediment budget of the beach and relate it to preceding energetic conditions

- What is the temporal variability of beach width and beach volume?
- To what degree is beach response alongshore uniform?
- How do the beach changes relate to variations in preceding wave conditions?

Objective 5. Integrate the daily morphologic changes with the seasonal morphologic variations

- Which daily morphologic changes appear after a storm and during the subsequent recovery?
- Which morphodynamic patterns are initiated by the seasonal variation in wave conditions?
- Do daily variations lead to seasonal variations in beach behaviour?

1.4 Dutch Coast - Noordwijk

The field site of this research project, Noordwijk aan Zee, is located along the Dutch coast, which is a sandy, storm-dominated coast with a micro- to mesotidal regime (Figure 1.2). The wave climate of Noordwijk, measured 9.5 km offshore at 18-m water depth (MPN; Figure 1.2), is dominated by sea waves and swell is limitedly present for only 20% of the time (Van Enckevort, 2001). The waves have an annual averaged offshore significant wave height $H_{1/3}$ of one meter and an accompanying wave period $T_{1/3}$ of 6 seconds (Wijnberg, 1995). Waves mainly approach the coast from SW to NNW (70° to −45° from shore normal). Seasonal variations in the wave climate comprise a mean $H_{1/3}$ of 1.2-1.3 m between October and March (i.e. winter) in contrast to a mean $H_{1/3}$ of 0.8-0.9 m between April and September (i.e. summer).

The microtidal water level fluctuations at Noordwijk are semi-diurnal and equal a mean tidal range of 1.8 m during spring tide and 1.4 m during neap tide. The

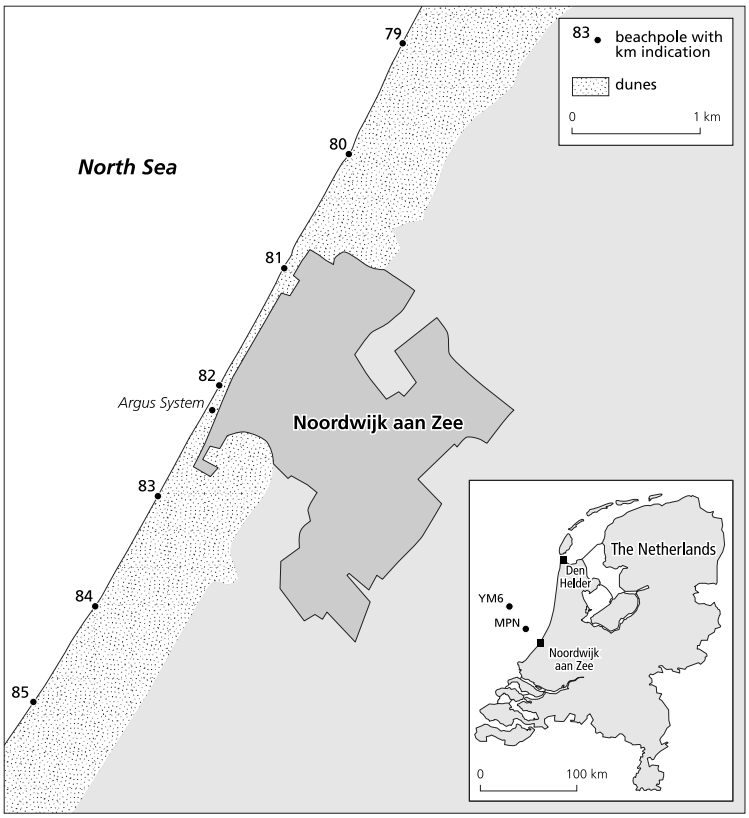

Figure 1.2 Map of the Netherlands with the hydrodynamic data collection sites: Meetpost Noordwijk (MPN) and IJmuiden (YM6), and a focus on Noordwijk aan Zee with the Argus monitoring system. Data collected at YM6 was used for about 2% of the time between November 2001 and November 2004, when there was data missing at MPN.

tidal signal shows an agger during spring tide, which almost disappears during neap tide conditions. The agger causes a stagnation of the water level for at least 2 hours at a vertical range between -0.3 and -0.6 m with respect to mean sea level for the predicted tide. Extra set-up or set-down of the mean water level is enforced by onshore or offshore-directed winds, respectively, and usually remains between +0.5 and -0.5 m, but may reach deviations of 1 m.

The coastal zone of Noordwijk aan Zee is characterized by a multiple bar system consisting of a single intertidal bar and two subtidal bars. Occasionally, a second intertidal bar may be formed on a pre-existing bar during low-energy wave conditions. The intertidal beach, located between the mean low- and high-water line, has an average width of 100 m and a slope of approximately 1:50. The beach sediments are well sorted and have a median size between 250 and 350 μm (Van Bemmelen, 1988). The two subtidal bars show a cyclic behaviour with a recurrence interval of about 4 years (Wijnberg & Terwindt, 1995). The cyclic pattern of the subtidal bars consists of (I) generation near the shore, (II) net seaward migration and (III) decay several hundreds meter from the shore. Van Enckevort & Ruessink (2003a) provides a detailed description of the subtidal Noordwijk bars on timescales from days to years. In the beginning of 1998, a shoreface nourishment of 1.25 x 10^6 m^3 sand was implemented seaward from the outer subtidal bar to mitigate shoreline retreat. This shoreface

nourishment stopped the net seaward sandbar migration of the inner bar for the first year, and overall strongly decelerated the net offshore migration of both bars for at least a period of 5.8 years (Ojeda et al., in prep). Initially, the beach volume increased after the execution of the shoreface nourishment, but the beach volume decreased again after three years (Quartel & Grasmeijer, 2007). Whether these volumetric beach changes and the shoreface nourishment relate directly is uncertain.

The beach and nearshore zone of Noordwijk have been monitored since 1995 by an Argus monitoring station. The system is mounted on the top of a hotel at a height of 62 m above mean sea level. Initially the system was composed by two black and white digital video cameras, but these were replaced by five full colour cameras in September 1998. The five cameras together view the coastal zone over 6 km in the alongshore direction, and 1.5 km in the cross-shore direction. Infrequently, malfunctioning of the local computer or the cameras led to data losses. But in general, the video system worked well and obtained its hourly images during day-time.

1.5 Thesis outline

The outline of the thesis reflects the five main objectives formulated in Section 1.3. Chapter 2 introduces the application of Argus imagery on intertidal beach morphology; it presents an object-oriented classification method which distinguishes three classes of sediment composition in a low-tide Argus image, leading to tripartite images from which the intertidal beach morphology can be derived. This classification method is applied to a 15-month data set of Argus low-tide images taken at Noordwijk aan Zee, the Netherlands. Delineation of the different classes in the tripartite images provides the cross-shore positions of the landward boundaries of both the intertidal bar and trough. Patterns of the daily cross-shore behaviour of these boundaries are described in Chapter 3 to examine seasonal effects in the cyclic behaviour of the bar - trough system. The daily behaviour of intertidal rip channels is studied in Chapter 4. Their characteristics are compared to offshore wave conditions as well as to the subtidal rip channel characteristics to study the forcing by waves and subtidal morphology. Both Chapters 3 and 4 focus on the impact of storm events on the beach morphology and its subsequent recovery. The effect of seasonal and interseasonal variation in storm frequency and subsequent calm conditions on the sediment budget of the beach is described in Chapter 5, with special emphasis on differences in beach response to comparable storms events. In addition to the Argus images, monthly elevation measurements were performed at the beach of Noordwijk aan Zee to create a complementary time series for the analyses of Chapter 5. Finally, Chapter 6 synthesizes all daily morphologic changes and seasonal variations and presents the conclusion with respect to the central aim of this study.

2 Extraction of beach morphology from video images

Quartel, S., E.A. Addink & B.G. Ruessink (2006) Object-oriented extraction of beach morphology from video images. International Journal of Applied Earth Observation and Geoinformation, 8, 256-269

Abstract

The Argus system is a shore-based, optical video system offering a suitable remote sensing technique for the purpose of long-term, high-resolution monitoring of coastal morphodynamics. Ten-minute time-exposure (timex) images obtained by the Argus cameras during low tide show the intertidal beach morphology (bars, troughs and rips) by the differences between water, wet sand and dry sand, where dry sand represents bars, and wet sand and water represent troughs and rips. A semi-automatic object-oriented algorithm was developed for classification of intertidal beach in low-tide video images and was tested on 13 low-tide Argus images collected at Noordwijk aan Zee, The Netherlands. Because of the strong relation between the visual observations and object-oriented image analysis, the Argus images are subdivided in small homogeneous areas (i.e. objects) by segmentation. Maximum likelihood classification creates a model for each day using a random selection of the objects, which are manually labelled, and their accompanying variables. Of the 3 classes, class wet sand had a classification fit of 43.4% when compared to an in-situ classification; class water was correctly classified for 90.1% and dry sand could be classified best (92.8%). By combining their cross-shore position and their classification, objects can be directly linked with the respective morphological features.

2.1 Introduction

Sandy beaches have an important recreational function and provide a natural defence mechanism for the coastline. The transition from land to sea is known as the intertidal zone, which extends from the mean low water level to the mean high water level. The presence of a bar, an elongated shore-parallel tabular body of sand, in the intertidal zone, influences the sediment budgets on the beach and protects the shoreward located dunes against erosion. A bar is always accompanied by a landward depression, referred

to as a trough (Figure 1.1), which drains the water during falling tide. In alongshore directions, rip channels may intercept the intertidal bars for drainage of the landward trough (Figure 1.1). The cross-shore length of a bar or a trough is in the order of tens of meters (Wijnberg & Kroon, 2002). The spacings between rips are in the order of ten to several hundreds of meters and tend to increase with offshore wave energy (Short, 1985).

Variations in offshore energy conditions (waves and tide) give rise to variations of the morphologic features on the intertidal beach. Intertidal bars, and therefore also the associated troughs and rips, are generally eroded during high-energy wave conditions and extreme water levels. The bars recover rapidly and new bars occur around the low water line during low- to moderate-energy wave conditions (Doeglas, 1955; Wright & Short, 1984). After generation of the morphologic features, they may migrate several to tens of meters a day (e.g. Owens & Frobel, 1977; Ranasinghe et al., 1999). The response of the features depends on the temporal variability and rate of change of the energy conditions (Wright & Short, 1984). However, the alternation of these energy conditions and the impact of the changing conditions on the morphology are not accurately known on a time-scale of weeks to years. This long time-scale is of special interest for coastal management, because it includes seasonal variabilities. Previous studies on morphological changes on short time scale (days to weeks) generally focused on measurements executed on cross-shore profiles, implying limited knowledge of alongshore morphologic variability.

Shore-based, optical video imagery offers suitable remote sensing data for the purpose of long-term, high-resolution monitoring of morphodynamic processes in the coastal zone (see Holland et al., 1997; Aarninkhof et al., 2003). Present-day applications of this remote sensing technique on intertidal beach morphology have mainly focused on shoreline detection, the transition between land and sea (e.g. Aarninkhof & Roelvink, 1999; Turner et al., 2000; Kingston, 2003). Color (RGB) video images show a visual contrast between the sub-aqueous (water) and sub-aerial (sand) beach, caused by the absorption of the red light component and the reflection of the blue light component by a water covered surface. The red light component is comparatively unaffected and thus reflected, for similar lightning conditions by a sandy surface (Lillesand & Kiefer, 1994). Yet the distinction between sand and water, as in shoreline detection models, is not sufficient to contour the morphological features. In this chapter focus is on accurate determination of the positions of intertidal morphology, i.e. bars, rips and troughs, using low-tide video images in which the morphology is often clearly visible to the human eye (Figure 1.1).

The human cognition system possesses the ability to generate image-objects from groups of neighboring pixels, which are spectrally similar. Subsequent analysis of the variables size, shape and spatial arrangement of the individual image-objects form a cognitive impression of texture (Hay et al., 1996). Similarly to the human cognition system, the object-oriented approach in image analysis creates image-objects by segmentation. For each image-object, spectral information is available, but also contextual and shape information. The conventional per-pixel approach includes only spectral information (for individual pixels) and is therefore hampered by the lack of

a spatial component (Hay et al., 1996). The shoreline detection models described above follow the per-pixel approach for image analysis. Because the object-oriented approach resembles the human cognition system closely (Blaschke et al., 2004), this approach seems to be the better option to obtain beach morphology from video images.

The aim of this chapter is to develop a methodology to extract intertidal morphologic features from video imagery in a (semi-)automated manner using object-oriented image analysis. The developed method was applied to a time series of routinely collected video images (i.e. Argus system), which shows the onshore migration of intertidal bars at Noordwijk aan Zee, The Netherlands. For each individual image the classification accuracy was determined by a percentage correctly classified objects and by comparing the classification to visual interpretation. Furthermore, the method was applied to an image recorded on a day when the bathymetry and morphology of the intertidal beach were determined in situ.

2.2 Argus video imagery

The video remote sensing system deployed here, pioneered by Holman & Sallenger (1986), is known as an Argus monitoring station, which typically comprises five color (RGB) video cameras mounted several tens of meters above sea level on a tower or a building. For this study the 10-minute time exposure (timex) images of the Argus video system in Noordwijk aan Zee, The Netherlands, were processed. This Argus system consists of five full color cameras, which were installed on the roof of hotel "Huis ter Duin" in September 1998. The advantage of using timex-images is that timex-images do not show moving objects like vehicles or people present on the beach, which can be seen on instantaneous images. The quality of the timex-images is influenced by weather conditions as fog, rain and/or sunlight exposure, because these conditions negatively affect the visibility of the morphology in the images.

The obliquely collected images undergo geometrical transformation to obtain a rectified plan view of the coastal zone. Prior to the transformation the images are corrected for radial distortions in the lens and pixel nonsquareness, which results from small differences in sampling frequency between camera and the image acquisition hardware. To perform the transformation the relation between image coordinates (u, v) and world location (x, y, z) is determined by solving collinearity equations. A rectification level (z) needs to be set for the transformation of a 2D to a 3D coordinate system. Holland et al. (1997) present a more detailed description about camera calibration and geometrical transformation for Argus imagery. The rectified images of the different cameras can be merged to create an image with a plan view over an alongshore coastal stretch. The distance of the alongshore stretch may cover up to 6 km, depending on station elevation and camera lens capacities. The accuracy of the photogrammetric transformation from image to ground coordinates is typically one pixel.

A rectified and merged Argus image at Noordwijk aan Zee offers a 180 $^\circ$ view over a SSW-NNE oriented, alongshore stretch of beach. In the present study we use

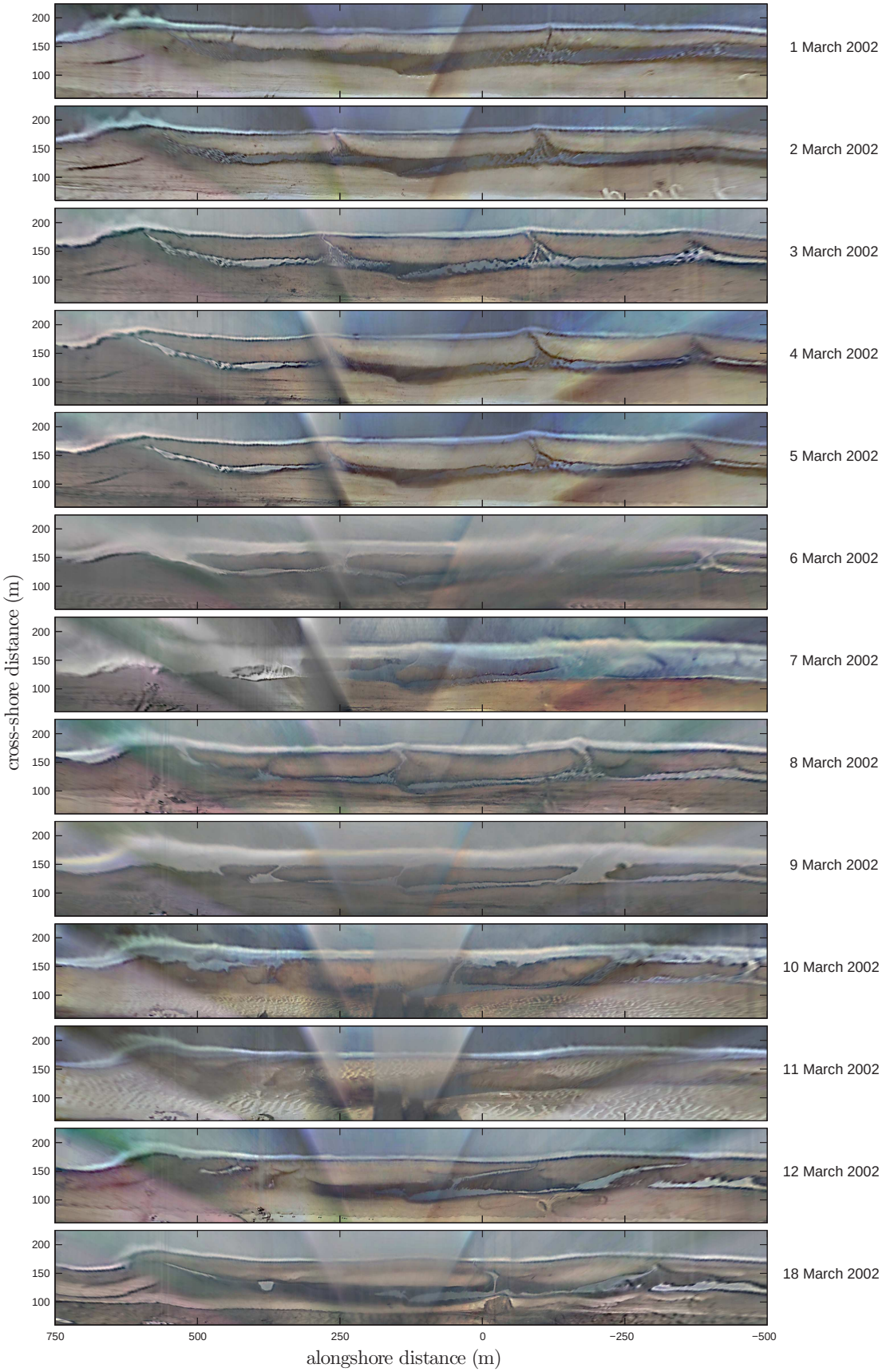

Figure 2.1a Time series of selected low-tide Argus images from 1 March (top) to 12 March and 18 March 2002 (bottom) with the standardized images (a) and...

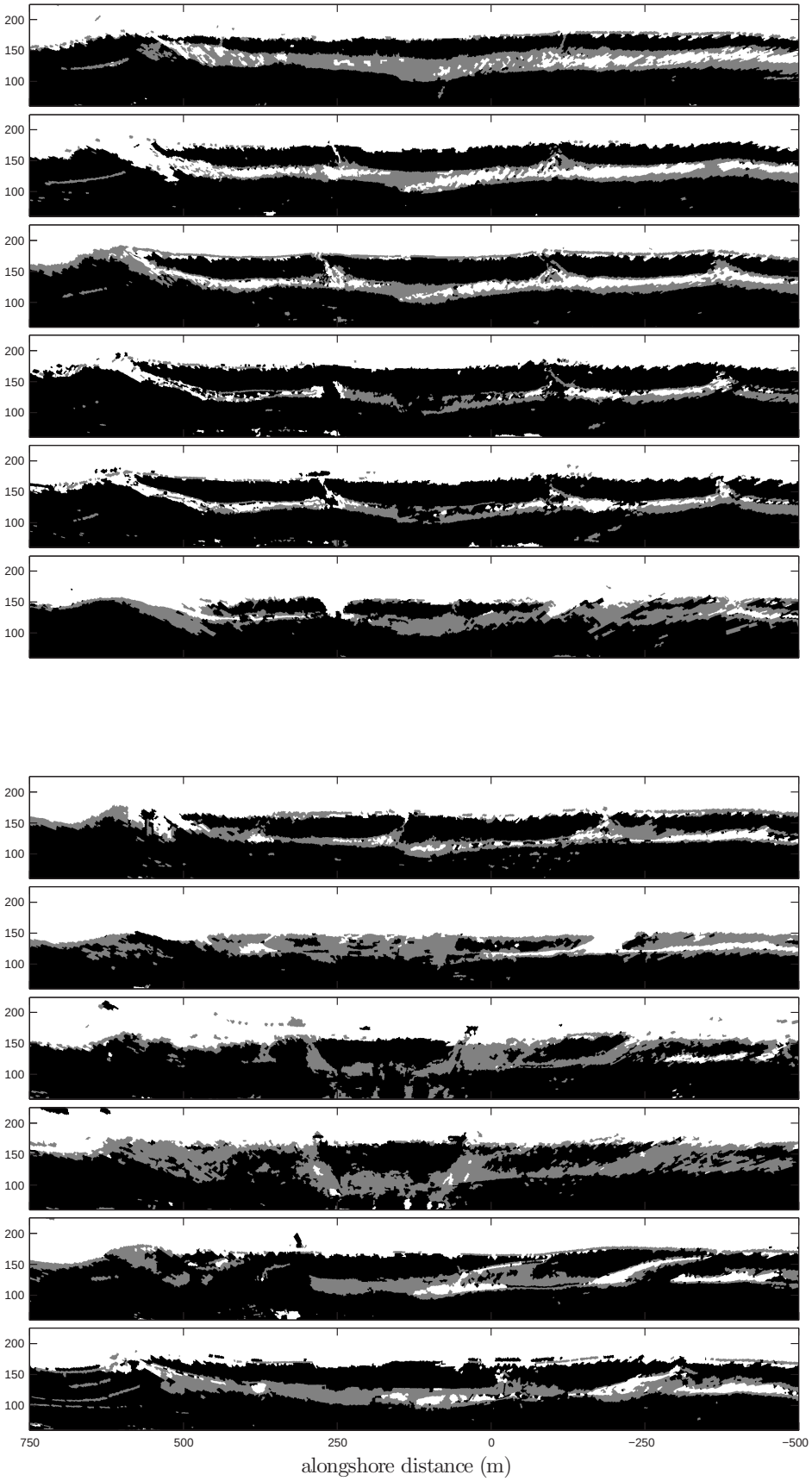

Figure 2.1b the classified images (b) representing dry sand class as black, wet sand class as grey and water class as white. The images show a part of the Noordwijk beach, stretching from SSW (left) to NNE (right).

merged images on a 0.5×0.5 m grid spanning 1250 m alongshore centered around the cameras and 165 m cross-shore, including the whole intertidal zone. The footprint pixel dimensions of the oblique images in the area of interest was less than a few meters in the cross-shore and alongshore direction, considerably less than the size of the morphological features in the intertidal beach.

A series of Noordwijk Argus images during low tide was selected for the period of 1 up to 12 March 2002 (Figure 2.1a). During the first five days, the intertidal bar migrated landward and the orientation of the rip channels, which intercepted the intertidal bar, changed from a northward to a southward direction. The intertidal morphologic features were not exposed on 6 March, although the image shows a change in rip orientation to shore-normal. On 7 March, the low tide water line and offshore wave energy were high resulting in a largely submerged morphology during low tide and therefore the image of this day was excluded from further processing. The shape of all morphologic features changed remarkably in the last five days, 8 up to 12 March. In the northern part of the image, the rip orientation shifted from shore-normal to strong oblique in a northward direction and the length of the rip doubled. The southern rip first disappeared, and subsequently a strong oblique rip developed. The shape of the intertidal bar changed from an elongated ellipse to an elongated diamond and the trough cross-section widened.

In addition to this time series, the low tide image of 18 March 2002 was selected, because field data were available for this day. The morphology discernible in the image consisted of an intertidal bar, which is intersected at three different locations by rip channels, and a trough. The orientation was different for all three rips (Figure 2.1a). A small through with a cross-shore position close to the high water line, was present in the south. On this day, 18 March, the bathymetry was determined in situ using a differential Global Positioning System (dGPS). The measurements were performed along cross-shore transects with an alongshore spacing of 50 m and sometimes between two transects due to the presence of rips around low tide while the intertidal beach was emerged. Measurements were classified as one of the three defined classes, or as a boundary between two classes, and subsequently used for the validation of the classification method. The dGPS data reflected an intertidal bar intersected by three rip channels with a corresponding trough and a small trough near the high water line in the north.

2.3 Classification algorithm

The visual difference between the morphologic features in the images is due to spectral differences between water and sand, but also due to variations in brightness caused by sand wetness. Dry sand appears light in an image, while wet sand appears darker (Lillesand & Kiefer, 1994) (Figure 2.2). The vertical position of bars on the intertidal beach is relatively higher compared to troughs and rips. Bars emerge earlier with falling tide and because of the permeable character of sand, the sand of bars is easily drained. The sand of the bar becomes dry and appears bright in the images. Dry

sand can also be seen on the upper beach. The upper beach is the area between the trough, or the most landward trough in case of several bar-trough combinations in the intertidal zone, and the dunes (Figure 1.1). The same process of drainage occurs on the upper beach, so this will also show a relatively high brightness. Sand of the troughs and rips, on the other hand, stays wetter and therefore appears darker in the images. Usually not even all water flows out of the troughs and the rips during low tide, and shallow pools and channels of water remain. The combination of water-sand and sand wetness differences led to the discrimination of three classes based on the surface composition in the low tide images: dry sand, wet sand and water. Classification of an Argus image into these three classes will allow delineation of morphologic features. The developed classification algorithm will be explained stepwise by use of the image of 1 March 2002 (Figure 2.2).

2.3.1 Pre-Processing

The three classes are easy to discriminate in an Argus image by eye, but different lightning conditions produce spatial and temporal variations that hamper automated classification of the images. Spatial variations are due to the different orientation of the five cameras ranging from SSW to NNE (through NWW), which induces varying sunlight exposure. Temporal variations are caused by varying sun positions during the day, but also during the seasons. The rising sun in the east may cast shadows of the buildings on the beach in the morning. In the afternoon, the sun may shine directly in the SSW oriented camera, while during sunset glare may influence all cameras. The incoming sunlight angle is larger in summer time than in winter time, causing seasonal variations. Standardization of the spectral bands (RGB) was applied to reduce light differences. The RGB bands were standardized to a mean of 128 and a standard deviation of 30 (Figure 2.2b). The latter was set to 30, because the standard deviation for bands of individual images was approximately 26 and a higher value will not suppress information as a lower value will. Every cross-shore pixel profile was standardized separately to smoothen the spatial variations of lightning in the alongshore direction.

Rough segments are created by applying an edge preserving smoothing (EPS) filter (compare Figure 2.2b and 2.2c). The EPS filter used here, divides a square symmetric neighborhood of 5x5 pixels in nine (slightly overlapping) windows, each window containing the central pixel (Figure 2.3; Nagao & Matsuyama, 1979). The total variance of the RGB bands is calculated for each of the nine windows and the central pixel value is replaced by the average of the most homogeneous window, i.e. the window with the lowest variance sum. The combination of averaging and homogeneity avoids filtering across edges in the image. The application of the EPS filter was repeated until the mean values of the individual bands remained unchanged.

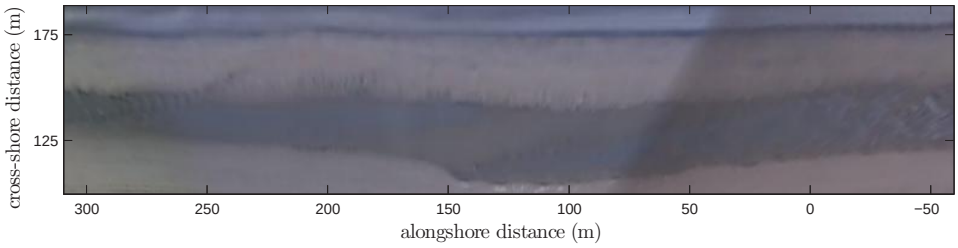

(a) Rectification and merging

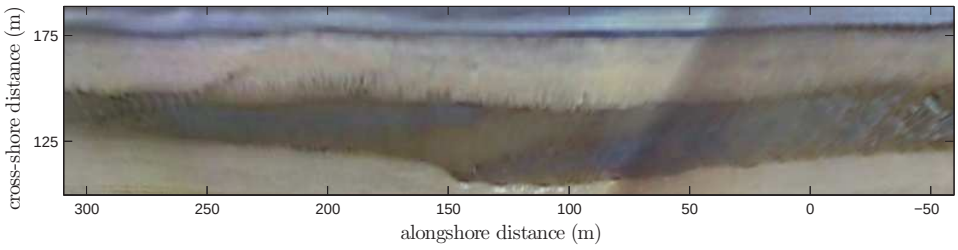

(b) Standardisation

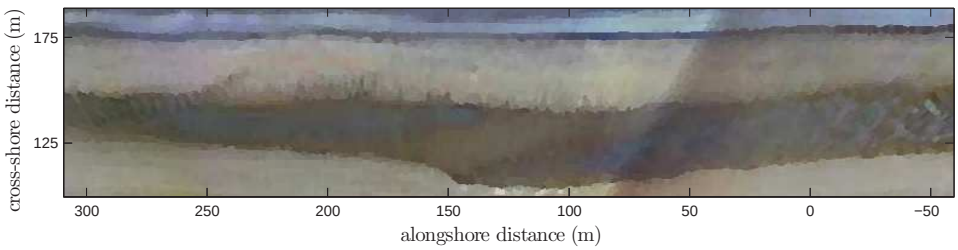

(c) Filtering

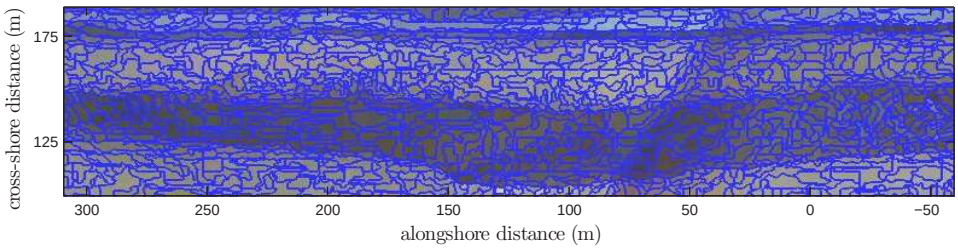

(d) Segmentation

Figure 2.2 Blow up of the Argus image of 1 March 2002, from top to bottom representing different phases in the classification algorithm: (a) original rectified and merged image; (b) image standardized for the RGB bands per cross-shore profile; (c) image after application of the edge preserving smoothing filter; (d) segmented image with scale parameter 10.

2.3.2 Segmentation

The process of image segmentation is the search for homogenous regions in an image. The method used here is a region-based segmentation approach (eCognition, 2002) and its segmentation algorithm is a bottom-up region-growing technique starting with single-pixel objects (Van der Sande et al., 2003). This method employs a randomly

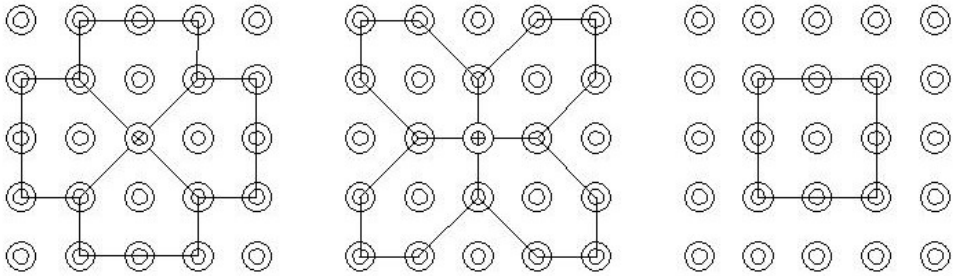

Figure 2.3 Edge-preserving smoothing filter. Black lines delineate the nine ares for which variance is calculated for each individual band. Per area the variances are summed and the one showing the lowest total variance is selected. For this area the mean values of the bands are calculated and assigned to the central pixel

chosen set of points on the image to define the objects. To eliminate the effect of this random point set, the EPS filter was applied. The merging decision for image segmentation is based on a local homogeneity criterion, described as the similarity between adjacent objects. The objects are pixels at the beginning of the process. The pair of objects with the smallest heterogeneity increase is merged. The process of merging ends when the smallest increase exceeds a user-defined threshold, which is called the scale parameter. Consequently object size increases with a larger scale parameter and vice versa (eCognition, 2002). Figure 2.2d shows part of the segmented image from 1 March 2002.

The image of 1 March 2002 was segmented for varying scale parameters (5, 10, 15, 20, 30, 40 and 50) to determine the scale parameter that creates the best classifiable objects. The scale parameter is a weighed combination of spectral values and shape properties, where the weight of the spectral values was set to 0.9 and the shape properties to 0.1, so emphasis was put on spectral characteristics. A higher scale pa-

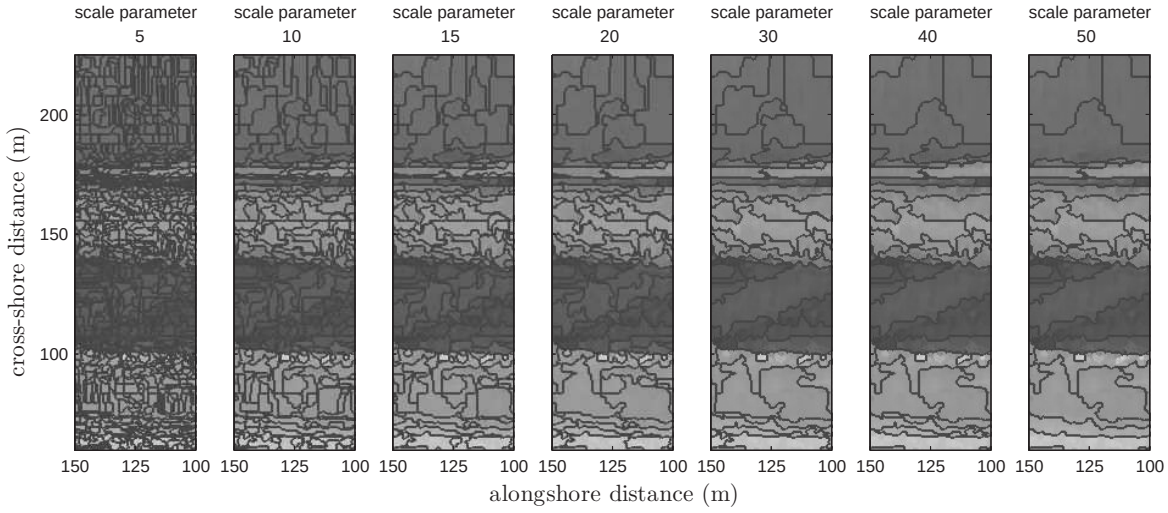

Figure 2.4 Zoom of the image of 1 March 2002, segmented with different scale parameters. From left to right: 5, 10, 15, 20, 30, 40 and 50.

Table 2.1 Cross-validation for maximum likelihood models to obtain suitable scale parameter

Scale	Number of	Classification fit				Range
parameter	objects	dry sand	wet sand	water	total	max - min
5	23,011	0.947	0.595	0.929	0.897	0.352
10	7,047	0.947	0.769	0.857	0.897	0.178
15	3,725	0.943	0.628	0.850	0.867	0.315
20	2,356	0.956	0.500	0.900	0.873	0.456
30	1,202	0.941	0.633	0.878	0.870	0.309

rameter entails more merging and fewer objects appear in a segmented image (Figure 2.4; Table 2.1).

2.3.3 Maximum Likelihood Classification

To obtain a classified image, all segments were labelled by use of maximum likelihood classification (MLC), in statistical terms known as quadratic discriminant analysis. MLC is a multivariate technique providing statistical classification of objects. The procedure begins with a set of objects where class and values of the variables are known, i.e. the training set. Performing a MLC on the training set results in a model that allows prediction of class membership for an object when only the object variables are known. MLC assumes unequal covariance matrices for the classes and makes use of quadratic functions of variables to describe boundaries between classification groups.

In the present work, spectral and contextual information were available for every object produced by the segmentation leading to 12 variables used in the classification. The Argus images are stored in jpeg format, which affects the shape of the objects. Consequently, shape variables were excluded from the classification process. The 12 included variables comprise:

- the mean and standard deviation of the red, green and blue color layer (6 variables);
- the ratio of the mean in each color layer to the sum of all 3 means (3 variables);
- the brightness, defined as the mean of the individual color means (1 variable);
- the difference between the highest and lowest color mean (1 variable);
- the object-averaged cross-shore location (1 variable).

To select the best scale parameter for the segmentation step, MLC was applied to the different segmented images of 1 March (with the scale parameter ranging from 5 to 50). A training set of 300 objects was randomly selected from each differently

segmented image and labelled as dry sand, wet sand or water through visual interpretation. Labelling of the objects resulting from segmentation with the scale parameter set to 40 and 50, was hampered by their size; they often incorporated more than one class. Consequently, the results for scale parameters 40 and 50 were excluded from Table 2.1. The average distribution of the classes in the training sets was 52% dry sand, 14% wet sand and 34% water objects. MLC created a classification model for each differently segmented image based on the training sets. Table 2.1 shows the results of the cross-validation of the training set after the MLC procedure. Two criteria defined the suitability of the different scale parameters: (I) Classification accuracy should be as high as possible (i.e. maximum value for total classification fit); and (II) the different classes should all be classified equally well (i.e. minimum value for range). Scale parameter 10 meets these criteria best and was thus selected as the default value for segmentation of the time series of Argus images.

For each segmented image of the time series, a training set of 300 random selected objects was interpreted and manually labelled. MLC created a classification model for each day using the labelled objects with their corresponding variables as input. The obtained classification model processed all objects of the segmented image resulting in a classified image.

The classification models also provide insight in the relation between class membership and the variables used to predict this membership, i.e. the importance of the respective variables for the distinction between two classes. For each variable, the values of the training set were used to calculate the difference in means ($\bar{X}_1 - \bar{X}_2$) and the standard error of this difference in means ($\sigma_{\bar{x}_1-\bar{x}_2}$) where subscripts 1 and 2 refer to two different classes. The difference in means was obtained by pairwise subtraction of the mean values. Because the variances were statistically different at the 95% confidence level, the standard error was computed as the separate variance estimate $\sigma_{\bar{x}_1-\bar{x}_2} = \sqrt{s_1^2/n_1 + s_2^2/n_2}$, in which s_1^2 (s_2^2) is the variance of the first (second) class and n_1 (n_2) is the number of objects of the first (second) class. The importance of a certain variable for the distinction between two classes increases with the t-value, $(\bar{X}_1 - \bar{X}_2)/\sigma_{\bar{x}_1-\bar{x}_2}$, of the two-sample t-test (McGrew, Jr. & Monroe, 1993).

2.3.4 Validation

Validation of the classification was carried out in a quantitative and qualitative manner. The quantitative validation consisted of the cross-validation of the training set, and of comparison of the classification of the 18 March image with in-situ classification. For the qualitative validation, class boundaries on the rectified image of 18 March 2002 were manually digitized. The digitized boundaries were draped over the classified image to compare the positions of these lines with the positions of class transitions obtained by the classification model.

2.4 Results

Figure 2.1a shows all images after standardization. The application of the EPS filter was repeated 9 times, after that the mean values of the RGB bands of all images remained the same. The number of objects for individual images ranged from 4,724 up to 7,536 after segmentation with a scale parameter of 10 (Table 2.2). For each image, MLC was performed on a training set of 300 manually labelled objects. The results of cross-validation are listed in Table 2.2. For 10 March 2002, the random selection of the training set provided a lack of wet sand objects disabling the cross-validation of the MLC results, but the number of wet sand objects was sufficient to perform MLC. The classification fit was lowest for wet sand class ranging from 38 to 85% with an average of 62%. The classification fits for both dry sand as well as water showed less variation and averaged at 93% and 91%, respectively.

The classified images are represented in Figure 2.1b. Note that in the first three and the last two images of the classified time series, the troughs and rips were well outlined by the transition between the classes dry sand and wet sand. The outlining of troughs and rips on 4 and 5 March was good too, but the models recognized quite some water areas as dry sand within the contours of these features. The models of 6 March as well as 8 March ascribed many objects of the upper beach to the class wet sand, so the transition between the trough and upper beach was harder to recognize. The lower part of the intertidal morphology was still flooded on 9 March during low tide, but the model was able to detect the dry sand of the intertidal bars quite well. The images of 10 and 11 March showed the morning shadows of "Huis ter Duin", the building on which the Argus station stands, as dark patches on the landward part

Table 2.2 Cross-validation for maximum likelihood models of the selected Argus image series

Day of	Number	Classification fit				Range
March 2002	of objects	dry sand	wet sand	water	total	max - min
1	7,047	0.947	0.769	0.857	0.897	0.178
2	7,465	0.921	0.615	0.929	0.883	0.313
3	7,529	0.932	0.851	0.934	0.920	0.083
4	6,703	0.914	0.708	0.876	0.847	0.206
5	6,822	0.938	0.685	0.911	0.883	0.253
6	4,724	0.877	0.565	0.912	0.870	0.346
8	6,978	0.935	0.543	0.920	0.883	0.392
9	4,892	0.939	0.389	0.974	0.923	0.585
10	7,536					
11	6,985	0.945	0.375	0.919	0.893	0.570
12	6,888	0.924	0.750	0.912	0.897	0.174
18	6,888	0.906	0.576	0.897	0.867	0.330

of the beach. This clearly disturbed the classification of image-objects around this area, since some of these dark patches were classified as water and contours of the shadows can be seen in the classified images. Besides this, the classified image of 10 March represented the surface composition reasonably well. The classified image of 11 March showed the boundary between trough and upper beach by the transition of wet sand to dry sand, but in the area between low water level and the trough-upper beach transition classification was not sufficiently accurate to recognize the correct outlines of the morphologic features.

Examination of the classification model produced by MLC also gives insight into the relationship between class membership and the variables. The relative importance of the variables for the distinction between two classes was, as outlined in Section 3.3, derived from the best estimate divided by the standard error. The three variables with the highest scores were selected from each pairwise comparison for the classification models. Table 2.3 shows an overview of the frequency that a variable was one of the three most important variables and gives the mean statistic t-value for these variables.

Ratio of red and blue, and cross-shore position were responsible for the distinction between the classes dry sand and water. The importance of red and blue ratio can be explained by the absorption of both bands by sand as against the absorption of red and the reflection of blue by water. The cross-shore position was important, because no water (dry sand) will appear in the landward (seaward) site of the beach. On two days (6 and 9 March) the variables composition was completely different. The visible resemblance of these two images (Figure 2.1a) are the gloomy appearance with the water being brighter than the sand, leading to the importance of mean of green and blue, and brightness for the distinction of dry sand from water. The statistic test values of mean green, mean blue, and brightness were high ($t > 20$, Table 2.3), implying a better distinction between water and dry sand on 6 and 9 March compared to the other days. The test statistics of ratio red, ratio blue and brightness were averaged over respectively 10, 8 and 9 days, but never reached the high t-values of mean green, mean blue and cross-shore position on 6 and 9 March.

The mean values of red and green, and the brightness were the main discriminators between dry sand and wet sand (Table 2.3). The importance of brightness confirmed that dry sand appears light on an image, while wet sand appears dark (Lillesand & Kiefer, 1994). Mean red was only excluded on 9 March, when the top-3 of distinguishing variables was entirely different and consisted of cross-shore position ($t = 7.2$), standard deviation blue ($t = 3.9$) and standard deviation red ($t = 3.8$). The standard deviations were only important on 9 March, while cross-shore position performed well on two other days (6 and 10 March) as well, both in combination with ratio blue.

The distinction between the classes wet sand and water is mainly defined by the variables mean values of green and blue and the brightness (Table 2.3). The importance of a blue component was most likely again due to its absorption near sand, and its reflection near water. This variable combination occurred in 9 out of 12 models. The whole composition altered only on 11 March to cross-shore position, ratio red and ratio blue, but t-values were relatively low: 12.2, 7.8 and 5.2. On that same

Table 2.3 Object variables with the frequencies (f) of being one of the three most important variables for the distinction between two classes and their mean t-value, based on the classification models of 1-12 March (excl. 7) and 18 March 2002.

Variable		Dry sand vs. water		Dry sand vs. wet sand		Wet sand vs. water	
		f	t	f	t	f	t
Red	Mean	0		11	12.5	1	18.9
	Std. Dev.	0		1	3.8	0	
	Ratio	10	17.0	1	10.1	2	9.3
Green	Mean	2	26.5	8	13.1	10	14.3
	Std. Dev.	0		0		0	
	Ratio	0		0		0	
Blue	Mean	5	20.3	0		10	14.5
	Std. Dev.	0		1	3.9	0	
	Ratio	8	16.5	3	7.9	2	7.4
Brightness		2	25.8	8	13.0	10	14.2
Maximum difference		0		0		0	
Cross-shore position		9	18.3	3	8.0	1	12.2

day, these variables were also most important for discriminating dry sand and water, though theirs performed better given their higher t-values: 23.5, 13.6 and 10.7 respectively. The t-values for discrimination of dry sand and water were overall higher compared to the discrimination of wet sand and dry sand or wet sand and water. The variables of wet sand contrasted less with dry sand and water, and will therefore be harder to classify. This corresponds with the lower classification fits of wet sand in the cross-validation (Table 2.2).

The dGPS survey of 18 March 2002 consisted of 606 data points, 556 of which were labelled in-situ into classes conform the classified images (293 points as dry sand, 152 points as wet sand, and 111 points as water, Table 2.4). The remaining 50 points were measured on transitions of two classes. The model classification of the 556 dGPS data points was extracted from the classified image of 18 March (Figure 2.1b). The vast majority (92.8%) of the in-situ dry sand points were recognized by the model in the Argus image (Table 2.4). The remaining in-situ dry sand points (7.2%) were identified as wet sand for 5.1%, which occurred over the complete alongshore distance near the transitions of the intertidal bar to the trough, and as water for 2.1%, what happened close to the low tide water line. Almost half of the wet sand data points were correctly classified by the model (43.4%). The model misclassified the same amount of wet sand points as dry sand points (44.1%). These misclassified points were mainly positioned in the northern part of the image. According to the dGPS data, a small trough with a width of 2 to 10 meters was positioned here, but this was not distinguished by the model. The remaining misclassified wet sand points were

positioned around the rips. Although the smallest number of data points belongs to the water class, the conformance between the in-situ and model classification was 90.1%. Misclassification of the water points happened primarily around the water line. The position of the water line changed during the dGPS survey, which lasted several hours. The 10 minutes exposure of the Argus image led to a relatively more stable position of the water line. The difference in water level position between the two data collecting techniques may easily have caused the misclassification for nearby located points. In total 78.8% of the dGPS points were labelled identically by the in-situ and the model classification.

The 50 transition data points represent three types of boundaries: (I) the transition between intertidal bar and trough reflected by the change of dry sand to wet sand or dry sand to water (15 data points); (II) the transition of trough and upper beach reflected by the change of wet sand to dry sand or water to dry sand (18 data points); and (III) the boundaries of the small trough on the upper beach in the north, in which wet sand represented the small trough and dry sand the upper beach (17 data points). The latter could not be analyzed, because the classification model was not able to distinguish this trough in the Argus image. The position of the other two boundary types was generally more seaward in the classified image than determined during the dGPS survey. The average difference between the boundaries found by classification and measured with the dGPS is 2.5 m; 0.4 m for the transition of the intertidal bar to the trough and 4.1 m for the transition of the trough to the upper beach.

Besides a quantitative validation, a visual comparison between a manual interpretation and a classified image was performed. The digitized lines of the Argus image of 18 March 2002 were draped over the classified image (Figure 2.5). In general, the digitized boundaries match the boundaries emerging from the classification well, but for some regions of the image the boundaries were different. The analogy of boundaries was high for the water class located in the trough between -500 and -400 m alongshore, for the intertidal bar-trough transition over the whole stretch of beach and for the trough-upper beach transition between -500 and +140 m alongshore. The conformance of the boundaries was quite good, but less compared to the preceding described boundaries, for the small trough found on the upper beach between +575 and +750 m (south), and for the digitized lines following the transition between water and wet sand in the trough between -400 and +400 m. Also the classified boundaries of the two rips in the north matched well with the digitized boundaries. The classified boundary of the rip in the south (about +550 m) showed some discrepancy with the

Table 2.4 Quantitative point validation of dGPS-data and classified image of 18 March 2002.

Field observations	Number of points	Model prediction			Fit
		dry sand	wet sand	water	
Dry sand	293	272	15	6	0.928
Wet sand	152	67	66	19	0.434
Water	111	4	7	100	0.901

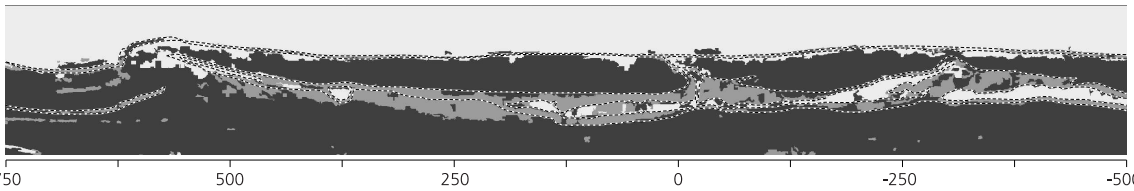

Figure 2.5 Digitized boundaries (dashed line) draped over the classified image of 18 March 2002. Dark grey represents dry sand, light grey represents wet sand and white represents water.

digitized boundary. This rip was hardly recognizable in the classified image. Some differences between digitized and classified boundaries were also found around the water line and the trough-upper beach transitions on the alongshore stretch between +140 and +550 m.

2.5 Discussion

In this chapter, a semi-automatic algorithm based on object-oriented image analysis was described for classification of video images showing the intertidal beach to enable beach morphology extraction. The classification model was built up by the classes dry sand, wet sand and water, as morphologic features in images can be recognized based on these surface composition. Thirteen Argus images of a time series ranging from 1 to 12 March and 18 March 2002 were preprocessed, segmented to reduce spectral confusion and classified. The spectral definitions of the classes are time and location specific, meaning that for each image a unique classification model has to be defined (Aarninkhof et al., 2003). The classified images show encouraging results (Figure 2.1b).

The efficiency of the classification may be influenced by sunlight. Exposure to sunlight is different over the five cameras at the end of the day, while the most left camera is facing SW, and the other cameras are facing W to NNE. The influence of sunlight is also noticeable by shades, mainly from buildings just landward of the beach, present on images taken in the morning (e.g. 11 March 2002; see Figure 2.1a). The effect of varying lightning conditions is reduced by the standardization per cross-shore profile, although it should be noted that the effect of sunlight is better eliminated than that of shade. Besides sun glint, weather conditions as fog and rain also reduce the contrast of the image, mainly causing the image to become blurry. These conditions were not present in this data set so their influence on classification is not clear yet, but it can be anticipated that the classification will become less accurate.

In each model, wet sand was classified with the lowest accuracy. The classification fit reached values between 65 and 80% when determining the best scale parameter (Table 2.1), and between 39 and 87% for classification of the time series (Table 2.2). Classification of wet sand is difficult, because it shows characteristics of both water and sand. In shoreline detection studies, distinction is made between the two classes water and sand by applying a per-pixel approach, but these classes are easily confused due

to the presence of wet sand (Aarninkhof et al., 2003). Besides the low classification fit, the class wet sand combined with the class water defines the morphological features rips and troughs. The intertidal bar and the upper beach are defined exclusively by the class dry sand. This might suggest that the classes wet sand and water could be merged into one class. However, distinction between the two classes provides valuable information on the orientation of rips. For example, on 12 March 2002 the shape of the rips is elongated and strongly oblique oriented looking at the water. But regarding to the wet sand, these rips have a very wide funnel shape oriented shore-normal (Figure 2.1a).

Quantitative validation of the classification model showed a good correspondence between the in-situ and the model classifications for the classes dry sand and water, both about 90%. The lower classification fit of wet sand was still around 43%. The highest classification fit of sandy surfaces (so comprising wet and dry sand) found by Yates et al. (1993) was only 68%. They used MLC on a LANDSAT5 Thematic Mapper data, which provides both visible and near-infrared spectral information, to classify intertidal surface sediments of an estuary. Furthermore, the lower classification fit of 43% of wet sand can be largely attributed to the small trough on the upper beach in the northern part of the image, which was not recognized by the model. The width of this trough varies between 2 and 10 m. The grid size of the Argus image is 0.5 m, though the accuracy of this chosen size varies with the distance of the grid cell from the camera. The position of the trough corresponds with cross-shore pixel footprint dimensions of approximately 1.0 m, which is still smaller than the trough width. However, the segment variables are not contrasting enough for the model to recognize it as wet sand. Maybe this trough is already drained too well causing the lack of contrast, because of its higher position on the upper beach compared to the other trough. During visual interpretation, this trough was not recognized either (Figure 2.5). The small trough (with similar width) in the south on the upper beach (between +575 and +750 m alongshore) was recognized by both the classification model and visual interpretation (Figure 2.5).

More classification confusion was found around the water level both with the quantitative and qualitative validation. However, the low water line does not define a boundary of a morphologic feature, although its shape reflects the shape of morphologic features (mainly the intertidal bar).

Average variation in class boundary positions computed by the model and estimated during the dGPS surveys was about 2.5 m cross-shore, with the modelled positions on average more seaward than the in-situ positions. The variation is five times the chosen pixel size of 0.5 m and exceeds the range of the cross-shore footprint dimension, which varies between 0.5 and 2 m. The variation depends on sharpness of the transitions, which varies for different boundary types. The crisp transition between bar and trough causes a variation of only about 0.4 m, which is smaller than the pixel size and the range of cross-shore footprint dimension. Whereas the trough-beach transition was more gradual causing a variation of approximately 4.1 m, which is comparable to the shoreline position errors found by shoreline detection models. In Egmond, located some 40 km north of Noordwijk and showing similar beach charac-

teristics, another Argus-station has been installed. Here, shoreline detection models using Argus images resulted in horizontal errors of the shoreline position between 4.5 and 6 m, which is deduced from the vertical displacement of the shoreline (Aarninkhof et al., 2003).

2.6 Conclusions

A semi-automatic object-oriented algorithm was developed for classification of intertidal beach morphology in low-tide video images. The algorithm comprises standardization of the images collected simultaneously by individual cameras, smoothing by an edge preserving smoothing filter, segmentation, and classification using maximum likelihood method. Tests of the algorithm on 13 low-tide Argus images collected at Noordwijk aan Zee, show that the bar/trough/rip morphological units can be classified by using the surface composition classes dry sand, wet sand and water. Of the 3 classes, dry sand could be classified best (92.8%) when compared to an in-situ classification, water was correctly classified for 90.1% and wet sand had a classification fit of 43.4%. Pairwise, classes dry sand - water were typically discriminated by the ratio in the red and blue layers, and cross-shore position, classes dry sand - wet sand were typically discriminated by the mean of the red and green layers, and the brightness, and classes wet sand - water were typically discriminated by the mean value of the green and blue layers, and the brightness. Application of this classification algorithm on longer time series of video images will provide valuable information on the dynamics of the intertidal morphologic features.

3 Cross-shore behaviour of an intertidal bar-trough system

Quartel, S., B.G. Ruessink & A. Kroon (2007) Daily to seasonal cross-shore behaviour of quasi-persistent intertidal beach morphology. Earth Surface Processes and Landforms, 32(9), 1293-1307

Abstract

In this study, an intertidal bar and trough system on the beach of Noordwijk, the Netherlands was monitored over a 15-month period to examine the daily to seasonal sequential cross-shore behaviour and to establish which conditions force or interrupt this cyclic bar behaviour. The beach morphology (bars/troughs) was classified from low-tide Argus video images based on surface composition. From the classified images, time series of the landward boundary of the bar and of the trough were extracted. The time series of the alongshore-averaged boundary positions described sawtooth motion with a period between 1 and 4 months, comprising gradual landward migration followed by abrupt seaward shifts. The abrupt seaward shift appeared to be a morphological reset induced by storm events, which lasted at least 30 hours with a large average root-mean-square wave height ($\geq$ 2 m) and offshore surge level ($\geq$ 0.5 m), and a small trough ($<$ 20 m wide) in the pre-storm beach morphology. The time series of the boundary positions exhibited very little variability longer (seasonal) scale, but somewhat larger variability on smaller (daily) scale. The bar boundary was found to be more dynamic than the trough boundary.

3.1 Introduction

The unconsolidated sandy material of the intertidal beach, located between the mean low- and high water level, is generally organized in one or more shore-parallel bodies of sand (bars) and accompanying depressions (troughs). In micro- to mesotidal conditions the sandbars typically have a definite steep, landward facing slip-face (Davis et al., 1972; Wijnberg & Kroon, 2002). Masselink et al. (2006) called these bars 'slip-face ridges', to distinguish them from the more subdued multiple bar systems typical of macro-tidal conditions.

During low-energy wave conditions slip-face ridges show a cross-shore cyclic behaviour, consisting of: (I) generation near the low tide water line; (II) landward migration; and (III) disappearance due to merging of the bar at the high water level. Following the disappearance, a new bar is rapidly generated near the low water line (Doeglas, 1955; Hayes & Boothroyd, 1969; Wijnberg & Kroon, 2002). The sequence from bar generation to disappearance has been observed to vary between several days (for non-tidal environments) to weeks (for meso-tidal environments) (Hayes & Boothroyd, 1969; Owens & Frobel, 1977). The cyclic pattern may however be interrupted at any moment by storm wave activity, causing flattening of the beach when the sand is eroded from the beach (Doeglas, 1955; Owens & Frobel, 1977). This erosional disappearance is also known as a morphological reset. The reset and the subsequent rapidly newly generated bar shows the quasi-persistent character of the slip-face ridge, because the bar seems to be continuously present on the beach, but indeed experiences relatively short moments of absence.

The behaviour of the slip-face ridges is often coupled to the type, intensity and duration of shallow water wave processes, i.e. swash, bores and breaking waves (e.g. Masselink & Short, 1993). Swash - backwash processes are responsible for the generation (I) and landward migration (II) of slip-face ridges (Kroon, 1994; Wijnberg & Kroon, 2002; Masselink et al., 2006). This landward migration occurs when sediment is entrained from the seaward flank by breakers, bores or swash motion, and subsequently deposited at the landward flank by swash motion, which overtops the crest of the slip-face ridge (Wijnberg & Kroon, 2002). Swash - backwash activity results in vertical bar growth when the swash motion does not overtop the bar and is active on the seaward flank only.

Landward migration of the slip-face ridges may occur during submergence as well. When the water depth above the bar-crest is at least 0.1 m, the onshore orbital motion under the bores exceeds the offshore wave stroke, whereas excess water transported over the bar is channelled alongshore to the nearest intertidal rip channels (Aagaard et al., 2006). Therefore, mean flows and subsequently the suspended sediment transport capacity at the bar crest are directed landward (e.g. Aagaard et al., 1997). Houser & Greenwood (2007) showed different behaviour of the submerged slip-face ridges during high-energetic wave conditions though: landward migration when waves break seaward of the bar crest, but seaward migration when waves break landward of the bar crest and erode the bar crest. Migration rates of intertidal bars are higher in non-tidal environments than in tidal environments (Davis et al., 1972), showing the influence of the residence time of hydrodynamic processes (Kroon & Masselink, 2002), which in tidal environments is obviously shorter than in a non-tidal setting. On macro-tidal beaches the short residence time may even result in multiple bar system with time independent cross-shore positions (Anthony et al., 2005).

The merging of slip-face ridges occurs during low-energy wave conditions (e.g. Wijnberg & Kroon, 2002). However, various studies for a micro-tidal beach in Denmark present merging of a slip-face ridge during high-energetic conditions (i.e. offshore wave heights about 2 m; Aagaard et al., 1997, 2006). Initially with these conditions, landward-directed currents above the crest of the slip-face ridge as a part of

the horizontal cell circulation led to landward-directed suspended sediment transport. Therefore, the slip-face ridge migrated landward and the accompanying trough infilled. When the trough was infilled, undertow became more important. As a consequence, the suspended sediment transport above the crest became seaward oriented and, subsequently, the beach started to erode.

Most observations and conceptual models of the sequential cross-shore behaviour of slip-face ridges are based on field experiments that lasted for a couple of days to some weeks at most (see Davis & Fox, 1972; Owens & Frobel, 1977; Kroon, 1994; Aagaard et al., 2005). It is thus uncertain how often such a sequence of generation, migration and merging or flattening occurs. Besides, existing analyses of bar systems often focus on bars only, although bars and troughs together form a so-called bar system. Anthony et al. (2005) found that strong alongshore currents in well-developed, deep troughs of multiple bar system on a macrotidal beach hinder cross-shore migration of the bars, showing the trough's importance in the morphodynamics of a bar system. Otherwise, little is known about the behaviour of the trough itself, and the (dis-) similarities between bar and trough behaviour.

The aim of this chapter is to examine the daily to seasonal sequential cross-shore behaviour of the intertidal bar - through system and to establish which conditions force or interrupt this cyclic behaviour. The study was carried out at the beach of Noordwijk aan Zee, the Netherlands (Figure 1.2; Section 3.2). Intertidal bars, i.e. slip-face ridges, and troughs were derived from daily, low-tide video images over a 15-month period. These video images were classified based on their surface composition (Quartel et al., 2006) and the positions of the intertidal bars and troughs, by use of their landward boundary, were extracted from the classified images (Section 3.3). The alongshore-averaged temporal variability of the cross-shore positions of the boundaries was used to quantify the cross-shore migration of the bar - trough system. As described in Section 3.4, several periods of gentle onshore behaviour were recognized, each ending after 1 to 4 months with a reset during prolonged storm conditions. Our results are discussed and summarized in Sections 3.5 and 3.6, respectively.

3.2 Study site

Noordwijk aan Zee, located on the central Dutch coast (Figure 1.2), is a sandy, wave dominated coast, whose beach and nearshore zone consist of a single intertidal slip-face ridge and two subtidal bars, respectively (Figure 3.1; e.g. Van Enckevort & Ruessink, 2003a). Occasionally, a second intertidal bar may be formed on a pre-existing bar during low-energy wave conditions. The intertidal beach, i.e. the area between the mean high water line and mean low water level, has an average width of 100 m and a slope of approximately 1:50 at Noordwijk (Figure 3.1). The sediments on the beach are well sorted and between 250 and 350 μm in grain size (Van Bemmelen, 1988).

The beach and nearshore zone of Noordwijk has been monitored since 1995 by a digital video camera system, known as an Argus monitoring station (see Holman & Sallenger, 1986). The system is mounted on the top of a hotel at a height of 62 m

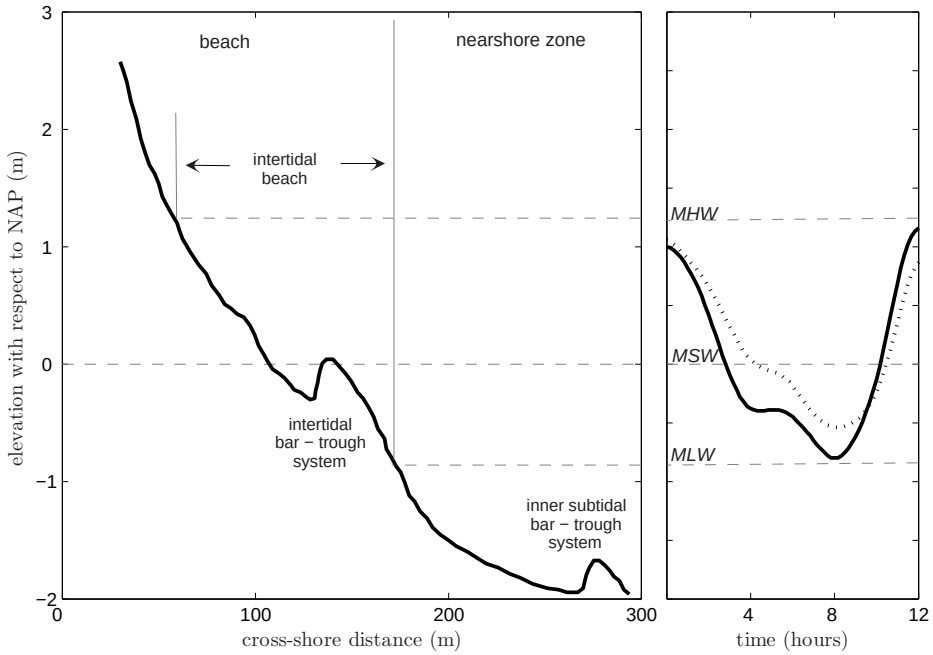

Figure 3.1 Left panel shows an example of a cross-shore profile of the beach and a part of the nearshore zone at Noordwijk. Right panel represents predicted water level, η_{pred0}, fluctuations at MPN for one tidal cycle. The black solid line represents spring tidal cycle with the agger at $t = 4 - 6$ hours around -0.4 m in height, and the black dashed line shows a neap tidal cycle. MHW and MLW represent the average high and low water level, respectively.

above mean sea level, and consists of 5 cameras that together view the coastal zone over 6 km in the alongshore direction, and 1.5 km in the cross-shore direction. The cameras collect every hour during daylight ten-minute time-exposure (timex) images, which are based on instantaneous snapshots sampled at 2 Hz. The oblique images taken daily at low tide for the period 19 October 2001 to 31 December 2002 were selected for the present study. Gaps due to technical malfunctioning of the Argus system exist for 5-7 January, 14-21 April, 25-28 April and 19-26 July 2002.

Offshore wind, waves and water levels were collected at Meetpost Noordwijk (MPN in Figure 1.2), which is positioned about 9.5 km offshore at 18-m water depth. Figure 3.2 presents the wind direction (θ_{wind}) and wind force, the root-mean-square wave height (H_{rms0}), the energy-weighted wave direction (θ_0), the peak wave period (T_{p0}) and the surge level (η_{surge}, defined as the measured difference between observed and astronomical water levels, $\eta_{\mathrm{obs0}} - \eta_{\mathrm{pred0}}$). The study period contained a number of events with strong wind (wind force > 10.8 m/s, marked by the largest dots), limited to an incident wind angle between -45° and 70° (Figure 3.2a), causing high wave conditions with H_{rms0} up to 4 m (Figure 3.2b). During these high wave conditions (for simplicity, high wave conditions were defined as $H_{\mathrm{rms0}} > 1.5$ m at this site, see also Kroon et al., 2003), T_{p0} varied between 7 to 10 s, with larger values when waves were incident from northern directions (Figures 3.2c and d). During the summer (April - September 2002), the high wave events occurred less frequently and involved smaller surge levels ($\eta_{\mathrm{surge}} \approx 0.3 - 1.0$ m) than during the winter (October 2001 -

March 2002 and October - December 2002; $\eta_{\text{surge}} \approx 0.5 - 1.7$ m) (Figure 3.2e).

Low-energy wave conditions (defined as $H_{\text{rms},0} < 1.5$ m for this beach) occurred with onshore and offshore directed winds and had $T_{\text{p}0}$ of about 5 s. During the less frequent periods of offshore directed winds ($\theta_{\text{wind}} < -90^\circ$ or $\theta_{\text{wind}} > 90^\circ$), $H_{\text{rms}0}$ remained below 1 m. Besides, the offshore winds also resulted in negative surge levels (Figures 3.2a and e), causing partial subaerial exposure of the intertidal morphology during high tide.

The tide at Noordwijk is semi-diurnal and microtidal (mean tidal range is 1.8 (1.4) m during spring (neap) tide). The tidal signal shows an agger during spring tide, which almost disappears during neap tide conditions. The agger causes a stagnation of the water level for at least 2 hours at a vertical range between -0.3 and -0.6 m with respect to mean sea level for the predicted tide (Figure 3.1).

3.3 Data acquisition and preliminary analysis

The collected low-tide oblique timex Argus images were geometrically transformed to obtain a rectified plan view of the beach and nearshore zone (Holland et al., 1997). The rectified images of the different cameras can be merged to create a combined plan view. The region of interest on such a combined Argus image covered 1250 m in the alongshore direction with the camera position in the middle and 165 m in the cross-shore direction, including the whole intertidal zone. The pixel size of the rectified images was 0.5×0.5 m (Figure 3.3).

The intertidal beach morphology is visible on the plan view images due to differences in surface sediment composition. Quartel et al. (2006) developed an object-oriented algorithm to classify the surface composition into water (W), wet sand (WS), or dry sand (DS) (Figure 3.3). The classes are distinguishable due to their spectral properties in the colour (RGB) images: W is marked by blue, WS and DS are marked by red, but WS is darker than DS. The extraction of the spectral information from images is done in an object-oriented manner. A small amount of the created objects (300 from, on average, 7000 objects) were labelled and used as a training set for a quadratic discriminant analysis, obtaining a model to classify all objects of one image. Morphologic features on the intertidal beach can be delineated after classification of the images.

3.3.1 Feature delineation

Contours of dry sand areas in the classified images mark the boundaries of the slip-face ridges and the transition between the most landward trough and the upper beach, which are the features of interest for this study. Because the classes WS and W together distinguish the trough from the upper beach and the slip-face ridges (DS), these two classes were combined and together considered as the class WWS. This results in the conversion of the tripartite classified image into a binary image (middle

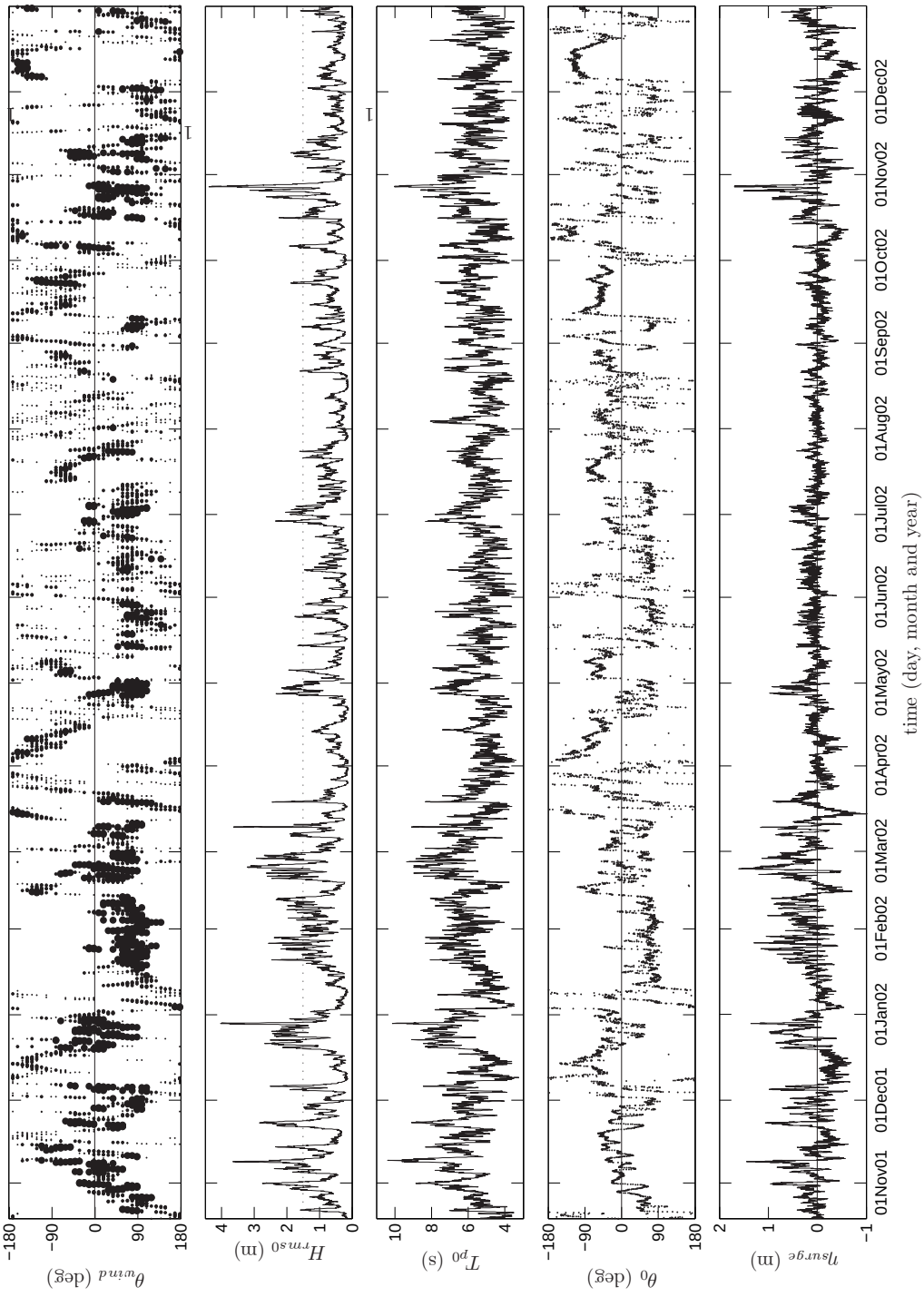

Figure 3.2 Wind, waves and water levels: upper panel shows the θ_{wind} combined with the wind force (small size, black dots represent wind force $\leq$ 5.4 m/s, middle size, dark grey dots 5.4 m/s $<$ wind force $\leq$ 10.8 m/s and large size, light grey dots wind force $>$ 10.8 m/s), the three middle panels show the wave characteristics H_{rms0}, θ_0 and T_{p0}, and the lower panel the surge level, η_{surge}. θ_{wind} and θ_0 are 298 $^\circ$ true N; positive numbers reflect incidence from southern directions and negative numbers reflect incidence from northern directions. Note: after a severe storm at the end of October 2002, the directional waverider at YM6 broke down and wave direction data was retrieved from Eierlandse Gat (about 90 km north of Noordwijk).

and lower image, respectively, in Figure 3.3).

Small patches of dry sand with a contour line shorter than 50 m were excluded from further study, because these small patches do not represent meso-scale features such as slip-face ridges. The type of boundary that the dry sand contour marks depends on its position and the presence of other contours on that cross-shore profile. Figure 3.3 shows four different cross-shore profiles from which the different boundary types can described. In case of only one contour in the profile, DS to WWS (see profile A), the transition marked the water line; apparently, no bar - trough system was present. In general, however, the intertidal beach consisted of one trough-bar system and the classified image entails three contours in a cross-shore profile as in profile B. Going in the seaward direction, the first contour marks the transition from DS to WWS, and corresponds to the trough - upper dry beach transition. The second contour is a WWS to DS transition and describes the landward boundary of the intertidal bar. The third and the most seaward contour (DS to WWS transition) is the water line. More than three contours could appear in the cross-shore profile when two bar - trough systems are present with the second bar positioned in the middle of the intertidal area or more towards the upper beach (profile C and D respectively).

Based on the amount and type of the class transitions, and their relative positions, the contours were labeled into different boundary types. Some manual interference was required; therefore the contours and accompanying boundary type labels were checked. The resulting boundary data are alongshore lines describing the cross-shore position of the detected landward boundary of the slip-face bar and the accompanying landward located trough, X_{lb} and X_{lt} respectively. A quadratic loess filter (Plant et al., 2002) was applied to the alongshore data to remove irregularities in the boundaries with the length scales < 50 m, which may have originated from misclassification of W, WS and DS.

3.3.2 Time Stacks

The detected feature boundaries are shown as colour time stacks in Figures 3.4 and 3.5. The horizontal axis in each time stack is the alongshore distance y and the vertical axis is time t. The colours are the cross-shore position x of the boundaries, with x increasing in the seaward direction. Each horizontal line represents the momentary cross-shore position of the landward boundary of the intertidal trough, $X_{lt}(y,t)$ (Figure 3.4), and the landward boundary of the intertidal bar, $X_{lb}(y,t)$ (Figure 3.5). The shape of the boundaries is visible by the alternation of warm and cold colours at a certain moment. The warm (cold) colours are the landward (seaward) protruding parts, also referred to as bays (horns). Gradual warming of the colours over time reflects the landward migration of features (e.g. from 27 December 2001 to 19 January 2002), while abrupt shifts to cold colours mark a reset in the morphology (see dotted lines in Figures 3.4 and 3.5). The alongshore shifting of the colour patterns represents alongshore migration.

Cross-shore positions $X_{lt}(y,t)$ and $X_{lb}(y,t)$ were not obtained for certain days

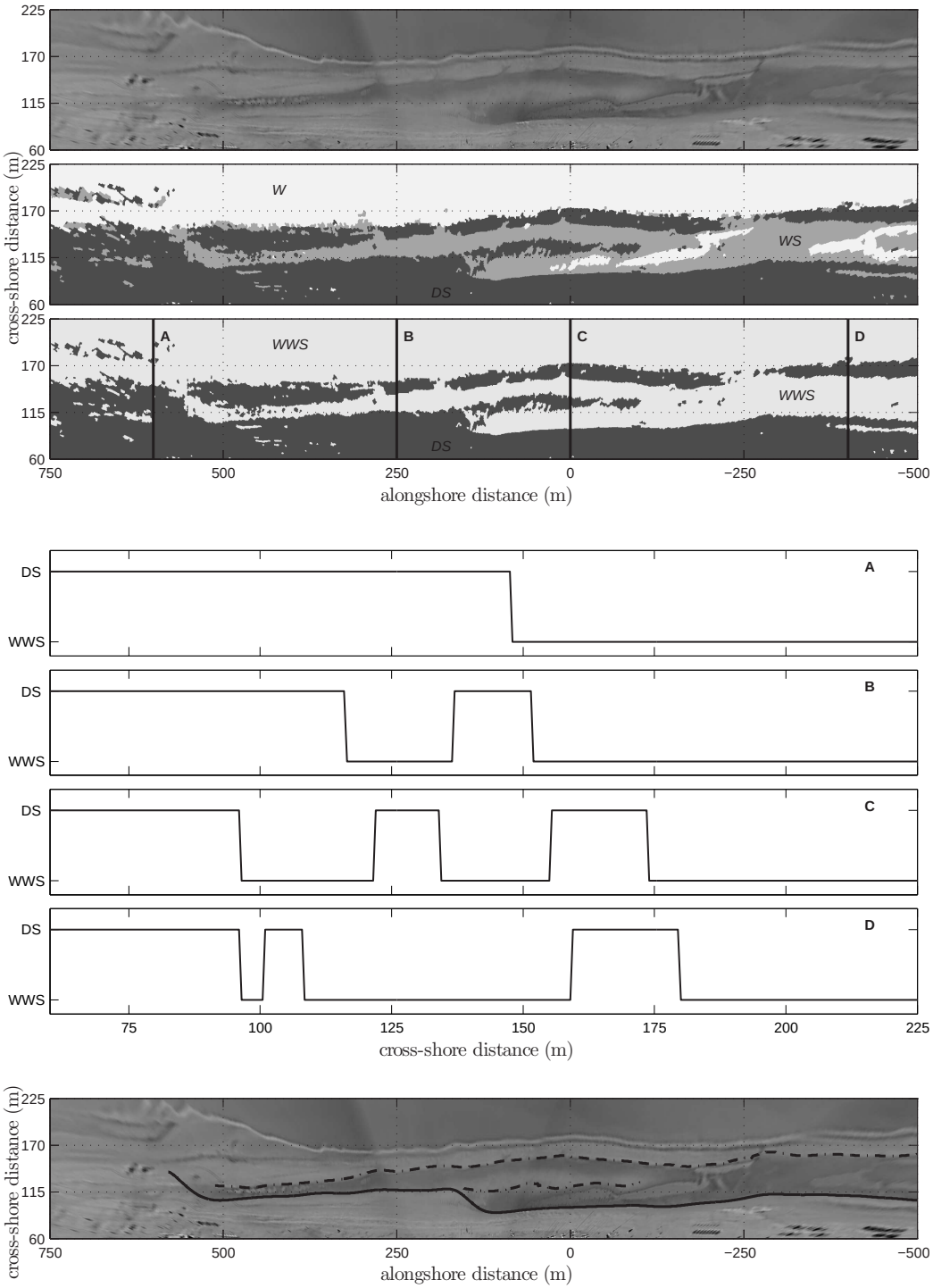

Figure 3.3 The upper three panels show the merged Argus image (top), tripartite classified image (middle) and binary image (lower) of 28 May 2002 at Noordwijk. Underneath are the four cross-shore profiles A, B, C and D which are marked in the classified binary image. The boundaries for 28 May are provided in the lowest panel, where the solid line represents the landward boundary of the trough and the dashed-dot line the landward boundary of the bar. Note: There are 2 landward boundaries of the bar and for further analysis the most landward positioned boundary, i.e. the boundary of the oldest bar, is used.

owing to high-energy conditions causing the features to remain submerged during the entire tidal cycle, inaccurate classification of the images, or unavailability of the images. Such no-data situations are reflected in the time stacks as white areas. In addition, the absence of the intertidal features on a good-quality image causes white areas in the time stacks. This concerns mainly the southern part of the beach ($y = +500 - +750$ m; Figures 3.4 and 3.5), which experienced long periods without a bar - trough system. Strikingly, this beach stretch also distinguishes itself from the remaining alongshore beach stretch ($y = -500 - +500$ m) by the relatively closer position of the inner subtidal bar to the beach (see Figures 4.5c and 4.6c). A relation between these two characteristics is feasible.

The plan-view Argus images from the 15-month study period were examined visually for days without bar - trough morphology. These days are listed in Table 3.1 as events 1 to 8, and correspond to the resets found in the time stacks, albeit that event 5 does not show up as a reset of X_{lt} (Figure 3.4). Usually, the low tide image previous to a reset showed a submerged intertidal morphology indicating high-energy conditions.

The storm events during the 15-month period were defined as the period between the moment H_{rms0} exceeded 1.5 m (i.e. high wave conditions; Section 3.2) and the moment H_{rms0} remained below 1.5 m for at least a half day (12 hours). In this way, 51 storm events with varying duration and intensity were identified. All morphologic resets data were found either within a storm event or within 15 hours after the end of a storm event. So the featureless beaches all involved preceding high-energy conditions. The duration and average H_{rms0}, θ_0, $\bar{\eta}_0$ and wind speed of the storm events of the resets are listed in Table 3.1.

3.4 Results

3.4.1 Average cross-shore position and migration

To examine the cross-shore behaviour of the bar - through system, $X_{lt}(y,t)$ and $X_{lb}(y,t)$ were alongshore averaged over $-500 < y < 500$ m to yield $\bar{X}_{lt,y}(t)$ and $\bar{X}_{lb,y}(t)$, respectively (Figure 3.6). The alongshore stretch of $y = 500 - 750$ m was excluded due to the frequent absence of the bar - trough system, and apparently dissimilar behaviour from the rest of beach. Because of seasonal differences in hydrodynamic conditions and varying tidal ranges due to spring and neap tide cycles, both alongshore-averaged time series were filtered to extract the seasonal, $\bar{X}_s$, and weekly, $\bar{X}_w$, component. The seasonal component $\bar{X}_s$ was obtained by low-pass filtering each $\bar{X}_y$ signal retaining time variability in excess of 91 days only. Subsequently, $\bar{X}_w$was computed by low-pass filtering $\bar{X}_y$-$\bar{X}_s$ with a cut-off period of 14.5 days. In each case the low-pass filtering was carried out with a quadratic loess filter (Plant et al., 2002). The remaining high-pass variability, $\bar{X}_y$-$\bar{X}_s$-$\bar{X}_w$, is referred to as the daily cross-shore variability, $\bar{X}_d$.

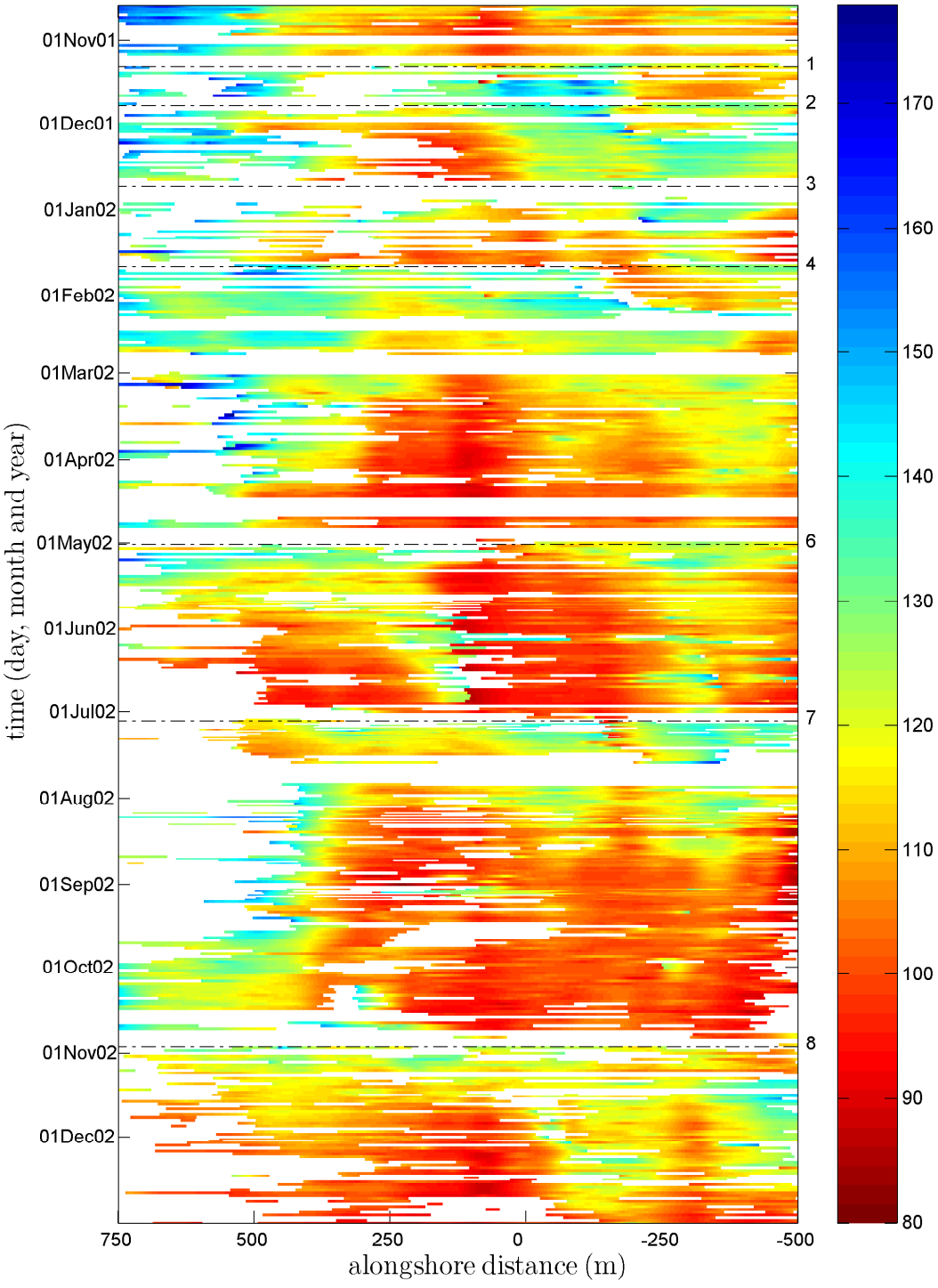

Figure 3.4 Colour time stack plot of the cross-shore position (colours) of the trough landward boundaries, $X_{lt}(y,t)$, with the alongshore distance, y, presented on the horizontal axis and the time, t, in downward direction on the vertical axis. The dashed-dotted lines refer to the moments with no morphologic features on the beach, which are listed by the event number.

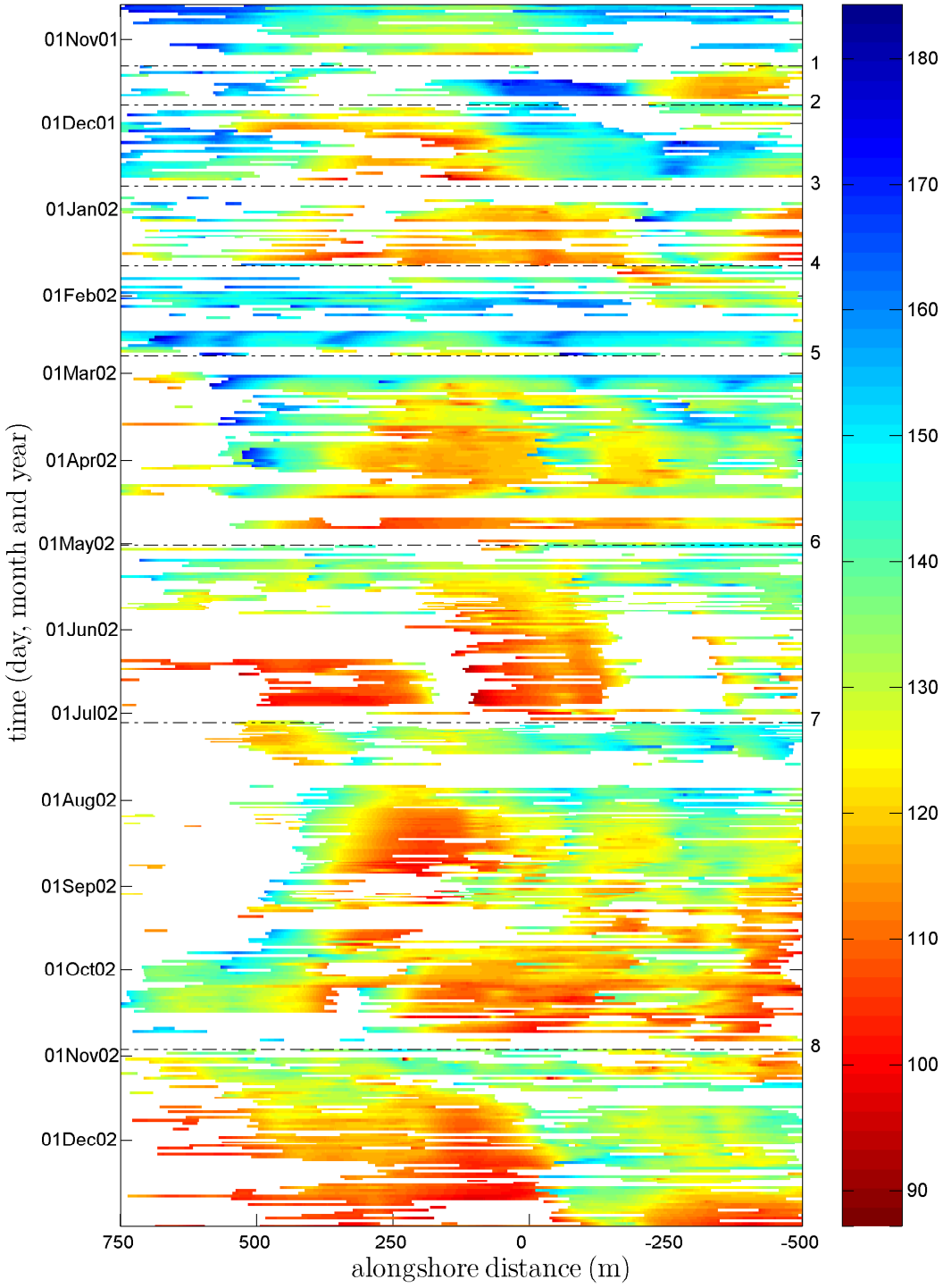

Figure 3.5 Colour time stack plot of the cross-shore position (colours) of the bar landward boundaries, $X_{lb}(y,t)$, with the alongshore distance, y, presented on the horizontal axis and the time, t, in downward direction on the vertical axis. The dashed-dotted lines refer to the moments with no morphologic features on the beach, which are listed by the event number.

The time series of $X_{lt}(y,t)$ and $X_{lb}(y,t)$ described a sawtooth pattern with abrupt shifts in the seaward direction followed by gradual displacements in the landward direction (Figure 3.6a). The abrupt seaward shifts are associated with the disappearance of the intertidal features during high-energy conditions and the subsequent regeneration of the features at a more seaward position, whereas the gradual landward displacements represent the onshore migration of the feature during low/intermediate energetic conditions (Figure 3.7). During the investigated period, 5 sequential sawtooth migration patterns were observed. The period of each sawtooth motion varied between a few weeks (in November and December 2001) up to 4 months (from July to October 2002) and thus lacked a clear seasonal component (Figure 3.6b). However, the weekly component ($\bar{X}_w$; Figure 3.6c) reflected the sawtooth motion quite well. The abrupt seaward shift of the sawtooth coincided with some of the events with featureless beaches.

Closer inspection of the data revealed that a decrease in $\bar{X}_{lt}(t)$ and $\bar{X}_{lb}(t)$ did not result from the reset of feature sequential behaviour only. Occasionally it was also due to a change from an elongated, shore-parallel bar-trough shape to a more oblique system, whereafter the landward feature boundaries partly occupied a more seaward position (Figure 3.8). Presumably, the maximum values of the seaward migration rate were associated by the regeneration after a storm, while the lower (average) values may be coupled to beach configuration changes. The difference between regeneration and migration may be made by focusing on the configuration on the individual boundary lines $X_y(t)$.

Table 3.1 Selected dates of Argus images with featureless beaches and the hydrodynamic and meteorologic conditions of the storm events, which preceeded or included these dates.

Event		Date	Area	Average preceeding conditions				
				Duration (hours)	H_{rms0} (m)	θ_0 (°)	η_0 (m)	Wind speed (m/s)
1		9 Nov ′01	partly (S)	73	1.92	−3	0.40	11.8
2		23 Nov ′01	partly	50	2.16	8	0.47	13.6
3	a	20 Dec ′01	partly	69	1.81	−25	0.36	11.2
	b	23 Dec ′01	total	69	1.81	−25	0.36	11.2
	c	27 Dec ′01	total	113	2.08	12	0.52	13.0
4		20 Jan ′02	partly	12	2.01	67	0.15	15.5
5		21 Feb ′02	partly	50	1.85	9	0.46	12.5
6		29 Apr ′02	partly (S)	41	1.78	61	0.41	13.9
7	a	29 Jun ′02	partly (S)	22	1.84	−29	0.35	12.1
	b	3 Jul ′02	total	39	1.58	68	0.24	13.2
8	a	24 Oct ′02	partly (N)	26	2.07	12	0.63	13.8
	b	28 Oct ′02	partly	58	2.41	33	0.72	15.8

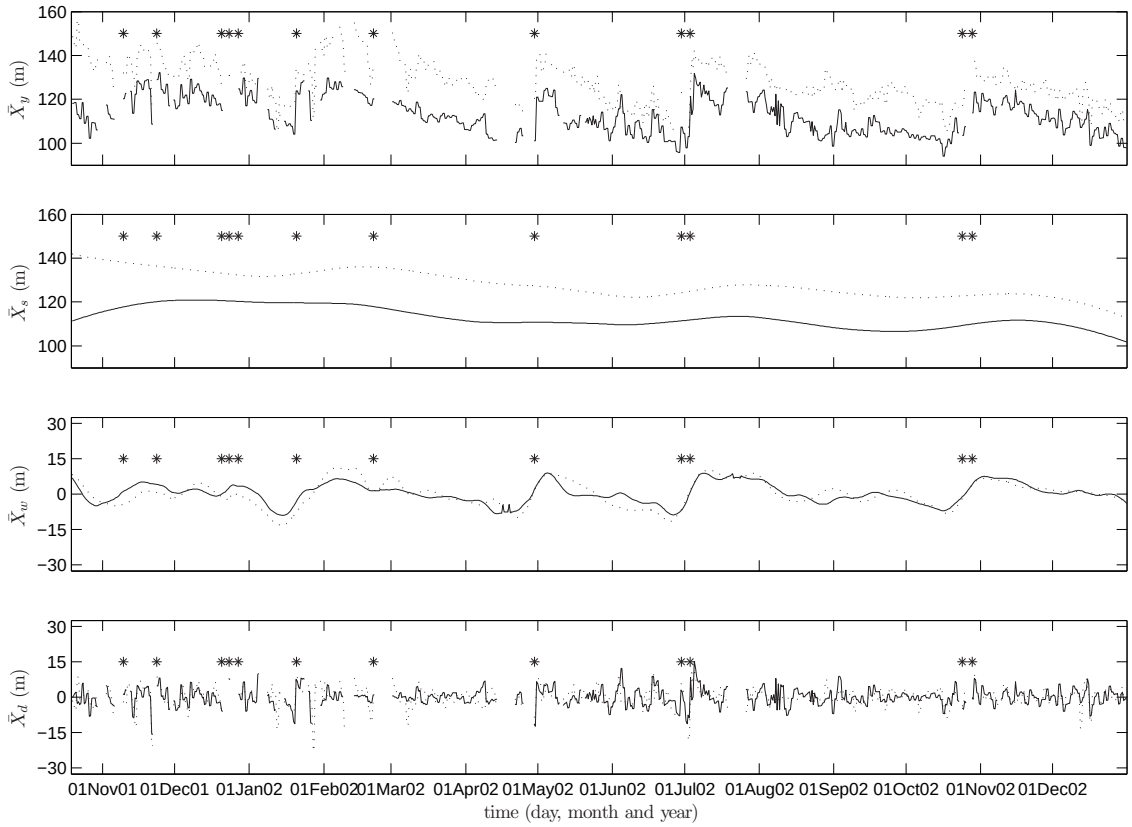

Figure 3.6 Time series of cross-shore positions and the seasonal, weekly and daily component of the landward boundary of the intertidal trough, $\bar{X}_{lt}(t)$ (solid line), and bar, $\bar{X}_{lb}(t)$ (dashed line). The asterisks ($*$) mark the events as listed in Table 3.1.

Values of $\bar{X}_{lt}(t)$ and $\bar{X}_{lb}(t)$ occurred within a limited cross-shore range (Figure 3.6a), which are used to investigate the similarity between the trough and bar behaviour. The difference between the most seaward position and most landward position of $\bar{X}_{lt}(t)$ was slightly over 30 m (Figure 3.9). Initially, the cross-shore range between the most seaward position and most landward position of $\bar{X}_{lb}(t)$ was around 50 m, but after March 2002 this was approximately 40 m (Figure 3.6a). The frequency of occurrence of $\bar{X}_{lb}(t)$ was about normally distributed with its mode at $\approx$ 125 m (Figure 3.9). The trough boundary position had a more positively skewed distribution with its maximum between 105-110 m (Figure 3.9). The cross-shore behaviour of $\bar{X}_{lb}(t)$ implies that it is more dynamic than the behaviour of $\bar{X}_{lt}(t)$ with regard to the larger range and the normal distribution of the cross-shore position. Figure 3.6a emphasizes the behaviour of $\bar{X}_{lt}(t)$ to be more asymmetric, because $\bar{X}_{lt}(t)$ follows an asymptotic trend towards the cross-shore position of approximately 105 m, which is most evident in the period between early July and mid-October.

The derivative of the cross-shore position time series (Figure 3.6) provided migration rates of the features for different timescales. The seasonal migration rate was derived from $\bar{X}_s$, the weekly migration rate from $\bar{X}_s+\bar{X}_w$, and the daily migration rate from $\bar{X}_y(=\bar{X}_s+\bar{X}_w+\bar{X}_d)$ (see Van Enckevort & Ruessink, 2003a), with which the positive (negative) values represent seaward (landward) migration rates. Table 3.2

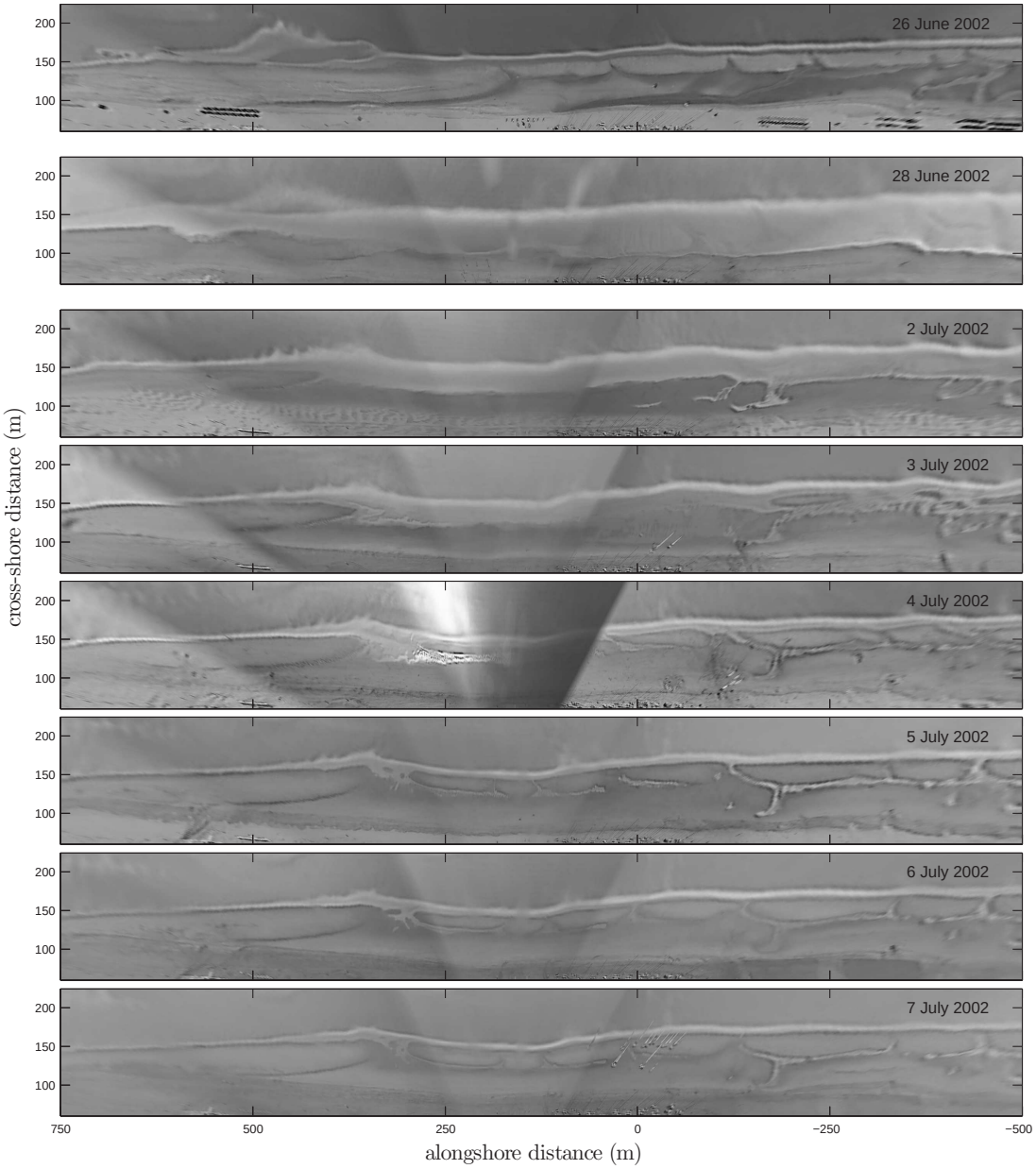

Figure 3.7 Argus image series of representing (from top to bottom) a beach with pre-storm morphology (26 June 2002), submerged morphology during the reset storm (28 June 2002), featureless (2 July 2002), partly regenerated bar at the low water line (3 July 2002) and fully regenerated bar which gradually migrates landward (4-7 July 2002). This sequence of morphology resulted in a (part of a) sawtooth motion.

shows the average values, standard deviations and maximum values of the computed migration rates. The seasonal migration rates of $\bar{X}_{s,lt}$ were small and almost equal in the landward and seaward directions (0.10 and 0.11 m/day respectively), but the migration rate in the landward direction of $\bar{X}_{s,lb}$ (0.13 m/day) was larger than the migration rate in the seaward direction (0.09 m/day). On weekly and daily timescale, the average landward migration rates and accompanying standard deviations of $\bar{X}_{lt}(t)$ and $\bar{X}_{lb}(t)$ were overall smaller than the seaward migration rates and accompanying

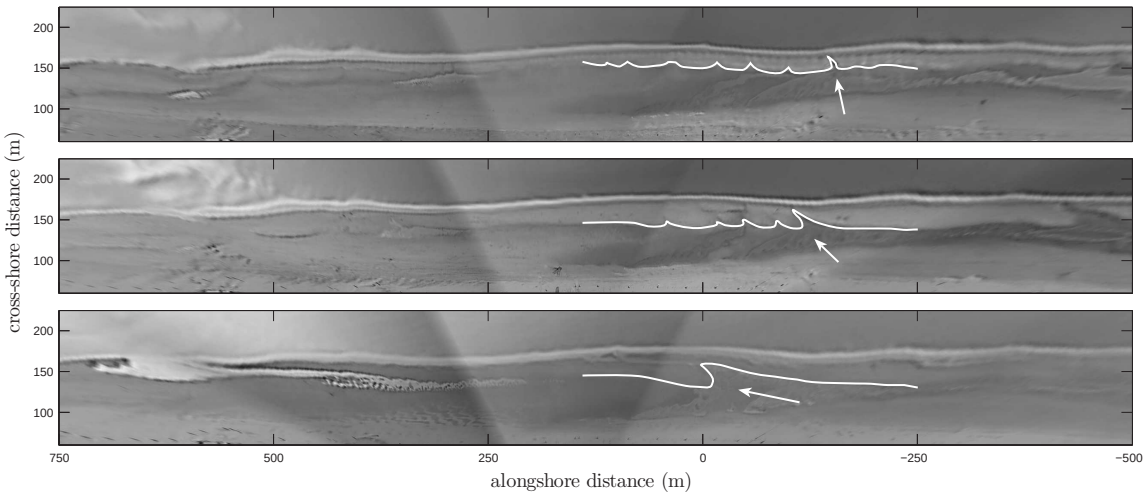

Figure 3.8 Argus image series showing the morphology configuration changes from linear to oblique between 2-4 May 2002 (from top to bottom). The white dashed-dotted line mark the landward boundary of the bar and the white arrows show the orientation of the rips, which determine the morphology configuration.

standard deviations, which corresponded with the gradual landward migration and abrupt seaward migration of the sawtooth motion. The large values of the weekly migration rates in the landward direction (5.9 m/day for $\bar{X}_{lb}(t)$) remained smaller than in the seaward direction (6.6 m/day), while the large values of the daily migration rate in the seaward direction (62.0 m/day) clearly exceed the extreme daily migration rate in landward direction (48.3 m/day). The latter would indicate the importance of the daily timescale in the abrupt seaward shifts of $\bar{X}_{lt}(t)$ and $\bar{X}_{bt}(t)$. Finally the larger daily and weekly migration rates for $\bar{X}_{lb}(t)$ than for $\bar{X}_{lt}(t)$ once more emphasize the behaviour of $\bar{X}_{lb}(t)$ to be more dynamic than $\bar{X}_{lt}(t)$.

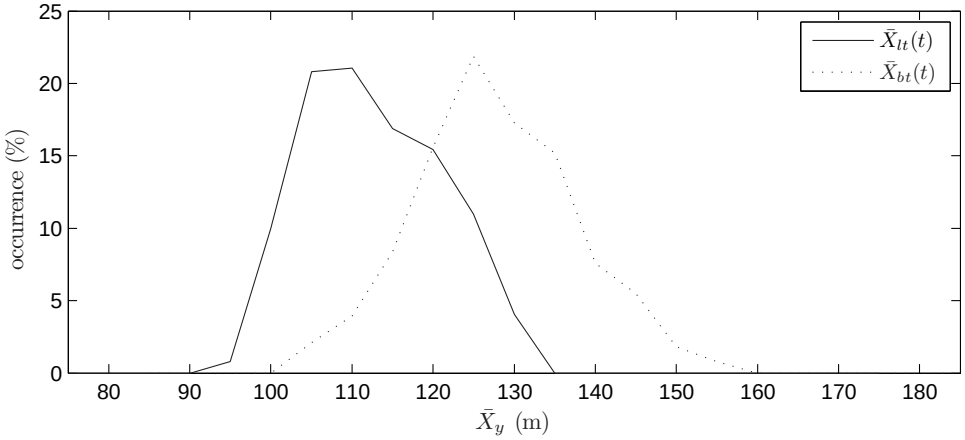

Figure 3.9 Frequency distribution of cross-shore positions, $\bar{X}_y$, of landward trough and bar boundaries.

Table 3.2 Cross-shore migration statistics of the landward boundary of trough and bar

		Landward migration (m/day)			Seaward migration (m/day)		
		seasonal	weekly	daily	seasonal	weekly	daily
Bar	mean	0.13	0.58	6.85	0.09	0.80	7.66
	st. dev.	0.08	0.48	6.84	0.05	0.83	8.98
	max.	0.42	6.60	48.34	0.19	5.90	62.00
Trough	mean	0.10	0.45	6.63	0.11	0.70	7.21
	st. dev.	0.09	0.51	5.91	0.09	0.75	7.04
	max.	0.38	7.09	32.26	0.35	6.45	39.71

3.4.2 Cross-shore sequences and the impact of storm events

The duration between successive resets exceeded the duration between individual storms, implying that not every storm resulted in a reset and thus that there were considerable differences between storm events, for instance in terms of duration or wave height average. Figure 3.10 shows the duration of the 51 storm events (Section 3.3.2) and their accompanying conditions as the computed mean and standard deviation of wave height, surge level, wave angle and wind speed. The variation in conditions during the storms was large, but the storms inducing the resets lasted in general the longest and typically had the largest average wave heights and surge levels. Most storms that caused a reset lasted for more than 2 or 3 successive tides (duration $>$ 30 hours) with largest average H_{rms0} ($\approx$ 2 m) and large η_{surge} ($\approx$ 0.5 m). The summer events 6 and 7 were exceptional in this sense, because H_{rms0} was clearly lower than those of the winter events. Figure 9 further suggests that θ_0 and wind speed did not discriminate the reset storm events from all storm event, because of the large variety in values.

An additional reason for a reset to take place during certain storms was found in the morphology. Five storms with a duration of 30 hours combined with large H_{rms0} and η_{surge}, were active within the measuring period, but did not enforce a reset. For only three storms, data on the morphology, i.e. $X_{lb}(y,t)$ and $X_{lt}(y,t)$, before and after the storm were available. These no-reset storm events (further referred to as events A, B and C) started on 31 October 2001, 8 February and 6 March 2002, and lasted for 33, 70 and 31 hours respectively. H_{rms0} was on average 2.08, 1.71 and 1.70 m combined with an average η_{surge} of 0.55, 0.37 and 0.58 m during events A, B and C respectively. The morphology before the reset and no-reset storm events was examined by use of $\bar{X}_{lb}(t)$ and $\bar{X}_{lt}(t)$ (Figure 3.11). Compared to the situation before reset storms, $\bar{X}_{lt}(t)$ before no-reset storm events occurred within a similar range of positions, but $\bar{X}_{lb}(t)$ previous to no-reset storm events seemed to appear more seaward. The latter became more apparent with the trough width, which was computed as the

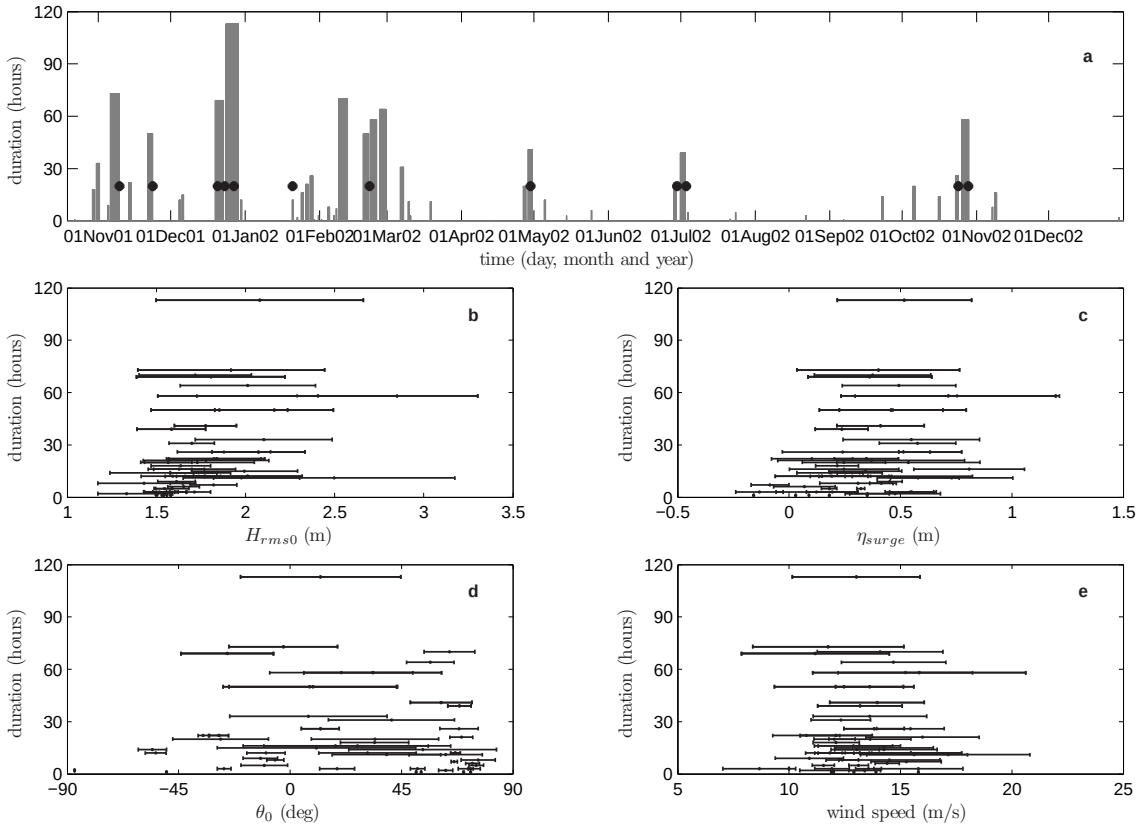

Figure 3.10 Characteristics of the 51 defined storms with in the upper panel a. time vs. duration of the storms as bars and the resets marked by $*$. The four lower panels (b-d) represent the duration on the vertical axis and in error bars on the horizontal axis the average value combined with standard deviation of hydrodynamic or meteorologic conditions during the storms. The storms inducing the morphologic resets are marked in black, while the others are in gray.

average of the difference between $X_{lb}(y,t)$ and $X_{lt}(y,t)$ (Figure 3.11). A trough width larger than 20 m occurred before no-reset storm events A-C, while the trough width was overall smaller than 20 m before reset storm events.

3.5 Discussion

The cross-shore sequential behaviour of a bar - trough system over a 15-month study period described a sawtooth motion of gradual landward and abrupt seaward migration with a period between 1 and 4 months (Figures 3.4, 3.5 and 3.6). The abrupt seaward migration coincided with the days when Argus images showed little or no bar - trough morphology, which were found by visual examination, and with the occurrence of storm events. After a reset storm beaches were rarely featureless for more than one day, while newly generated bars rapidly appeared near the low water line, confirming the typical quasi-persistent character of the slip-face ridges (e.g. Doeglas, 1955; Kroon, 1994; Masselink et al., 2006).

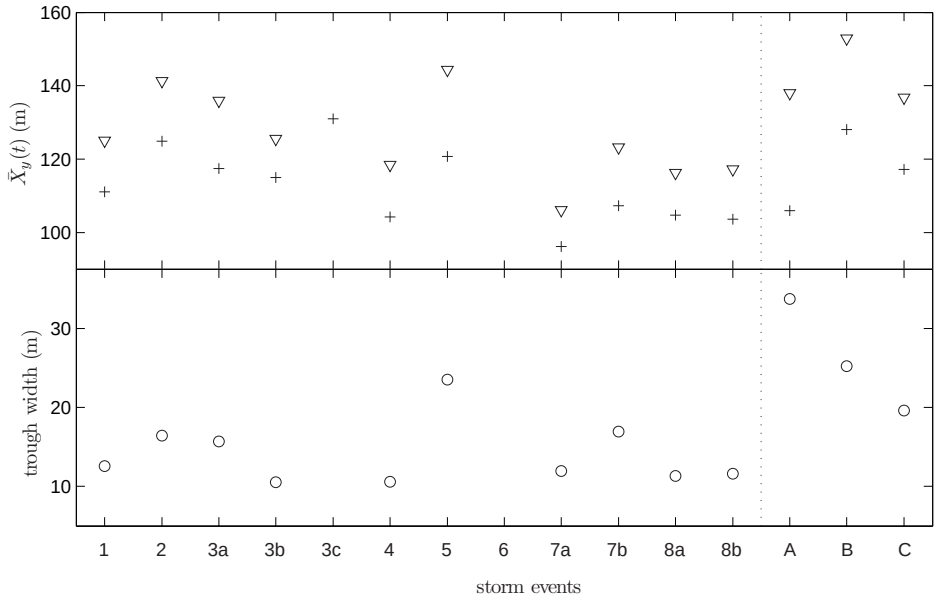

Figure 3.11 The upper panel represents the $\bar{X}_{lb}(t)$ ($\triangledown$) and $\bar{X}_{lt}(t)$ (+) before the reset storm events 1-8 and no-reset storm events A-C. The trough width ($\circ$) previous to these events was computed as the average of the distance between $X_{lb}(y,t)$ and $X_{lt}(y,t)$, and is presented in the lower panel.

Welding of the bar - trough system to the high water line during persistent low-energy wave conditions, as suggested in literature (e.g. Doeglas, 1955; Hayes & Boothroyd, 1969; Wijnberg & Kroon, 2002), was not found in the Argus images of this beach during the 15-month study period. The slip-face ridges were almost always submerged during high tide conditions, except for a few days with pronounced offshore winds causing a set-down of 0.5 m. Apparently, the position of the slip-face ridge was not close enough to the high water line, which is needed for a bar to weld at the high water line. The cross-shore position of the slip-face may be limited by the agger and the asymmetry present in the tidal signal. The agger initiates a long residence time for certain hydrodynamic processes to occur on the seaward flank of a *mature* slip-face ridge stimulating vertical bar growth (Figure 3.1), in which *mature* means that the slip-face ridge experienced some landward migration after its generation. The tidal asymmetry results in a relatively longer period of a tidal cycle for vertical bar growth processes than bar migration processes, especially during spring tide conditions (Figure 3.1). If the potential for vertical bar growth exceeds bar migration, the cross-shore bar position becomes more stable. The asymptotic trend shown by $\bar{X}_{lb}(t)$ in Figure 3.6 may confirm this hypothesis. Furthermore, the trough becomes deeper compared to the bar crest during vertical bar growth. This may, subsequently, mitigate cross-shore bar migration as described by Anthony et al. (2005), leading to a more stable position of the slip-face ridge.

The stable cross-shore position of these slip-face ridges differs though from the stable cross-shore position multiple bar system. The latter shows stability due to the short residence time of wave processes acting on the intertidal bars (see Kroon & Masselink, 2002; Anthony et al., 2005). But then again, the association of a long

residence time and little migration is in contrast to the long residence time of processes in non-tidal environments which leads to large cross-shore migration rates (Davis et al., 1972).

Storm conditions inducing the morphologic reset occurred over the whole 15-month period and were not restricted to certain seasons, although the winter season experienced more resets than the summer period. The reset storm conditions may be distinguished from other events based on a combination between storm duration (> 30 hours), large H_{rms0} (≥ 2 m) and large positive values of η_{surge} (≥ 0.5 m), but with these characteristics also no-reset storm events were found. Our analysis indicated that the trough width was larger (smaller) than 20 m before a no-reset (reset) storm event. Reset storm event 5 was exceptional with a trough width of 23.5 m, but Figures 3.4 and 3.5 already showed that only a reset of $X_{lb}(y,t)$ took place. Therefore, the trough width of the morphology previous to the storm event seemed to be an additional factor in inducing a reset.

The reason for the trough width being an additional factor can be explained by assuming a positive relation between the width and the depth of a trough. The mean flow may be undertow dominated during high-energy conditions when the trough is narrow and shallow, leading to beach erosion (Aagaard et al., 2006) and a reset. In contrast, horizontal cell circulation may be more pronounced during high-energy conditions in a morphology with a wide and deep trough; as the mean flow over the bar is now landward, and no reset is induced.

The importance of dimensions (i.e. width, depth) of the intertidal bar - trough system is shown by multiple bar systems. On beaches with multiple bar systems, storm conditions do not result in a reset, but in flattening and seaward migration of the bar - trough systems (e.g. Mulrennan, 1992; Masselink et al., 2006). Such bar - trough systems are hard to erode entirely, because the intertidal bars contain large amounts of sand (Anthony et al., 2005).

While behaviour of the intertidal bar - trough system is usually described by the behaviour of the bar only, this study showed that bar and accompanying trough may behave differently. The landward boundary of the bar, $\bar{X}_{lb}(t)$, appeared to be more dynamic than the landward boundary of the trough, $\bar{X}_{lt}(t)$, as indicated by the larger migration rates and standard deviations of the former (Table 3.2). $\bar{X}_{lb}(t)$ migrated landward and seaward resulting in an approximate normal distribution of $\bar{X}_{lb}(t)$, while the trough's net migration was directed landward resulting in a skewed distribution of $\bar{X}_{lt}(t)$ (Figure 3.9). Therefore, one needs to deal with the bar and trough dynamics separately when the behaviour of intertidal bar - trough systems is studied.

3.6 Conclusions

Over the 15-month study period, the cross-shore sequential behaviour of the intertidal bar - trough system of the microtidal, sandy beach of Noordwijk, the Netherlands, described a sawtooth motion of gradual landward and abrupt seaward migration with

a period between 1 and 4 months. The abrupt seaward shifts took place when the storm duration was longer than 30 hours, the average root-mean-square wave heights and surge levels were larger than 2 m and 0.5 m, respectively, and the trough of the pre-storm morphology was less than < 20 m in width. The largest variability of the alongshore-averaged cross-shore position of the landward boundary of the bar and trough occurred on daily and weekly scale, while seasonal variability was little. The bar and trough boundary behaved differently: the landward boundary of the bar showed more dynamic behaviour than the landward boundary of the trough.

4 Alongshore behaviour of intertidal rip channels

Quartel, S. (in prep) Temporal and spatial behaviour of rip channels in a multiple-barred coastal system.

Abstract

Alongshore bar systems are frequently intercepted by local depressions (i.e. rip channels) through which water is transported seawards. A 15-month data set of daily time-averaged video images (Argus) has been analyzed to describe the spatial and temporal variability of the rip channels on a multiple barred coast at Noordwijk aan Zee, The Netherlands. Intertidal and subtidal bar lines were derived from the Argus images in which local maxima represent the cross-shore and alongshore location of the rip channels. The average intertidal rip spacing ($\bar{\lambda}$) was 243 m, but the rips were not spaced regularly ($\sigma_\lambda/\bar{\lambda} = 0.47$). Some intertidal rips were observed to fill up during falling tide, but the majority remained open. The filled intertidal rip channels had more landward positions and migrated slower (2.4 vs 4.6 m/day) in the alongshore direction than the open intertidal rip channels. The amount and the alongshore migration rate of open intertidal rip channels increased with the preceding wave heights ($r = 0.26$, $p < 0.01$) and alongshore component of the offshore wave power ($r = 0.25$, $p < 0.01$), respectively. The intertidal bar lines were always coupled to the subtidal barlines, suggesting that intertidal morphology is also forced by subtidal alongshore variability. The phase of two bar lines could vary from in-phase (0°) to out-of-phase (180°). The gradual phase changes due to different alongshore migration rates of the intertidal and subtidal bar lines.

4.1 Introduction

Rip channels are ubiquitous features along barred, sandy coasts and appear as cross-shore depressions in a shore-parallel bar or in between shore-connected transverse bars. The strong (up to 1-2 m/s) offshore-directed subtidal rip currents may endanger the beach and swimming safety (see MacMahan et al., 2006) and therefore receive considerable attention in coastal management issues (e.g. Short & Hogan, 1994; Jiménez et al., 2007). Rip currents are part of horizontal cell circulation patterns, in which they compensate for the onshore mass flux of breaking waves across a sand bar. While

rip channels are present in both the subtidal (e.g. Bowen & Inman, 1969; Van Enckevort & Ruessink, 2003b; Holman et al., 2006) and intertidal (e.g. Kroon & De Boer, 2001; Lafon et al., 2005; Van Houwelingen et al., 2006) zone, the temporal evolution (from generation to decay) of the intertidal rip channels has received little attention, especially in microtidal settings.

Rip channels prevail as a quasi-rhythmic pattern with characterizing spacings in the alongshore direction of which the origin is under debate. Now that the initial hypothesis of the forcing of rip channels by alongshore standing edge waves (Bowen & Inman, 1969) has proven to be generally incorrect (e.g. Holman et al., 2006; Turner et al., 2007), attention has shifted to self organization. Rip channels emerge as a response to random perturbations in the initial sea bed bathymetry due to the self-organizing nature of the coastal system (e.g. Deigaard et al., 1999). Self organization models suggest the alongshore rip spacing increases with an increase in (time-independent) wave height (e.g. Deigaard et al., 1999; Reniers et al., 2004). In the field, this relationship has not been convincingly demonstrated (Short, 1985; Huntley & Short, 1992; Lafon et al., 2005; Turner et al., 2007). It might be that rip spacing is more sensitive to the bathymetry preceding the pattern development than to the variability in the wave forcing (Calvete et al., 2007). Wave conditions have proven their forcing due to the correspondence in the direction of wave propagation and rip migration leading to a relation between the migration rates and the alongshore component of the wave energy flux (Ruessink et al., 2000; Van Enckevort & Ruessink, 2003b; Holman et al., 2006). Other theoretical studies based on self-organization of the rip channels have hypothesized rip spacing also to depend on morphologic variables, such as the distance between the shoreline and the bar crest (Deigaard et al., 1999), the cross-sectional area of the trough (Deigaard et al., 1999), or the elevation of the bar (Calvete et al., 2007). However, field observations frequently do not support the relations between these morphologic parameters and the development of the rip channels (Ranasinghe et al., 1999; Holman et al., 2006).

The coupling with the offshore-located alongshore-variable morphology, such as rip channels and crescentic patterns in an outer bar, is a third theory on the generation of rip channels in an inner bar. The outer rip channels allow higher waves to reach the inner bar than shoreward of the outer-bar shoals. The wave height variability on the inner bar generates set-up gradients resulting in a cell circulation pattern and the generation of rip channels in the inner bar. Under shore-normal waves, the inner-bar rip channels will develop shoreward of the outer-bar shoals; the rhythmic patterns of the inner and outer bar system are thus out-of-phase (180°; Haas et al., 2003). Sonu (1973) indeed found this out-of-phase relation between the two rhythmic patterns, but several studies also found that the two patterns had no out-of-phase relation or even were non-coupled (Greenwood & Davidson-Arnott, 1975; Van Enckevort & Ruessink, 2003b; Lafon et al., 2005). The lack of coupling may imply the dominance of self-organization processes within the bar systems over coupling processes between the bar systems. Moreover, Ruessink et al. (2007) showed an inner and outer bar system to change from an initially uncoupled to a coupled system in response to the onshore propagating, increasingly non-uniform outer bar. Besides, the out-of-phase relation suggests the spacings of the rip channels to be identical for both systems, whereas

field studies frequently showed the rip channel spacing of the inner bar system to be smaller than the rip channel spacing of the outer bar system (e.g. Hom-ma & Sonu, 1962; Sonu, 1973; Greenwood & Davidson-Arnott, 1975). Castelle & Bonneton (2004) demonstrated in a numerical study the rip channel spacings of an inner bar system to be half the rip channel spacings of the outer bar system. Here, waves diverging shoreward of the outer-bar shoal and waves converging shoreward of the outer-bar rip channel induce circulation cells at the inner bar system with half the spacing of the circulation cell of the outer bar system. Overall, the studied coupling of two rhythmic patterns refers usually to two subtidal bar systems or to a subtidal bar system and the shoreline, and much less to a subtidal and a intertidal bar system.

The aim of this chapter is to investigate the spatial and temporal dynamics of intertidal rip channels and their relation with offshore wave characteristics and with subtidal rip channel characteristicss on a microtidal, storm-dominated beach. Daily positions of intertidal and subtidal rip channels over a period of 15 months were derived from Argus video observations of a microtidal beach at Noordwijk aan Zee, the Netherlands (Sections 4.2 and 4.3). The spatial and temporal variability of the rip channel amount, spacing and migration rates demonstrated the daily behaviour of the intertidal rip channels and revealed a coupling with hydrodynamic parameters as well as subtidal rip channel characteristics (Section 4.4). Coupling of the intertidal and subtidal alongshore bar rhythmicities confirmed the influence of the subtidal morphology on the intertidal bar system (Section 4.5).

4.2 Study site

Noordwijk aan Zee, located on the central Dutch coast (Figure 1.2), is a sandy, wave dominated coast characterized by a single intertidal bar and two subtidal bars (Figure 4.1; e.g. Van Enckevort & Ruessink, 2003b). During low-energy wave conditions, a second intertidal bar may form on a pre-existing bar (Quartel et al., 2007). The intertidal beach has an average width of 100 m and a slope of approximately 1:50. The cross-shore behaviour of the intertidal bar describes a sawtooth motion comprising gradual landward migration followed by abrupt seaward shifts, with a 1-4 month period between consecutive shifts. The abrupt seaward shift can be considered as a morphological reset as a pre-existing bar is erased and a new one forms near the low-water line, for further details see Quartel et al. (2007). The subtidal bars show a net offshore migration with a cyclicity of about 4 years (Wijnberg & Terwindt, 1995), although since 1998 this migration has been strongly decelerated by a shoreface nourishment (Quartel & Grasmeijer, 2006; Ojeda et al., in prep).

The beach and nearshore zone of Noordwijk has been monitored since 1995 by an Argus video system (see Holman & Stanley, 2007). The system is mounted on the top of a hotel at a height of 62 m above mean sea level, and consists of 5 cameras that together view the coastal zone over 6 km in the alongshore direction, and 1.5 km in the cross-shore direction. Every day-light hour, the cameras collect ten-minute time-exposure (timex) images by averaging snapshots sampled at 2 Hz. The oblique

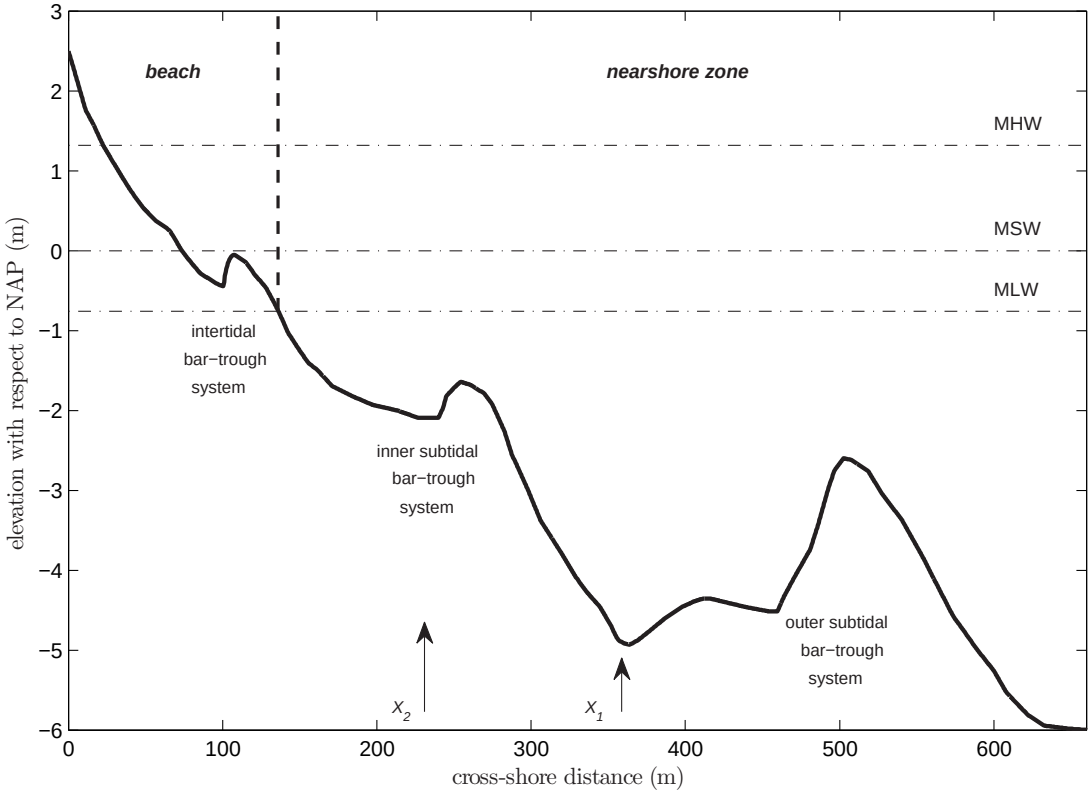

Figure 4.1 Cross-shore profile of Noordwijk showing the intertidal and two subtidal bar systems. The arrows X_1 and X_2 indicate the locations of the computed hydrodynamics which were used for coupling of the inner subtidal and intertidal, respectively, rip channel characteristics.

images taken daily at low tide for the period 19 October 2001 to 31 December 2002 were selected for the present study. Gaps due to technical malfunctioning of the Argus system exist for 5-7 January, 14-21 April, 25-28 April and 19-26 July 2002.

The collected low-tide oblique timex Argus images were geometrically transformed to obtain a rectified plane view of the nearshore zone (Lippmann & Holman, 1990; Holland et al., 1997). This process has a typical error of one pixel with the pixel footprint increasing at larger distances from the camera. Therefore, the pixel size for the intertidal zone was set on 0.5×0.5 m and the pixel size for the subtidal zone on 2.5×2.5 m. The rectified images were then merged to create a plan view (e.g. Figure 4.2a). The region of interest regarding the intertidal zone on a merged image covered 1250 m in the alongshore direction centered around the cameras and 165 m in the cross-shore direction (Figure 4.2b). The subtidal zone with the inner subtidal bar was studied for the same 1250 m in the alongshore direction, but the region of interest extended 200 m in the cross-shore direction. In both images, positive x is in the offshore direction and positive y is in the southward direction.

Offshore wave and water level data were collected at Meetpost Noordwijk (MPN in Figure 1.2), which is positioned about 9.5 km offshore at 18-m water depth. Missing

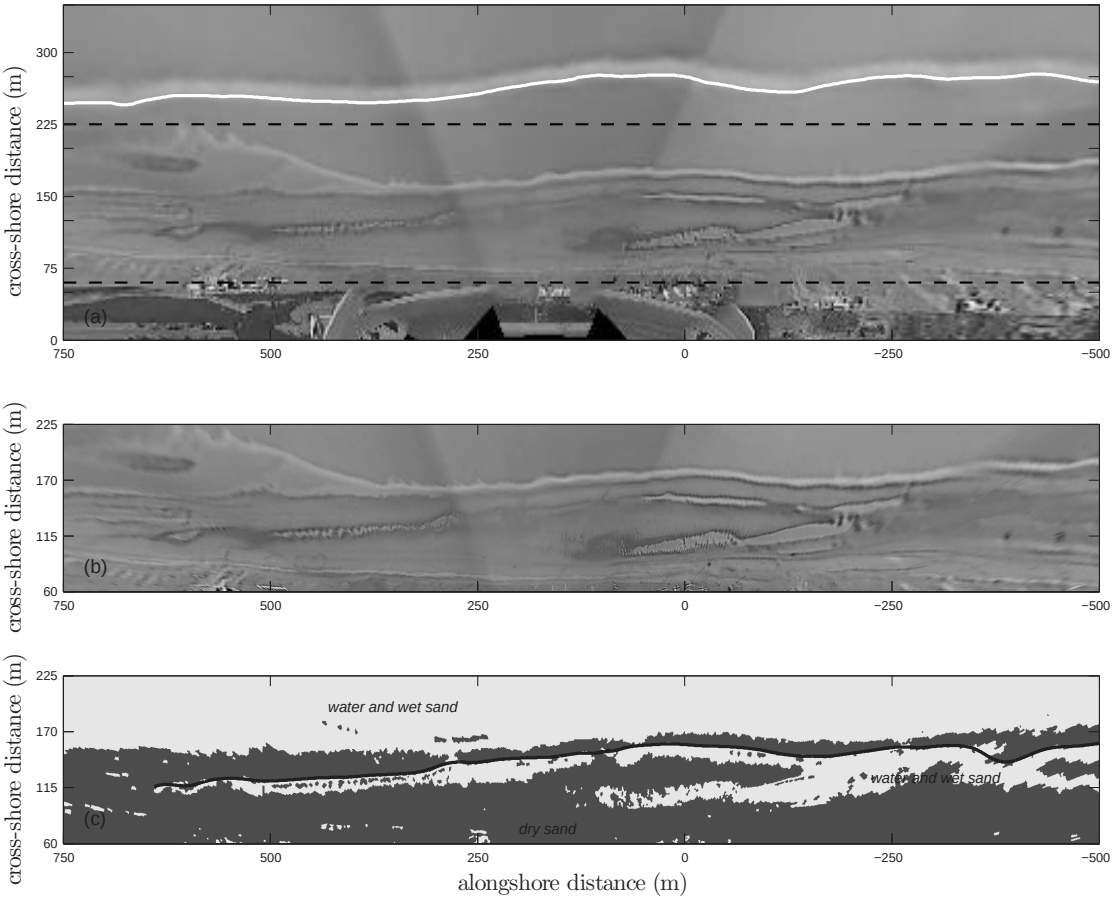

Figure 4.2 Rectified and merged Argus image taken around low tide on 27 May 2002 (a) showing the dunes, the beach (region of interest of intertidal zone marked by dashed line) and a part of the subtidal zone with the inner bar line (white solid line). The region of interest regarding the intertidal zone was produced with a higher resolution (b) and consequently classified based on the surface composition (c) with the intertidal bar line (black solid line).

wave data (10% in time) were replaced by wave data from the Ymuiden buoy (YM6 in Figure 1.2). Figure 4.3a presents the root-mean-square wave height (H_{rms0}) during the study period. The storm events that lead to morphologic resets on the intertidal beach have a H_{rms0} in excess of 2 m over a period of at least 30 hours, and a offshore surge level larger than 0.5 m (Quartel et al., 2007). These storm events in the study period are indicated in Figure 4.3a.

4.3 Methods

4.3.1 Bar lines

Two different methods were used to obtain the cross-shore position of the intertidal and inner subtidal bar from the Argus images. The intertidal bars are visible on

low-tide plan-view images as dry sand patches encircled by wet sand or water (Figure 4.2b). An object-oriented algorithm was used to classify the surface composition of the beach area in the Argus images into the classes water, wet sand or dry sand (Quartel et al., 2006). Subsequently, the classes water and wet sand were combined, because the bars are distinguished from its surroundings by dry sand versus the other two classes (Figure 4.2c). The landward part of the contour of the dry sand patch is defined as the landward boundary of the intertidal bar. The resulting boundary data are alongshore bar lines describing the cross-shore position of the detected landward boundary of the intertidal bar (Figure 4.2c). A quadratic loess filter (Plant et al., 2002) was applied to the alongshore data to remove irregularities in the boundaries with length scales < 50 m, which may have originated from misclassification of the three classes. For a more detailed description of the intertidal bar line detection method, see Quartel et al. (2007).

Subtidal bars are visible on Argus images as an alongshore high-intensity band owing to wave breaking (Figure 4.2a; Lippmann & Holman, 1990; Van Enckevort & Ruessink, 2001). An alongshore series of intensity maxima (Figure 4.2a) is referred to as a subtidal bar line in the following. The obtained cross-shore position of the subtidal bar line was corrected for the differences in water level elevation of each

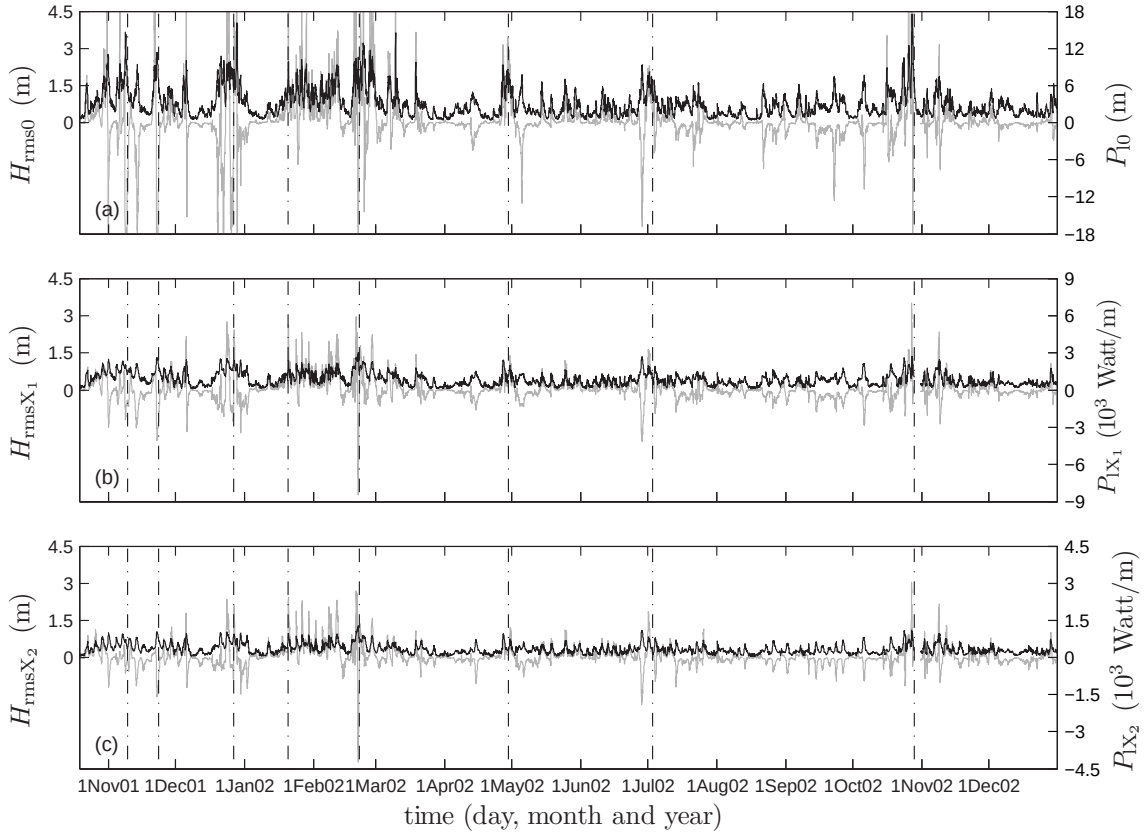

Figure 4.3 Time series of the hydrodynamic parameters H_{rms} (black) and P_{l} (grey) at the offshore location MPN (a), location X_1 (b) and location X_2 (c). Storm events which induced a morphologic reset on the intertidal beach are marked by vertical dash-dot bars. Note the different vertical scales of the P_{l}.

Argus image, which otherwise would lead to extra temporal variability of the cross-shore position (Van Enckevort & Ruessink, 2001).

4.3.2 Rip channel characteristics

Alongshore patterns of the bar lines include seaward perturbations, whose maxima represent the position of a rip channel. In the remainder of this chapter, a rip channel in the intertidal zone is referred to as an IRC and a rip channel in the subtidal zone as a SRC. All maxima were checked visually, and those that did not correspond to rip channels were culled from the data set. Misclassification of the intertidal beach may have resulted in the absence of certain maxima in the bar line meaning that some rip channels were missed with this detection technique. The detected rip channels were followed in successive images by visual inspection. When rip channels could be followed in time, the alongshore positions Y of the rip channels were smoothed (Y_{i}) to remove noise resulting from the detection method. An adaptive window was needed to apply a quadratic loess filter because of the irregular time interval between the rip channels positions. The size of the applied adaptive window contained 10% of the data points to obtain a 10% smoothing level.

The IRCs were subsequently classified as either a filled or open rip channel (fIRC or oIRC, respectively). An oIRC has a landward located funnel with a clearly visible seaward channel connecting the trough with the sea (Figure 4.4), which implies that this rip still drains the beach during low tide. A fIRC only consists of a funnel; its channel is filled with sediment (Figure 4.4).

The alongshore positions of the IRCs and SRCs are presented in Figures 4.5a and 4.6a, respectively, as a function of time. The amount of rip channels were summed in bins with an alongshore width of 50 m leading to the spatial variability of the rip channel occurrence N (Figures 4.5b and 4.6b), and on a certain moment leading to the temporal variability (Figures 4.5d and 4.6d). The rip spacing was computed as the alongshore distance between two adjacent rip channels, making no distinction between the IRC type. The changes in time of the smoothed alongshore positions

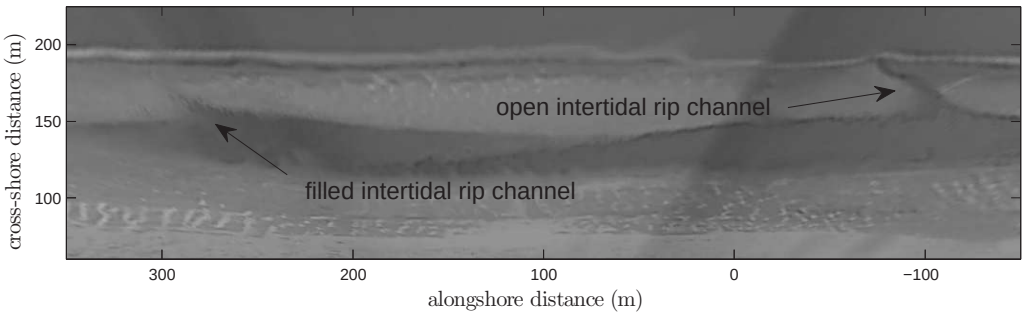

Figure 4.4 Blow up of an Argus image with examples of a filled intertidal rip channel (left; fIRC) and an open intertidal rip channel (right; oIRC).

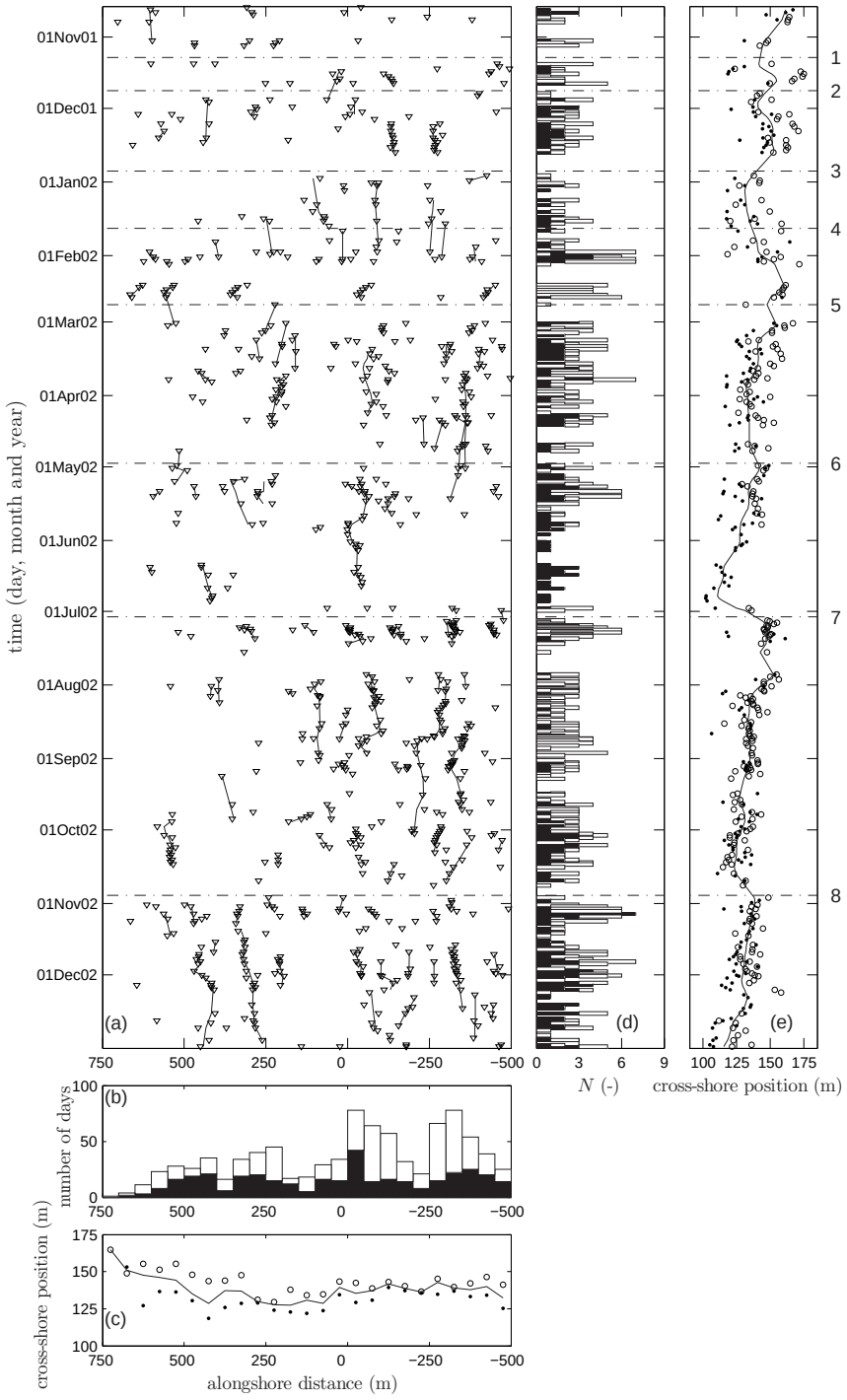

Figure 4.5 Time series of IRCs (▽) from 19 October 2001 to 31 December 2002 with the alongshore position versus time (a) including their smoothed position (solid line). Spatial variability of the number of days rip channels appeared (b) and the time-averaged cross-shore position (c), and temporal variability of the number of rips N (d) and alongshore-averaged cross-shore position (solid line shows the filtered data with a window of 14 days; e). Except for a, the distinction of IRC type was made: fIRCs reflected by black-filled bars or dots, and oIRCs by unfilled, white bars or dots. The extreme storm events are numbered and marked by horizontal dash-dot bars.

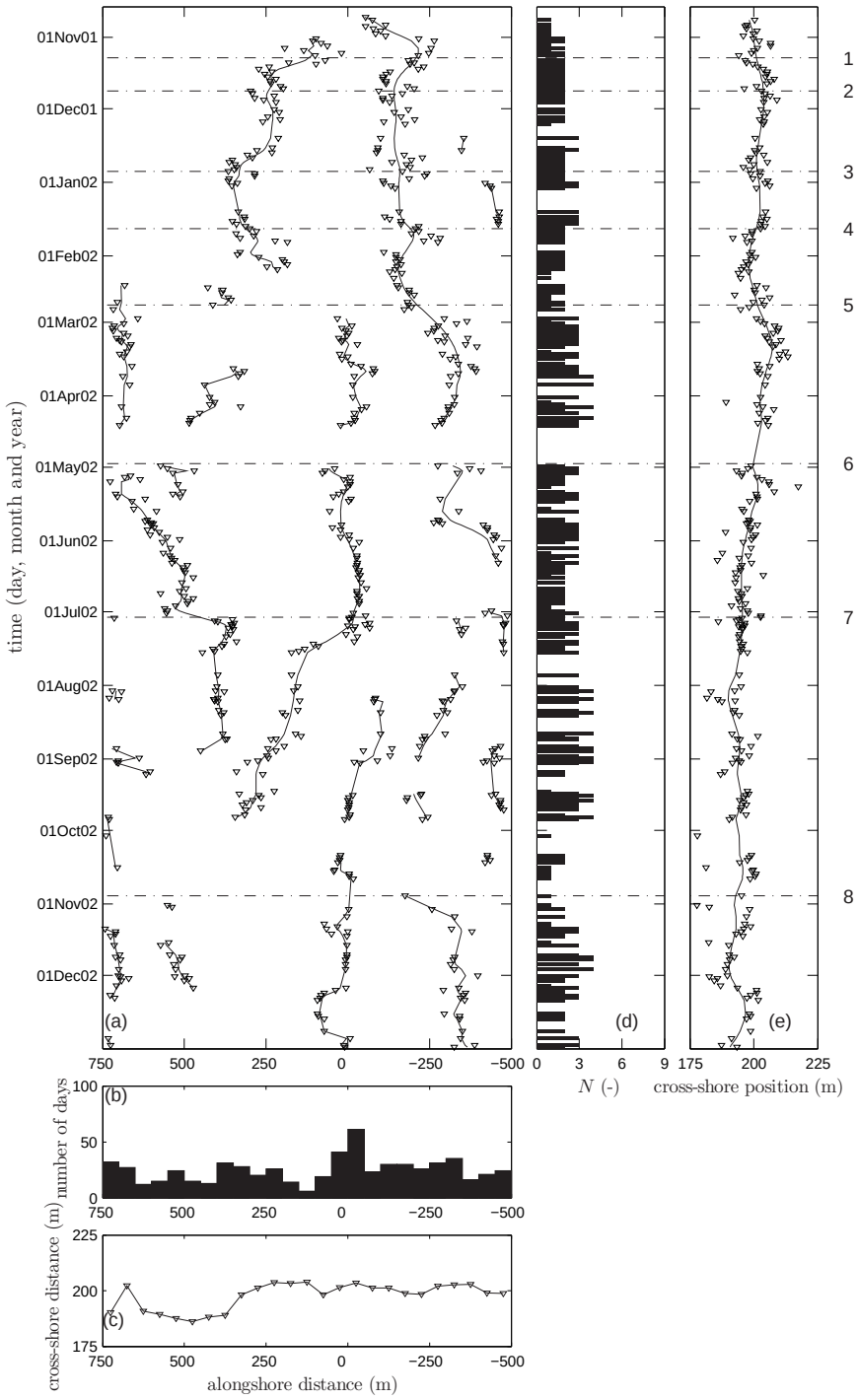

Figure 4.6 Time series of SRCs (▼) from 19 October 2001 to 31 December 2002 with the alongshore position versus time (a) including their smoothed position (solid line). Spatial variability of the number of days rip channels appeared (b) and the time-averaged cross-shore position (c), and temporal variability of the number of rips N (d) and alongshore-averaged cross-shore position (solid line shows the filtered data with a window of 14 days; e). The extreme storm events are numbered and marked by horizontal dash-dot bars.

Y_i were converted into alongshore migration rates $c_{\mathrm{Y_i}}(t)$ by dividing the difference in smoothed alongshore location (ΔY_i) located in two subsequent images with the time difference of those two subsequent images (Δt). The alongshore and temporal variability of the cross-shore positions of the IRCs and SRCs positions is displayed in Figures 4.5c and e and Figures 4.6c and e, respectively.

4.3.3 Hydrodynamic parameters

Temporal and spatial rip channel variability have often been found to be correlated with incoming wave energy and (proxies of) the alongshore current (e.g. Short, 1985; MacMahan et al., 2006). In this study, H_{rms0} was used to indicate the amount of incoming wave energy (see also Holman et al., 2006) and the alongshore component of the wave power P_{l0} as a proxy of the alongshore current (see also Ruessink et al., 2000; Van Enckevort & Ruessink, 2003b). The alongshore component of the wave power is computed as (Komar, 1998)

$$P_{\mathrm{l0}} = \frac{\rho g^2}{32\pi} H_{\mathrm{rms0}}^2 T_{\mathrm{p0}} \sin\theta_0 \cos\theta_0 \tag{4.1}$$

where $\rho = 1025\mathrm{kg/m^3}$ is the sea water density, $g = 9.81\mathrm{m/s^2}$ is the gravitational acceleration, T_{p0} is the offshore peak wave period, θ_0 is the energy-weighted wave direction from shore normal. The time series of P_{l0} is shown in Figure 4.3a.

The amount of wave energy affecting the inner bar system and consequently the intertidal bar system is smaller than the offshore wave energy due to energy dissipation by wave breaking. Therefore, the wave model of Battjes & Janssen (1978) was used to estimate the amount of wave energy at the locations with the largest water depths just seaward of the inner subidal and intertidal bar systems (X_1 and X_2, respectively; Figure 4.1). The computed $H_{\mathrm{rmsX_1}}$ ($H_{\mathrm{rmsX_2}}$) and $P_{\mathrm{lX_1}}$ ($P_{\mathrm{lX_2}}$) are presented in Figure 4.3b (c).

In earlier work (e.g. Short & Brander, 1999; Holman et al., 2006), the hydrodynamic parameter was averaged over one antecedent day to investigate its effect on rip channel characteristics. However, Wright et al. (1985) suggested that the beach changes may be related to wave conditions averaged over a few preceding days, but the amount of antecedent days was variable. Therefore, H_{rms} and P_{l} are expressed here as an average of the preceding hourly H_{rms} and P_{l} over a variable amount of D days by $\bar{H}_{\mathrm{rms}} = \frac{\sum_{i=0}^{D} H_{\mathrm{rms}}(t)}{D}$ and $\bar{P}_{\mathrm{l}} = \frac{\sum_{i=0}^{D} P_{\mathrm{l}}(t)}{D}$, where $i = 0$ is the moment of the low tide image. The largest correlation r between the rip channel characteristic and $\bar{H}_{\mathrm{rms}}$ or $\bar{P}_{\mathrm{l}}$ from $D >= 1$ was selected and the accompanying D was noted. For the correlation of $\bar{H}_{\mathrm{rms}}$ and $\bar{P}_{\mathrm{l}}$ with $c_{\mathrm{Y_i}}$, the hydrodynamic parameters were averaged over $D = \Delta t$.

4.4 Spatial and temporal rip channel variability

4.4.1 Rip number

A total of 875 IRCs were found on 320 different low-tide images of the 438-day measuring period. Of all detected IRCs, 58% were identified as oIRCs and 42% as fIRCs. In total, the alongshore occurrence of IRCs was alongshore non-uniform with two peaks around $y = -50$ m and $y = -300$ m, whereas only a few IRCs were found at $y > 500$m (Figure 4.5b). The standard deviation of the rip channel occurrence σ_N per 50-m bin was computed and normalized by the mean rip channel occurrence $\bar{N}$ of that bin resulting in a coefficient of variability CV of the alongshore location. The oIRCs showed more variability in their alongshore locations, Y, than the fIRCs ($CV_{Y,fIRC} = 0.76$ and $CV_{Y,oIRC} = 0.59$).

Almost 20% of the IRCs (188) were detected on one image only. These one-image IRCs could either indeed have a one-day lifetime or they may posses a longer lifetime that was not detected in the successive images possibly owing to the inaccuracy of the detection method. More one-day IRCs were classified as fIRCs (59%) than oIRCs (41%) suggesting the appearance of fIRCs was less persistent in time. The remaining 693 IRCs were followed in time and had an average lifetime of 10 days. Most of these IRCs remained the same type (79%) during their lifetime, but some IRCs changed from fIRC to oIRC and visa versa (21%). The transition from oIRC to fIRC happened a little more frequently (58%) than the other way around. After an IRC disappeared, the following IRC often appeared around the same alongshore position, which led to the double peaks in the spatial alongshore distribution of the rip channels (see Figure 4.5b).

Immediately after a storm which induced a morphologic reset, there were no rip channels due to the absence of the intertidal bar system. Subsequently, a maximum amount of IRCs (6 or 7) were present within ten days after a morphologic reset of the beach (e.g. event 7; Figure 4.5d). Indeed, the amount of oIRCs increased with $\bar{H}_{rmsX_2}$ and this relation was strongest averaging with $D = 15$ days ($r = 0.26$), but this r value was already nearly reached for $D = 10$ days (Table 4.1). Persistence of certain conditions or extreme wave conditions will lead to differentiation of $\bar{H}_{rmsX_2}$ over a period as long as $D = 10$ days, meaning that the amount of oIRCs was quite constant. On the contrary, the amount of fIRCs decreased with an increasing $\bar{H}_{rmsX_2}$ and this relation was strongest for the hydrodynamic conditions averaged over one antecedent day ($r = -0.13$, $D = 1$ day). This implies short-term and immediate variability of the fIRCs to the wave conditions.

In the inner subtidal bar, 649 SRCs were found in 285 images. The SRCs were more alongshore uniformly spaced than both types of IRCs ($CV_{Y,SRC} = 0.45$). Most SRCs were positioned in the $y = -50 - 0$ m bin, which is the same beach bin in which the amount of IRCs peaked as well. The average SRC lifetime was 39 days about 3 times as long as the IRC lifetime. When we compare Figure 4.5a with Figure 4.6a, we can see that the SRCs reveal a more temporal consistent pattern than the IRCs

Table 4.1 Correlation coefficient r between rip channel characteristics (rip number, spacing and alongshore migration rate c_{Y_i}) and time-averaged hydrodynamic conditions ($\bar{H}_{rms}$, $\bar{P}_l$).

		$\bar{H}_{rms0,t}$ (m)		$\bar{P}_{lo,t}$ (Watt/m)		SRC
		D	r	D	r	r
number (-)	fIRC	1	−0.13	16	−0.07	−0.12
	oIRC	15	0.26	15	0.34	−0.13
	SRC	4	−0.27	9	−0.26	
spacing (m)	IRC	4	0.10	15	0.10	0.10
	SRC	4	0.16	4	0.29	
c_{Y_i} (m/s)	fIRC		0.07		−0.05	−0.16
	oIRC		0.08		0.25	0.11
	SRC		−0.01		0.30	

implying the SRCs to be more temporally persistent than the IRCs. Furthermore, the temporal variability of the SRC suggests that the SRCs can split up ($y \approx -200$m, mid-February 2002) or merge ($y \approx 300$ m, start of September 2002) trough time (see also Van Enckevort et al., 2004). The SRCs did not change during the storm events that induced morphologic resets of the intertidal beach (Figure 4.6). The inverse relations from the SRC number with $\bar{H}_{rmsX_1}$ and $\bar{P}_{lX_1}$ showed that the SRCs merge during high-energy conditions and split during low-energy conditions (Table 4.1; Van Enckevort et al., 2004). When the amount of SRCs was small, the amount of fIRCs and oIRCs was large as indicated by the inverse relations between the IRCs and SRCs ($r = -0.12$ and $r = -0.13$, respectively, $p < 0.01$).

4.4.2 Rip channel spacing

Naturally, rip spacing λ is inversely related to the amount of rip channels. On the intertidal beach however, this relation between number of IRCs and spacing was noteworthy weak ($r = -0.19$). Besides, the time-averaged spacing with two or three IRCs was almost identical (approximately 250 m), which seemed to be the result of the non-uniform alongshore occurrence of the IRCs and, additionally, the absence of the IRCs along the southern part of the beach ($y > 500$ m; Figure 4.5b). Another consequence of this non-uniform alongshore occurrence was the time-averaged λ_{IRC} obtained from all images being approximately half of λ_{SRC} (243 and 446 m, respectively), although they were computed for the same alongshore stretch of coast. The SRCs were more regularly spaced over this alongshore coastal stretch than the IRCs with $CV_{\lambda,SRC} = 0.23$ vs. $CV_{\lambda,IRC} = 0.53$). Neither the $\bar{H}_{rmsX_1}$ nor $\bar{P}_{lX_1}$ were statistically significantly correlated to λ_{IRC} at $\alpha = 0.05$ (Table 4.1). $\bar{H}_{rmsX_1}$ and $\bar{P}_{lX_1}$ were both related to λ_{SRC} ($r = 0.16$ and $r = 0.29$, respectively) with their largest r at

$D = 4$ days for both parameters. The latter suggests that a period of higher waves needs to last at least 4 days to affect λ_{SRC}.

4.4.3 Alongshore migration

The temporal variability of the alongshore position of the rip channels (with a lifetime longer than one image) was converted into migration rates (Figure 4.7). On average, the oIRCs migrated faster than the fIRCs ($\bar{c}_{\mathrm{Y_i,oIRCs}} = 4.6$ m/day and $\bar{c}_{\mathrm{Y_i,fIRCs}} = 2.4$ m/day, respectively). This suggests fIRCs to have a more stable alongshore position than oIRCs. The peak migration rates were about 12 m/day for the fIRCs, a factor of 3 lower than the peak migration rates of the oIRCs (36 m/day). The alongshore mobility of the SRCs was comparable to that of the oIRCs. Due to the consistent pattern of the SRCs (Section 4.4.1; Figure 4.6), the temporal variability of $c_{\mathrm{Y_i,SRCs}}$ appeared less noisy than the temporal variability of $c_{\mathrm{Y_i,oIRCs}}$ (compare Figures 4.7a and b).

The individual migration rates, $c_{\mathrm{Y_i}}$, of the oIRCs and SRCs are statistically significantly coupled to $\bar{P}_{\mathrm{l}}$ (Table 4.1). Despite simultaneously occurring RCs sometimes migrated in opposite direction, the oIRCs and SRCs migrated generally in identical direction forced by the anticipated alongshore current (Figure 4.7). This was shown in a positive relation between $c_{\mathrm{Y_i,oIRC}}$ and $c_{\mathrm{Y_i,SRC}}$. However, albeit the absence of a

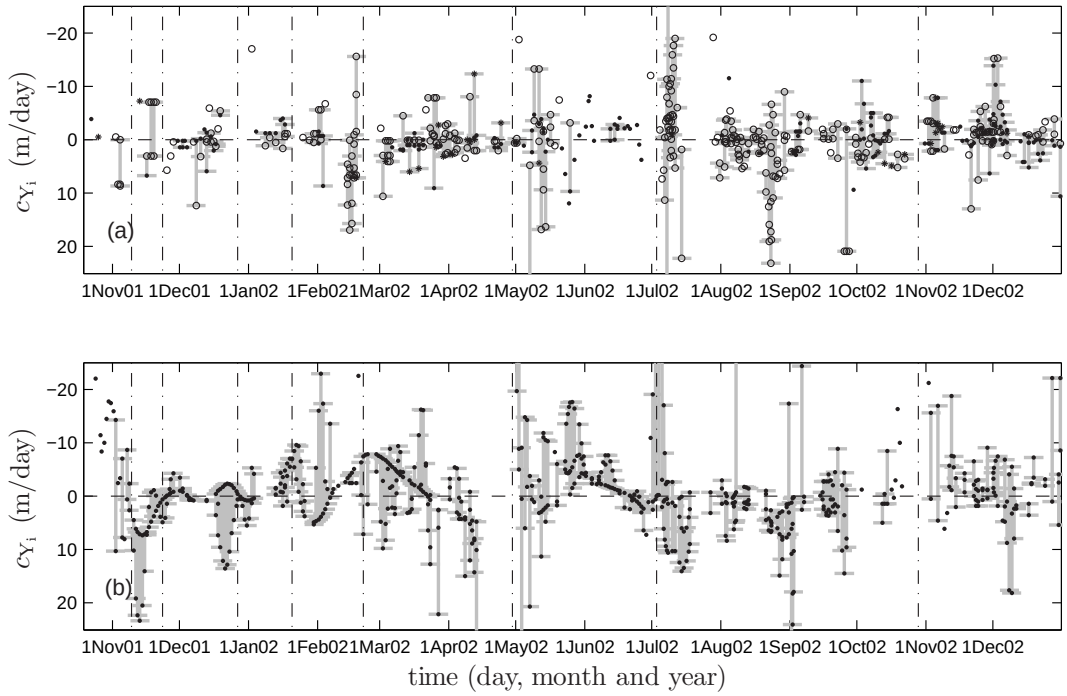

Figure 4.7 Migration rates of the rip channels in the intertidal zone (a) with fIRCs (•) and oIRCs (○) and in the subtidal zone (b; SRCs). The errorbars (in gray) show minimum and maximum value found on a day, when more then one migration rate was found, to indicate the variability in alongshore migration. Negative migration rates are directed to the north. The extreme storm events are marked by vertical dash-dot bars.

relation between $c_{\mathrm{Y_{i,fIRC}}}$ and $\bar{P}_{\mathrm{l}}$, $c_{\mathrm{Y_{i,fIRC}}}$ was inversely related to $c_{\mathrm{Y_{i,SRC}}}$ (Table 4.1). The inverse relation between $c_{\mathrm{Y_{i,fIRC}}}$ and $c_{\mathrm{Y_{i,SRC}}}$ suggests that fIRCs migrated in the opposite direction of the SRCs. Thus, the alongshore migrating of the SRCs influenced the alongshore migration of both types of IRCs.

4.4.4 Cross-shore behaviour

The cross-shore positions of the fIRCs were about 10 m more landward than those of the oIRCs (Figure 4.5c). The time- and alongshore-averaged cross-shore positions of the two types were significantly different at a 95% confidence level. The more landward position of fIRCs automatically involved higher beach elevations, which could explain the infilling of these rip channels. Less water needed to be drained at larger beach elevation and the decrease in drainage function of a IRC provided the possibility to fill up during falling tide by the net landward sediment transport of swash.

From February 2002 onwards, the temporal variability of the alongshore-averaged cross-shore position of the IRCs $\bar{X}_{\mathrm{Y,IRC}}$ revealed a sawtooth movement consisting of gradual landward migration and abrupt seaward migration (Figure 4.5e). This sawtooth motion was also observed for the cross-shore behaviour of the bar line itself (Quartel et al., 2007) implying that the bar line behaves as a whole in the cross-shore direction. The storm events led to the temporary disappearance of the bar, trough and associated rips after which they reappeared at comparable alongshore, but more seaward positions.

The SRCs also displayed a sawtooth motion comprising a gradual landward migration and an abrupt seaward migration (Figure 4.6e). The time-averaged SRC position was 198 m. In general, however, the SRCs were located more landward in the southern ($y > +350$m) part of the study area than in the northern part. Recall that the southern part of the beach was also characterized by less occurring IRCs and the frequent absence of the intertidal bar (Section 4.4.1). The landward located SRCs was associated with a more landward position of the subtidal bar line, which suggests that the more landward position of the subtidal bar line created different boundary conditions for the intertidal beach and hindered the development of an intertidal bar.

4.5 Nearshore morphologic template

The relations between characteristics of the IRCs and SRCs found in the previous section indicated the potential influence of the subtidal bar line and associated rip channels on the intertidal bar line and rip channels. Whether the alongshore (quasi-)rhythmic patterns of both bar lines were also related, was tested by a cross-correlation analysis implemented on the intertidal and subtidal bar lines. The largest r varied from 0.17 to 0.95 (all statistically significant at $\alpha = 0.01$; $\bar{r} = 0.58$ and $r_{\mathrm{std}} = 0.15$), which means that the rhythmicity of the two bar lines were always coupled.

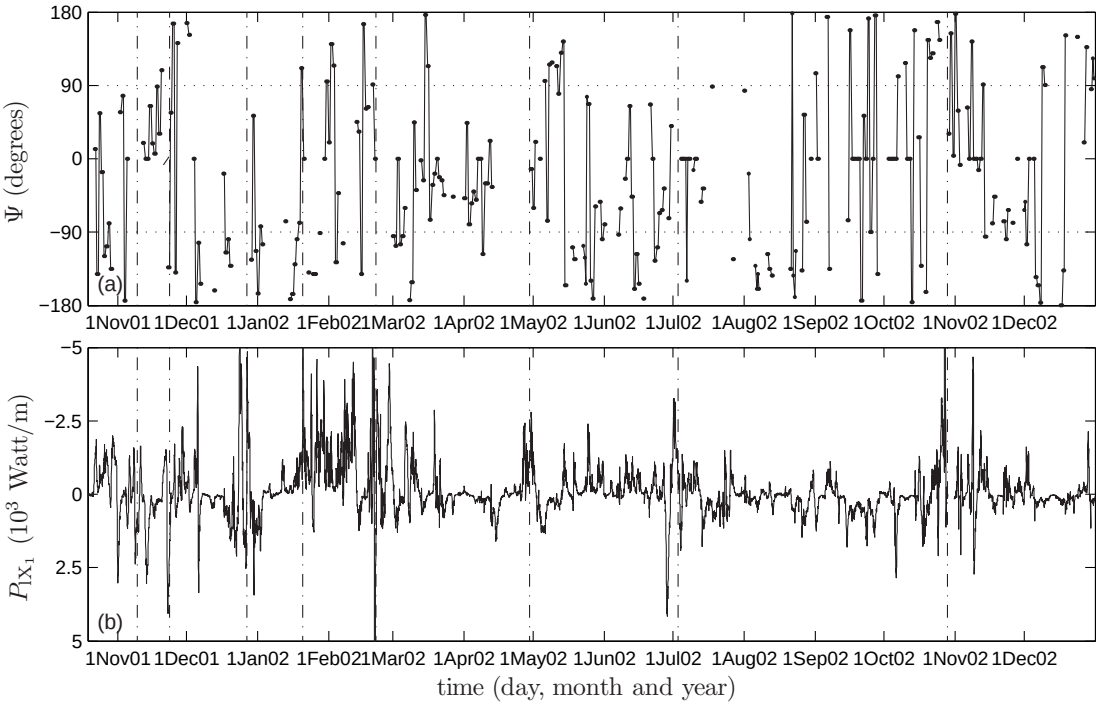

Figure 4.8 Time series of phase differences Ψ between the intertidal and subtidal bar lines (a) and of P_{lX_1} (b) in which positive values represent a southward directed alongshore current and negative values represent a northward directed alongshore current. The beach-reset storm events are marked by vertical dash-dot bars.

The ratio of the lag associated with the largest r to the average spacing of the SRC ($\lambda_{SRC} = 446$ m) was defined as the phase difference Ψ between the two bar lines and is presented in Figure 4.8a. When Ψ was between -90 ° and +90 °, the rhythmicities were in-phase with the ultimate in-phase situation for $\Psi = 0$ °. Then the IRCs were located exactly landward of the SRCs. The rhythmicities were defined as out-of-phase for $-180° < \Psi < -90°$ or $+90° < \Psi < +180°$ in which Ψ equalled -180 ° or +180 ° for an exact out-of-phase relation. Then the two rhythmicities appeared when the alongshore position of a IRC was in the middle of two SRCs. Furthermore, the subtidal rhythmic pattern was positioned south of the intertidal pattern when Ψ was negative, and visa versa. During the measuring period, the bar lines were just as much in phase as out of phase (48% and 52%). The rhythmic pattern of the subtidal bar line was positioned more frequently south of the intertidal bar line pattern whereas negative values of Ψ occurred more frequently (52%) than positive values (32%). The phases did not depend on the hydrodynamic parameters. Even storm events did not affect the phases, because generally the phase after the storm event was comparable to the phase before the storm event (Figure 4.8a). Evidently, coupling of the intertidal and subtidal rhythmicities maintained during variable wave conditions or the coupling was restored immediately after a storm event at similar phase.

The Ψ values repeatedly changed gradually in time including transitions from in-phase to out-of-phase (e.g. November 2001 and start of May 2002; Figure 4.8a).

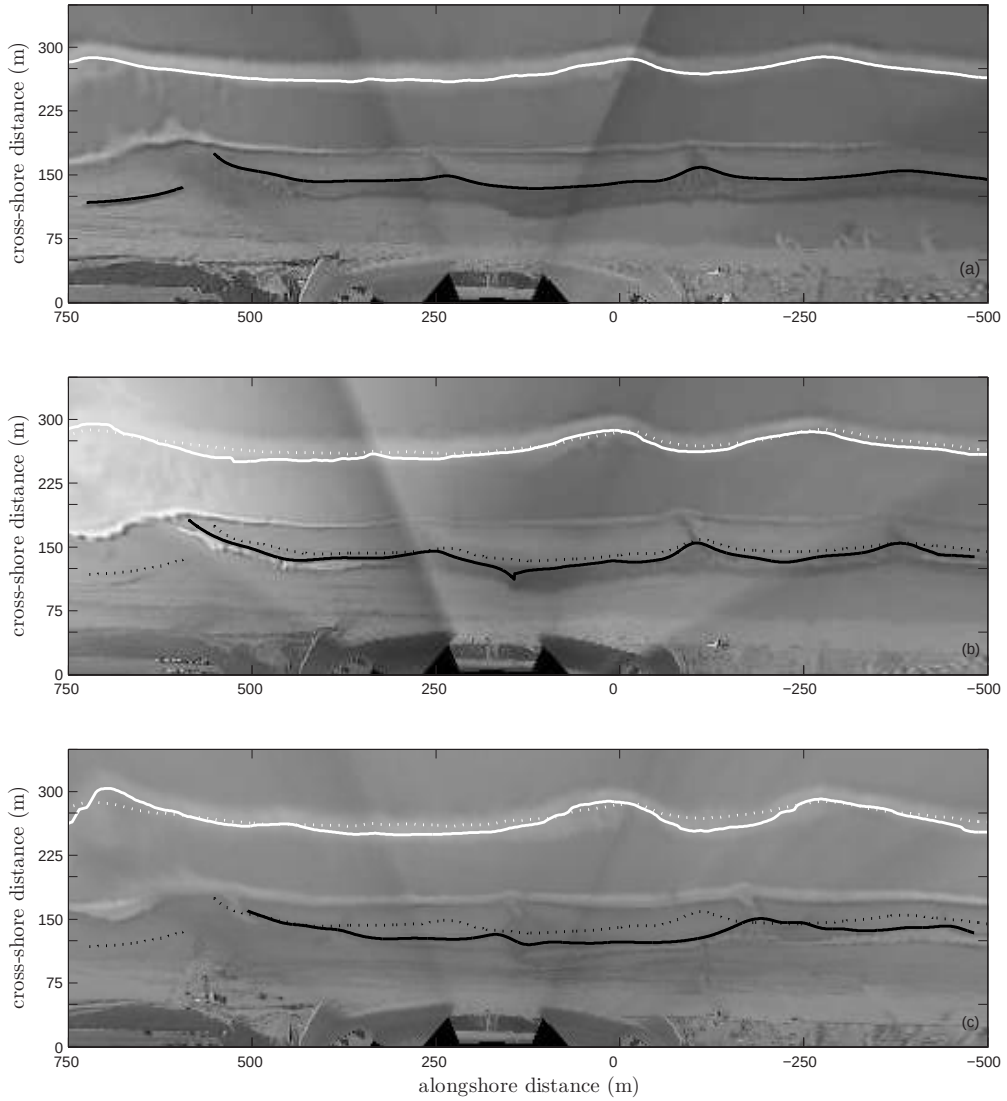

Figure 4.9 Example of a gradual changing phase of the intertidal and subtidal rhythmicities. Starting on 2 March 2002 (a) shows the initial intertidal (black solid) and subtidal (white solid) bar line, which will be presented in the subsequent images with identical colours, but as dashed lines. The subsequent images are from 4 March 2002 (b) and 8 March 2002 (c).

Phase changes reflect different migration rates of the bar lines. An example is shown in Figure 4.9 starting on 2 March 2002. During the subsequent days with small southward directed $\bar{P}_l$, both the intertidal and subtidal bar line moved several meters landward and in the southern direction (Figure 4.9b). The phase difference remained around $-105°$. Subsequently from 4 March 2002 up to 8 March 2002, the incident waves were mainly shore-normal (small $\bar{P}_l$), but ended with northward directed $\bar{P}_l$ peak (Figure 4.8b). Throughout these days, the SRCs maintained their alongshore position (Figure 4.9c). Whereas the intertidal bar migrated about 50 meters in the northern direction. The difference in the alongshore migration of the intertidal and subtidal bar line resulted in a change from $\Psi = -105°$ to $\Psi = -170°$ (Figure 4.8a).

In this example, the intertidal bar line migrated faster than the subtidal bar line. However, occasionally the subtidal bar lines also moved faster alongshore than the intertidal bar lines. Between 15 and 19 January 2002 for instance, the subtidal bar line migrated some 3 m/day northward, while the intertidal bar line moved 1 m/day northward only. Consequently Ψ changed from $-171°$ to $-99°$. These examples show that phase changes result from different alongshore migration rates of the intertidal and subtidal bar line.

4.6 Discussion

4.6.1 Intertidal rip channel types

Around low tide on the intertidal beach, two types of rip channels were discriminated being an open (oIRC) or filled rip channel (fIRC). A rip channel likely fills up when the drainage from the upper beach is small and the net swash sediment transport is landward. The fIRCs were located more landward than the oIRCs. Landward located bars are likely to be flooded for a shorter period than seaward located bars, which means less drainage during falling tide and rip channels intercepting these landward located bars can fill up. Presumably the short period of being flooded might also be the reason for $\bar{c}_{\mathrm{Y_i,fIRC}}$ to be smaller than $\bar{c}_{\mathrm{Y_i,oIRC}}$. Less time is available for the alongshore current to move fIRCs, but the alongshore current becomes smaller in landward direction. The fIRCs were more difficult to recognize on Argus images. The wet sand in their funnels was often misclassified as dry sand (Quartel et al., 2006), which results in the absence of a local seaward deviation in the intertidal bar line, and thus, in the failure to detect filled rip channels. This failure might explain the many one-day fIRC lifetimes.

4.6.2 Intersite comparison

The time-averaged spacing of the IRCs was $\approx$ 250 m and spatially variable with a coefficient of variation CV of 0.53. This CV was larger than that reported by Lafon et al. (2005) for IRCs on a meso- to macrotidal beach ($CV = 0.39$) and by Holman et al. (2006) for SRCs at an embayed, microtidal beach ($CV = 0.39$), but comparable to the spatial variation reported by Turner et al. (2007) for SRCs at a straight, microtidal beach ($CV = 0.47$). Despite the variability in CV values, all the studies indicate that rips are not spaced regularly in the alongshore. Spatial and temporal variability in rip channel spacing appears to be inherent to natural conditions because rips merge and split in response to time-varying offshore wave conditions (Van Enckevort et al., 2004). Van Enckevort et al. (2004) and Holman et al. (2006) argued that the non-zero CV indicates that the modelling of rip behaviour should be approached with non-linear models, such as that of Reniers et al. (2004), because linear models (e.g. linear stability models) result in $CV = 0$ by definition.

The time-averaged alongshore migration rates of the fIRCs and oIRCs were $O(1$ m/day). Lafon et al. (2005) reported similar migration rates of IRCs on a swell-dominated, meso- to macrotidal beach. However, these migration rates were obtained from two subsequent satellite images with an interval of 2 months. The net alongshore migration over the 2 month period was thus between 100 and 200 m on this swell-dominated beach, larger than the net 30 m/month alongshore migration of IRCs on a storm-dominated, macrotidal beach (Van Houwelingen et al., 2006). This difference in net IRC migration on beaches with large tidal ranges emphasizes the influence of swell or sea waves affecting beach morphology. Besides, IRCs on macrotidal beaches live longer than a few months, whereas the lifetime of the IRCs on the microtidal beach was on average only 10 days. This corresponds with the morphology of macrotidal beaches being more static than the morphology of microtidal beaches (Wijnberg & Kroon, 2002; Masselink et al., 2006).

4.6.3 Subtidal morphologic coupling

The amount and alongshore migration rates of the IRCs were weakly, but statistically significantly at the 99% confidence level, related with the amount and alongshore migration rates of the SRCs. A more landward location of the subtidal bar resulted in the absence of an intertidal bar ($y > +350$ m; Figures 4.5c and 4.6c). The IRCs preferred certain alongshore positions of which some coincided with the preferable alongshore positions of the SRCs (e.g. $Y \approx 0$; Figures 4.5b and 4.6b). Furthermore, the alongshore variability of the intertidal bar resembled the alongshore variability of the subtidal bar lines ($\bar{r} = 0.58$). These aspects imply that the behaviour of the IRCs was not only forced by wave conditions, but also by the subtidal morphology. The intertidal and subtidal bar lines were always coupled, suggesting that the alongshore variability in the subtidal sandbar governed the generation and the subsequent evolution of the intertidal rip channels.

The time-averaged IRC spacing was approximately halve the time-averaged SRC spacing, which implies spatial differences in the alongshore variability of both bars (note that the correlation coefficients were indeed always less than 1). Possibly, the persistent SRCs induce a persistent alongshore variability of the beach with an alongshore spatial scale identical to the SRCs spacings. This alongshore variability is likely to prevail over the whole intertidal beach zone. The (quasi-persistent) intertidal bar system may be superimposed on the larger-scale alongshore variability. The seaward deviation of the large-scale alongshore variability, induced by the alongshore position of the SRCs, may become preferable locations for the IRCs.

The phase between the intertidal and subtidal bar lines was observed to gradually change in time due to differences in alongshore migration rates of both bars. Lafon et al. (2005) found IRCs to migrate faster alongshore than SRCs. However, in this study, the IRCs migrated both slower and faster than the SRCs did, which may cause the somewhat weak relation between the migration rates of the IRCs and the SRCs (Table 4.1). The differences in migration rates suggest that the importance of forcing by wave conditions and the forcing by the subtidal morphology for the IRC

behaviour alters in time. The data used in the present study is, however, insufficient to examine which hydrodynamic and morphologic conditions induced the slower and faster migration rates of the IRCs with respect to the SRCs.

4.7 Conclusions

A 15-month data set of intertidal and subtidal bar lines has been analyzed to describe the spatial and temporal variability of the rip channels on a multiple barred coast at Noordwijk aan Zee, the Netherlands. The alongshore distribution of intertidal rip channels was non-uniform ($\sigma_\lambda/\bar{\lambda} \sim 0.47$). The cross-shore behaviour of the intertidal rip channels comprises gradual landward migration during low-energy conditions and a abrupt landward shift during a storm. Some of the intertidal rips filled up during falling tide, whereas the majority remained open. The filled intertidal rip channels had more landward positions and migrated slower (2.4 vs 4.6 m/day) in the alongshore direction than the open intertidal rip channels. The number of open rip channels increased with the incident wave height and the open rip channels migrated in the same direction as the anticipated alongshore current. Cross-correlation analysis revealed that the intertidal bar system was always coupled to the alongshore variability in the subtidal bar. The phase-difference between the intertidal and subtidal bar lines changed gradually in time due to differences in the alongshore migration rates of the both bar lines.

5 Seasonal patterns of the beach sediment budget

Quartel, S., A. Kroon & B.G. Ruessink (in review) Seasonal accretion and erosion patterns of a microtidal sandy beach. Marine Geology

Abstract

Monthly elevation surveys of a 1.5 km stretch of coast at Noordwijk, the Netherlands, were made (1) to quantify seasonal variability in the cross-shore position of high-, mean- and low-tide contours, beach width and beach volume, and (2) to examine the dependence of the variability on the offshore wave characteristics. Additionally, daily cross-shore positions of contours obtained from video images were used to examine daily beach response to wave characteristics between successive surveys. The more intense and frequent storm events in winter than in summer resulted in a seasonal change from a wide beach with a small volume at the end of winter to a narrow, large-volume beach in summer. The seasonal pattern in beach width resulted from the cross-shore sediment exchange between the supratidal and lower-intertidal part of the beach. In contrast to the coupling between beach behaviour and wave-characteristics on a seasonal scale, beach variability between successive surveys was unrelated to day- to week-averages of the preceding offshore wave conditions partly due to the precise timing of a storm relative to the two survey moments. Moreover, daily variability determined from the video images showed that differing antecedent morphology to storms and alongshore variations in beach morphology contributed to spatially and temporally variable beach response.

5.1 Introduction

Sandy beaches function as a natural sediment buffer for coastal systems. Periods of accretion and erosion of this sediment buffer alternate over time and are generally coupled to low and high-energy wave conditions. Low wave conditions supply sediment for the beach to accrete, while high-energy wave conditions erode sand from the beach by offshore directed currents such as undertow.

Various conceptual models for the alternation of beach accretion and erosion have been developed to distinguish different beach states based on beach characteristics.

A well-known model is the 'storm - post-storm' model, which predicts rapid sediment erosion during storms and slower accretion in the post-storm period (e.g. Nordstrom, 1980; Dubois, 1988; Stive et al., 2002). The erosion during a storm event is caused by offshore sediment transport induced by wave breaking and undertow processes on the intertidal beach during increased surge levels. This flattens the barred beach morphology. The accretion during post-storm conditions is caused by propagating bores and swash (Houser & Greenwood, 2007). The onshore orbital motion, and subsequently the sediment transport capacity, under the bores exceeds the offshore wave stroke, whereas excess water transported over the bar is channelled alongshore to the nearest intertidal rip channels (Aagaard et al., 2006). Therefore, bores and swash rush up the seaward flank of the bar transporting sediment to the bar crest or even up to the landward located trough. This causes vertical growth or landward migration, respectively, of the intertidal bars, which eventually may merge with the upper part of the beach near the high water line (e.g. Hayes & Boothroyd, 1969; Mulrennan, 1992; Masselink et al., 2006). This model is appropriate to a large variety of storm-dominated beaches, although, in detail, differences in morphologic response will be found due to the differences in settings such as the tidal regime, the number of bar-trough systems and the wave climate (e.g. Davis et al., 1972; Wijnberg & Kroon, 2002; Anthony et al., 2005).

Swell-dominated beaches show an alternation of accretion and erosion on a longer temporal scale, commonly in phase with the seasons. These swell-dominated beaches follow the 'bar - berm' model formulated by Shepard (1950) for Californian beaches. A steep beach face and berm are created by low-energy swell waves during the summer, while a flat profile including a new-formed temporal subtidal bar is created by storm-generated waves during the winter (Winant et al., 1975; Aubrey, 1979; Harper, 1980).

The 'storm - post-storm' model may also possess a seasonal aspect. Storms are possible throughout the year, but the frequency and intensity of storm occurrence is higher during winter months than during summer months. Normally, the response of the beach to high-energy wave conditions is faster than to low-energy wave conditions (Wright & Short, 1984). The impact of a storm can be immediately seen on a beach. However, the beach needs more time to respond to low-energy wave conditions and to recover. The adaptation time of the barred beach depends on the storm intensity, the storm duration and the pre-existing morphology during the storm event (Wright et al., 1985). The recovery time for the barred features on the beach is also strongly influenced by the length of the period between two successive storm events. The temporal variability of the wave conditions is higher in winter than in summer. Continuously changing wave conditions and short time periods between successive storms events may not allow the beach to adjust to the new conditions. Consequently, beaches may have a certain memory in their response and beach morphology may be best related to wave conditions averaged over a few antecedent days, rather than the immediately preceding conditions (Wright et al., 1985). Overall, the influence of the seasonal variability in energy conditions and storm events on storm-dominated beaches is unclear.

The 'storm - post-storm' model represents the morphological changes coupled to periods of accretion or erosion, and thus provides a qualitative description. For

quantification of accretion and erosion, information on the increase and decrease of sediments amounts is essential, and therefore changes in the actual sediment volume are often used (Allen, 1981). Variations in beach characteristics, such as the cross-shore position of the shoreline (Morton et al., 1995; Guillén et al., 1999) and beach width (Aarninkhof et al., 2003), are used to approximate accretion and erosion quantitatively as well. The correlation between sediment volumes and these beach characteristics is not always obvious though. For instance, a flattening of the beach implies a wider beach without coinciding necessarily with a volume loss or gain.

The aim of this chapter is to investigate seasonal patterns of beach accretion and erosion in monthly observed morphologies at a storm-dominated coast and to relate these patterns to variations in the wave forcing conditions. The study site, Noordwijk aan Zee (Figure 1.2), is located along the Dutch coast and characterized by a single quasi-persistent intertidal bar system and two persistent subtidal bar systems. The beach accretion and erosion are described by monthly variations in beach width and volume. These beach characteristics were derived from interpolated beach levellings over a 3-year period. Beach contours derived from hourly Argus video-images were used to examine the daily beach response to environmental conditions, and to investigate the net result of the daily variations on the monthly changes in beach characteristics.

5.2 Data acquisition and methodology

The data for our analysis consisted primarily of beach elevation data from a 1.5 km north-south oriented beach stretch (Figure 1.2) collected monthly between November 2001 and November 2004. Hourly Argus images from the same beach stretch were also acquired for several time spans between two successive beach surveys.

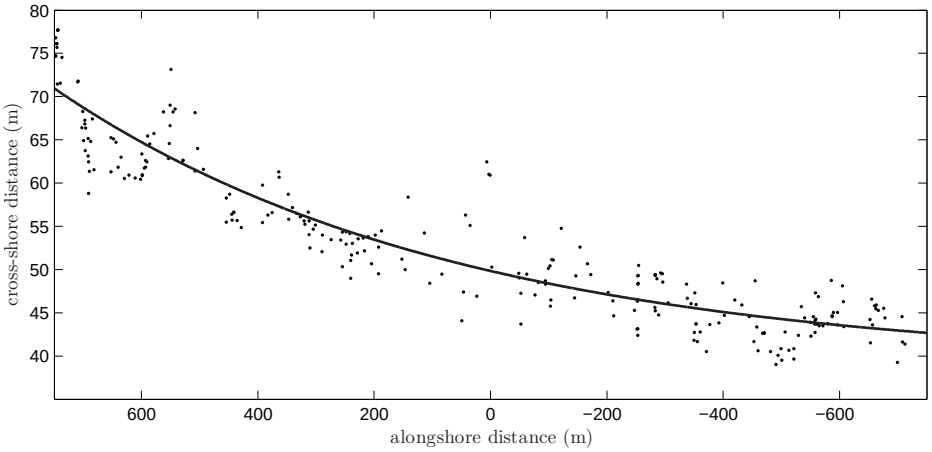

Figure 5.1 Alongshore position of the dunefoot between November 2001 and November 2004 (dots) with the exponential fit presented as the solid line.

5.2.1 Beach elevation

Bed levels were measured using a differential Global Positioning System (dGPS) with an accuracy of about 2.5 cm in the horizontal (x and y) and 4 cm in the vertical (z). The measurements were carried out around low tide every 4 weeks during spring tide conditions (typical range of 1.8 m), and the data were collected along 31 cross-shore transects with a 50-m alongshore spacing. Additional measurements between transects were carried out to capture details of small rips. Each transect stretched from just below the momentary water level to well above the dune foot at +3 m NAP (= Dutch ordinance level, $\approx$ mean sea level). The height of the momentary water level varied strongly with offshore wave energy conditions and storm surge levels. The water levels were 0.5 to 1.5 m above predicted tide levels during high-energy wave conditions due to storm surges and wave set-up. The lowest bed levels ≈ -1.5 m NAP were reached during low-energy wave conditions.

Bed level maps $Z(x, y, t)$ of each survey (t) were created by kriging interpolation of the bed level measurements (x, y, z). Several pre-processing steps were made to optimize the interpolation results. Firstly, a local coordinate system was introduced with the dunefoot (+3 m NAP) position, which is the landward boundary of the beach, as the zero reference line. For this purpose, the alongshore spatial trend of the dune foot was obtained by an exponential fit through the position of all bed levels at $z = 3.0 \pm 0.05$ m collected over the 3-year period ($r = 0.97$; Figure 5.1). This alongshore trend was extracted from all data sets. The small variations around this trend (Figure 5.1) had an anthropogenic cause. The seaward perturbations correspond to beach access points.

Secondly, the bed levels above +4 m and below -1.5 m NAP were culled from the data set. Thirdly, the cross-shore trend was estimated for each survey by nonlinear least-squares fitting of an alongshore-averaged mean beach profile $z_{trend}(x, t)$ to the remaining cross-shore distributed bed level data (Figure 5.2). We used (Kroon, 1994)

$$z_{trend}(x, t) = [1 - x_*^b]\Delta z + z_{x_{\min}}, \tag{5.1}$$

where x_* is the normalized cross-shore distance ($= x/\Delta x$), Δx is the width of the beach zone ($= x_{\max} - x_{\min}$), b is an exponent, and Δz is the difference in height between the boundaries ($= z_{x_{\min}} - z_{x_{\max}}$). The alongshore and cross-shore detrended data were used in an omnidirectional variogram, from which a day-specific spherical model was derived (Burrough & McDonnell, 1998; Swales, 2002). With this model the detrended data were interpolated on a 1×1 m grid. The three-dimensional bed level maps, $Z(x, y, t)$, were finally obtained by adding the cross-shore trend of the mean beach profile $z_{trend}(x, t)$ to the interpolated data (Figure 5.2).

5.2.2 Beach zonation

Beach changes were quantified as variations in beach width and beach volume for a number of beach zones (Figure 5.3), because cross-shore behavior is expected to differ

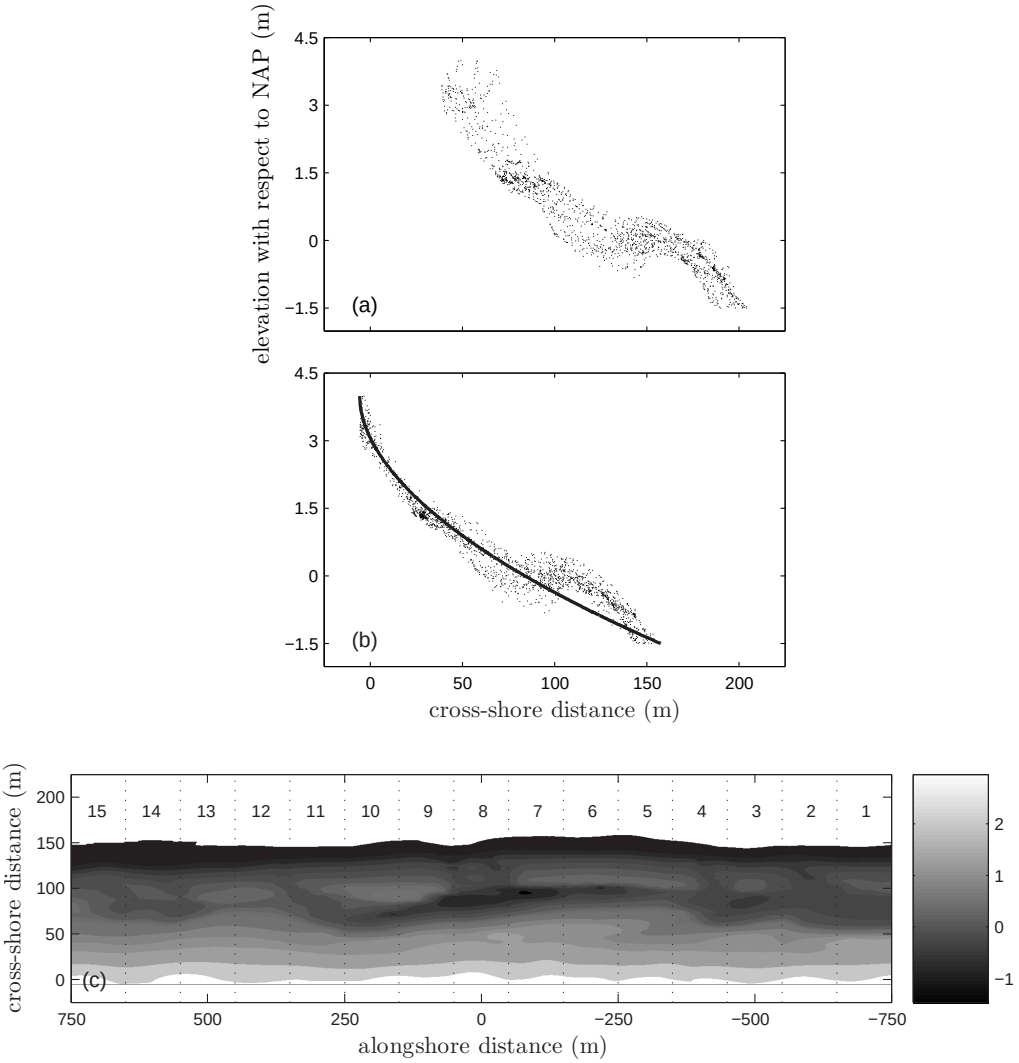

Figure 5.2 The result of alongshore detrending for the cross-shore distribution of the elevation data of 16 February 2002. Upper panel (a) shows the original data, middle panel (b) the alongshore-detrended data with the *mean beach profile* (solid line) and lower panel (c) the elevation map of this day with the defined beach sections.

due to differences in frequency and duration of tidal submergence. The heights used to divide the four different zones were based on long-term hourly records of offshore (18-m depth) wave parameters (root-mean-square wave height H_{rms0}, peak period T_{p0}) and measured water levels (η_0; Figure 5.4) based on the shoreline elevation model of Aarninkhof et al. (2003). In the time series of η_0 over the 3-year measuring period, moments of high and low tide ($\eta_{0,\mathrm{ht}}$ and $\eta_{0,\mathrm{lt}}$ respectively) were determined by finding a local maximum and minimum every 12 hours. Subsequently, the wave set-up and vertical swash excursion were calculated with the shoreline elevation model for these moments, with water level elevation at the shore at high tide (η_{ht}) given by

$$\eta_{\mathrm{ht}} = \eta_{0,\mathrm{ht}} + \eta_{\mathrm{sl}} + 1.3\frac{\eta_{\mathrm{osc}}}{2} \tag{5.2}$$

and at low tide (η_{lt})

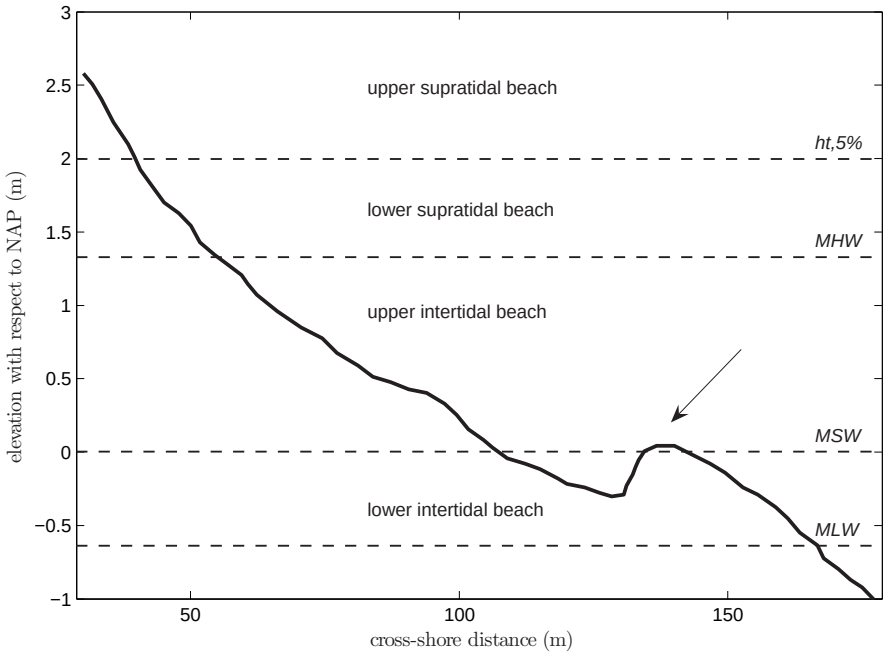

Figure 5.3 Cross-shore beach profile showing the different vertical zones and their boundaries. The arrow indicates the location of an intertidal bar in the upper intertidal beach.

$$\eta_{\mathrm{lt}} = \eta_{0,\mathrm{lt}} + \eta_{\mathrm{sl}} - 1.3\frac{\eta_{\mathrm{osc}}}{2}, \tag{5.3}$$

where η_{sl} represents the increase in water level due to wave breaking-induced set-up and η_{osc} represents the vertical swash excursion (see Aarninkhof et al. (2003) for parametrization details). The swash term in Eqs. 5.2 and 5.3 was added and subtracted, respectively, to ensure that η_{ht} (η_{lt}) is the higher (lower) vertical limit of the water level. The mean value of all η_{ht} (η_{lt}) resulted in the elevation of the mean high (low) water line at the shore, henceforth denoted MHW (MLW).

The main division of beach zones is marked by MHW ($z_{\mathrm{MHW}} = +1.32$ m NAP) leading to a supratidal and an intertidal beach, where the first is infrequently submerged and the second is submerged almost every tide. In addition, both the supratidal and the intertidal beach zones were split into an upper and a lower part (Figure 5.3). The supratidal zone was divided by the elevation exceeded by only 5% of the high tide water levels ($z_{\mathrm{ht,5\%}} = +2$ m NAP), and the intertidal zone was divided by mean seawater level ($z_{\mathrm{MSW}} = 0$ m NAP).

The cross-shore distance between MLW ($z_{\mathrm{MLW}} = -0.76$ m NAP) and the dunefoot ($z_{\mathrm{df}} = +3$ m NAP) is defined as beach width, W_b. The cross-shore distance between MLW and MHW is the width of the intertidal zone, W_{iz}. The amount of sediment within W_b represents beach volume V_b. Additionally, sediment volumes were computed separately for the four vertical zones.

Returning to Figure 5.4, it can be seen that there are more frequent high-energy wave conditions ($H_{\mathrm{rms0}} > 1.5$ m) during winter months (October to March) than during summer months (April to September; Figure 5.4). Individual high-energy

events in general experienced higher waves (H_{rms0} between 3 to 4.5 m) and larger surges (i.e. measured difference between observed and predicted water level, η_{surge} up to 1.5 m) during winter months than during summer months (H_{rms0} around 2 m and η_{surge} about 0.5 m).

5.2.3 Video-derived contours

Argus video images originate from a shore-based monitoring system (Holman & Sallenger, 1986). At Noordwijk, the Argus station consists of five colour (RGB) video cameras, which are mounted approximately 60 m above sea level on the roof of a hotel. Every daylight hour, 10-minute time exposure (timex) images are collected by averaging over 1200 snapshots sampled at 2 Hz. These oblique images undergo geometrical transformation (Holland et al., 1997) after which a 180 ° plan view over

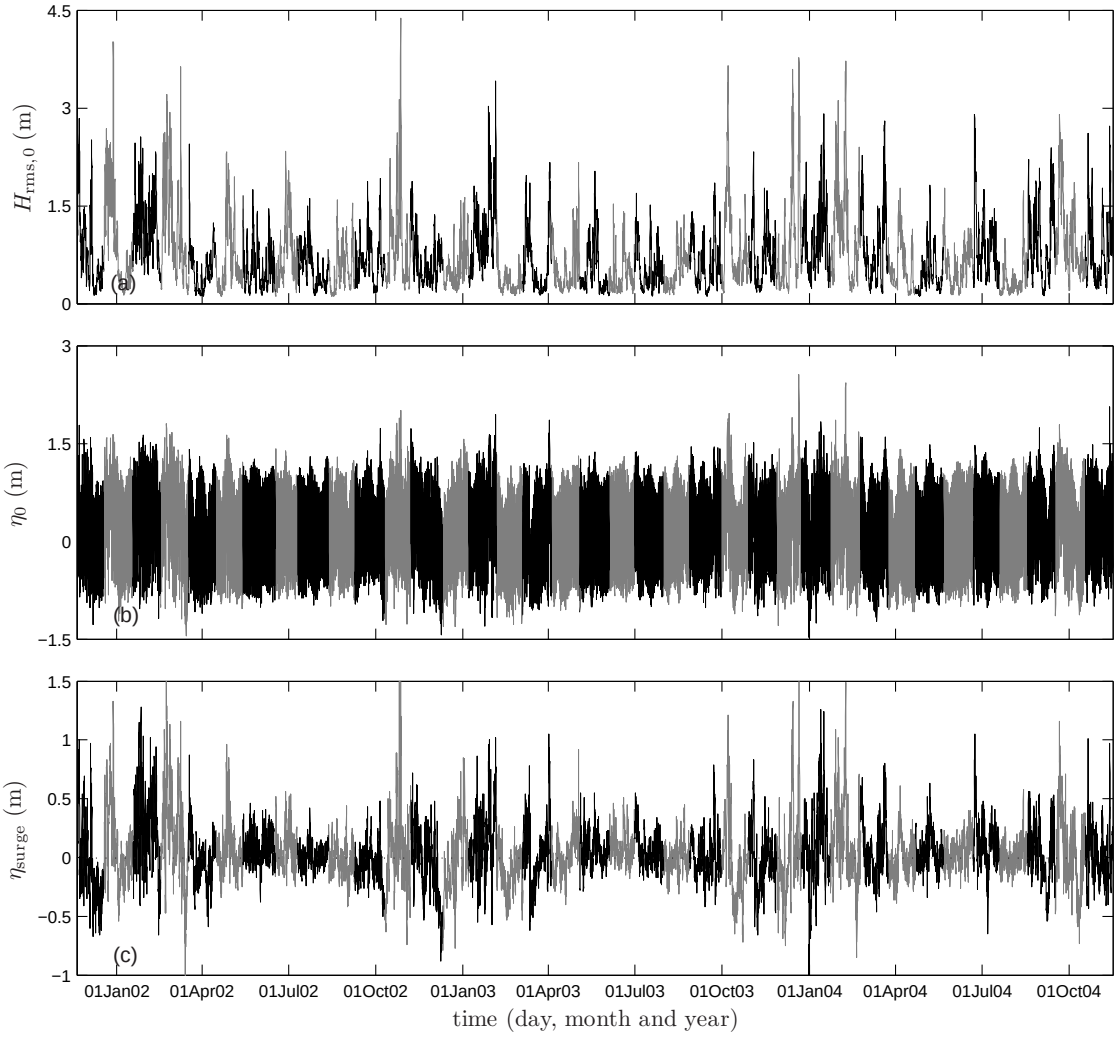

Figure 5.4 Wave and water levels from November 2001 to November 2004: upper panel (a) is the H_{rms0}, middle panel (b) η_0, and lower panel (c) η_{surge}. The grey and black colours indicate the different periods between two successive surveys.

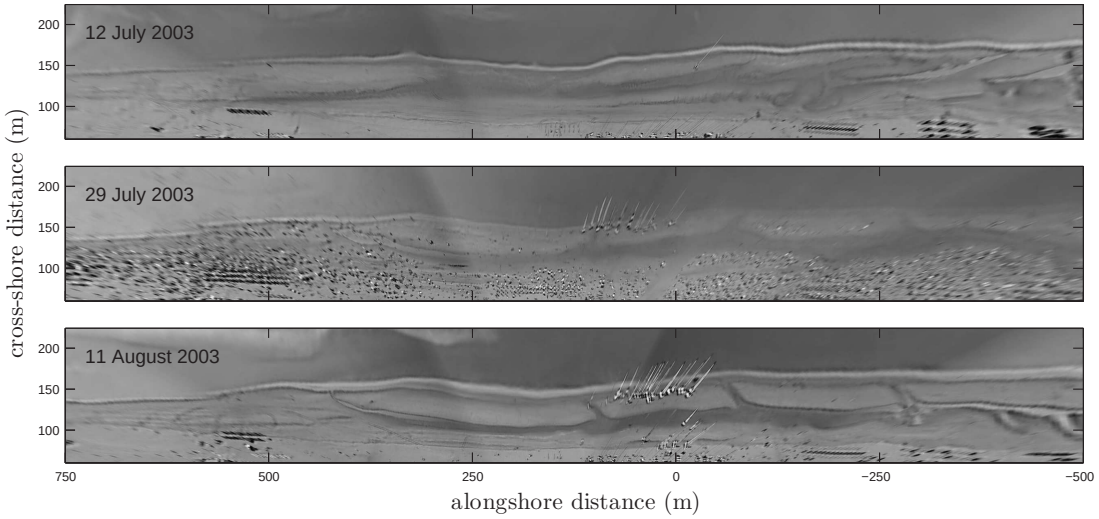

Figure 5.5 Three Argus images from 12 July, 29 July and 11 August 2003. These images show the visual contrast between water and sand. Moreover, these images were taken around low tide, thus exposing the intertidal beach morphology, so that the alongshore non-uniformity and the morphological changes of the beach can also be seen.

the selected alongshore beach stretch is available (Figure 5.5).

Shoreline elevations were computed with Equation 5.2 from hourly-measured offshore hydrodynamic conditions between two successive surveys. On each day between the two successive surveys, the moments of the shoreline approaching the elevation of MHW, MSW and MLW were listed and the timex Argus images of these moments were selected. On colour images, a visual contrast between water and sand is present resulting in the possibility of shoreline detection (Figure 5.5). For this set of Argus images, the shoreline detection model used was based on the difference in hue and saturation between water and sand pixels (Aarninkhof & Roelvink, 1999). The detection of the shoreline resulted in the cross-shore position of the shoreline at any given moment.

The elevations of the video-detected shorelines were close, but not identical to either MHW, MSW or MLW. The video-derived cross-shore positions were corrected for the cross-shore position of either MHW, MSW or MLW using the local slope from the time- and alongshore-average cross-shore beach profile, $\bar{Z}_y(x)$ (Figure 5.6a). This was done to avoid artificial temporal variability in the cross-shore position of either of the 3 contours because of a temporal variability in the water elevation of the selected Argus images.

5.2.4 Alongshore uniformity

The dunefoot, MHW, MSW and MLW contours were derived from both data-sets to quantify beach changes in terms of beach width and volume. The relative importance of the alongshore component of beach changes was examined with the alongshore uniformity of the beach elevation data $Z(x, y, t)$, because beach changes are likely to be

composed of an alongshore and a cross-shore component (Anthony et al., 2004). The alongshore uniformity of the beach was tested by estimating the fraction of the total temporal variance that was uniform alongshore, following the methodology of Plant et al. (1999). To this end, $Z(x, y, t)$ is divided into a time-averaged beach elevation, $\bar{Z}(x, y)$, and deviations from the mean, $Z'(x, y, t) = Z(x, y, t) - \bar{Z}(x, y)$. Figure 5.6a shows the alongshore-average of $\bar{Z}(x, y)$, denoted $\bar{Z}_y(x)$. The total variance ($S_Y^2(x)$) is estimated as the root-mean-square deviation of $Z'(x, y, t)$, averaged in time and alongshore direction. The square-root of $S_Y^2(x)$ is the standard deviation profile $S_Y(x)$ shown in Figure 5.6b. Alongshore averaging of $Z'(x, y, t)$ results in the alongshore-uniform component, $Z'_Y(x, t)$, the root-mean-square averaged value of which, over time, is the temporal variance, $s_Y^2(x)$. The ratio of $s_Y^2(x)$ to $S_Y^2(x)$ is the ratio of alongshore-uniform to total variance as a function of cross-shore distance. The alongshore-uniform variance fraction computed over the entire length of the study area was below 0.6 (Figure 5.6c). Thus, the observed changes resulted from both alongshore and cross-shore variations.

The whole beach stretch was subsequently divided into 15 beach sections of 100 m length each (Figure 5.2). The $\bar{Z}_Y(x)$ and $S_Y(x)$ profiles in the 15 sections were fairly similar to that of the entire 1.5 km wide study area (Figures 5.6a and b). In

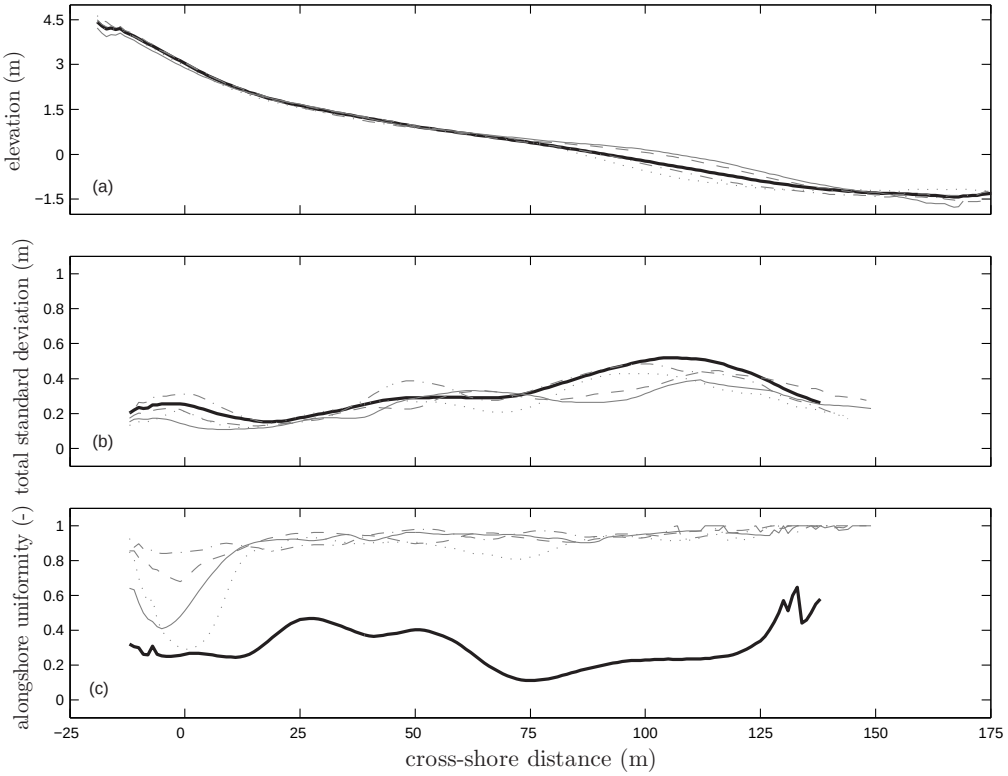

Figure 5.6 Profiles of the time- and alongshore-averaged beach elevation $\bar{Z}_Y(x)$ and the standard deviation $S_Y(x)$ are presented in a and b, respectively. The fraction of the temporal component of the total variance, reflecting the alongshore uniformity, is presented in c. Black lines are computed over the 1.5-km wide study area, while the grey lines are computed over different beach sections as defined in Figure 5.2 (section 3 is solid, 6 is dashed, 9 is dash-dotted and 12 is dotted).

contrast, the alongshore-uniform variance fraction was notably higher (Figure 5.6c), being over 0.8 for $x > 10$ m, meaning that beach changes within the sections were mainly due to cross-shore variations. The smallest values for the alongshore-uniform variance fraction were at $x \approx 0$ m and were largely of human origin (Section 5.2.1). Beach changes were also studied for the individual 100-m wide sections, because of the influence of the alongshore component on change exhibited by the entire beach.

5.3 Beach dimensions and variations

Variations in W_{b}, W_{iz} and V_{b} are due to the changes in the cross-shore positions of the dunefoot, MHW and MLW. The alongshore-averaged (over the entire 1.5 km wide study area) cross-shore position of the dunefoot, $\bar{X}_{\mathrm{df}}(t)$, fluctuated around 0 m and showed a pattern of gradual seaward migration and abrupt landward shifts (Figure 5.7a). The landward shift of $\bar{X}_{\mathrm{df}}(t)$ in general took place during winter months (October to March), when storm events occurred more frequently (Figure 5.4). The alongshore range in $X_{\mathrm{df}}(t)$ and $\sigma_{\mathrm{df}}(t)$ decreased simultaneously with the landward

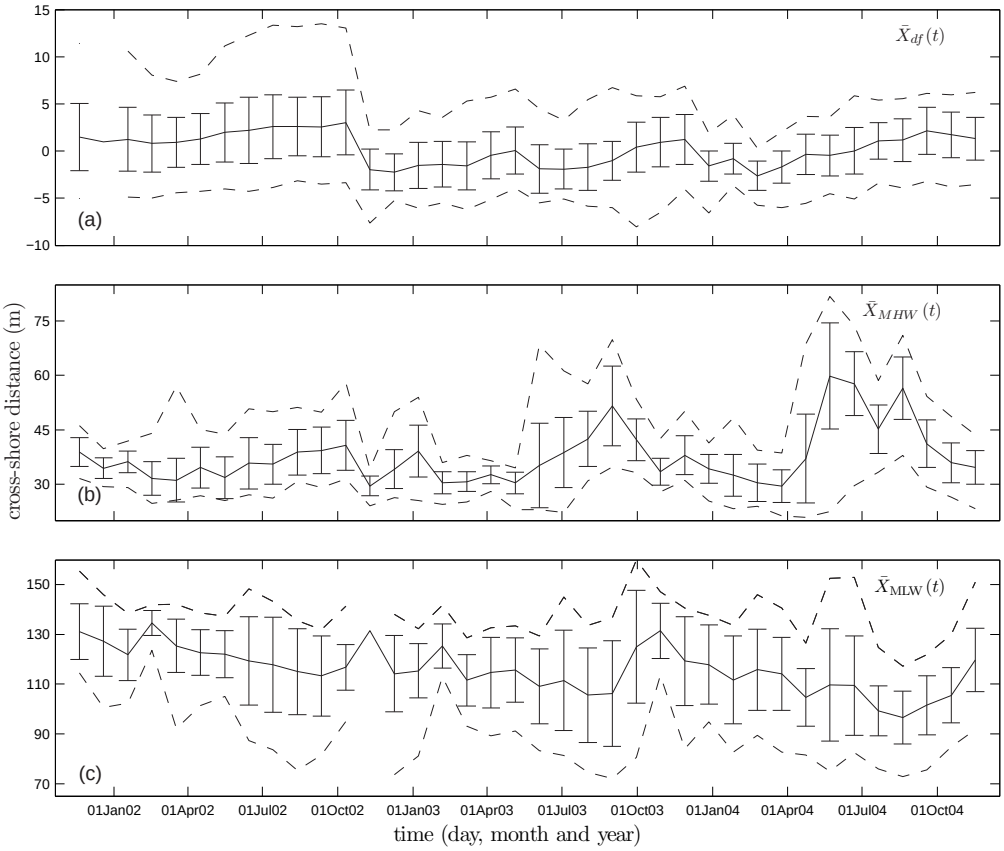

Figure 5.7 Cross-shore positions of the dunefoot (a), MHW (b) and MLW (c) contours with the solid line representing the alongshore-average position ($\bar{X}(t)$) and the error bar the standard deviation ($\sigma(t)$) between November 2001 and November 2004. The dashed lines show the minimum and maximum cross-shore positions ($\bar{X}_{\mathrm{min}}(t)$ and $\bar{X}_{\mathrm{max}}(t)$), i.e. together comprising the range.

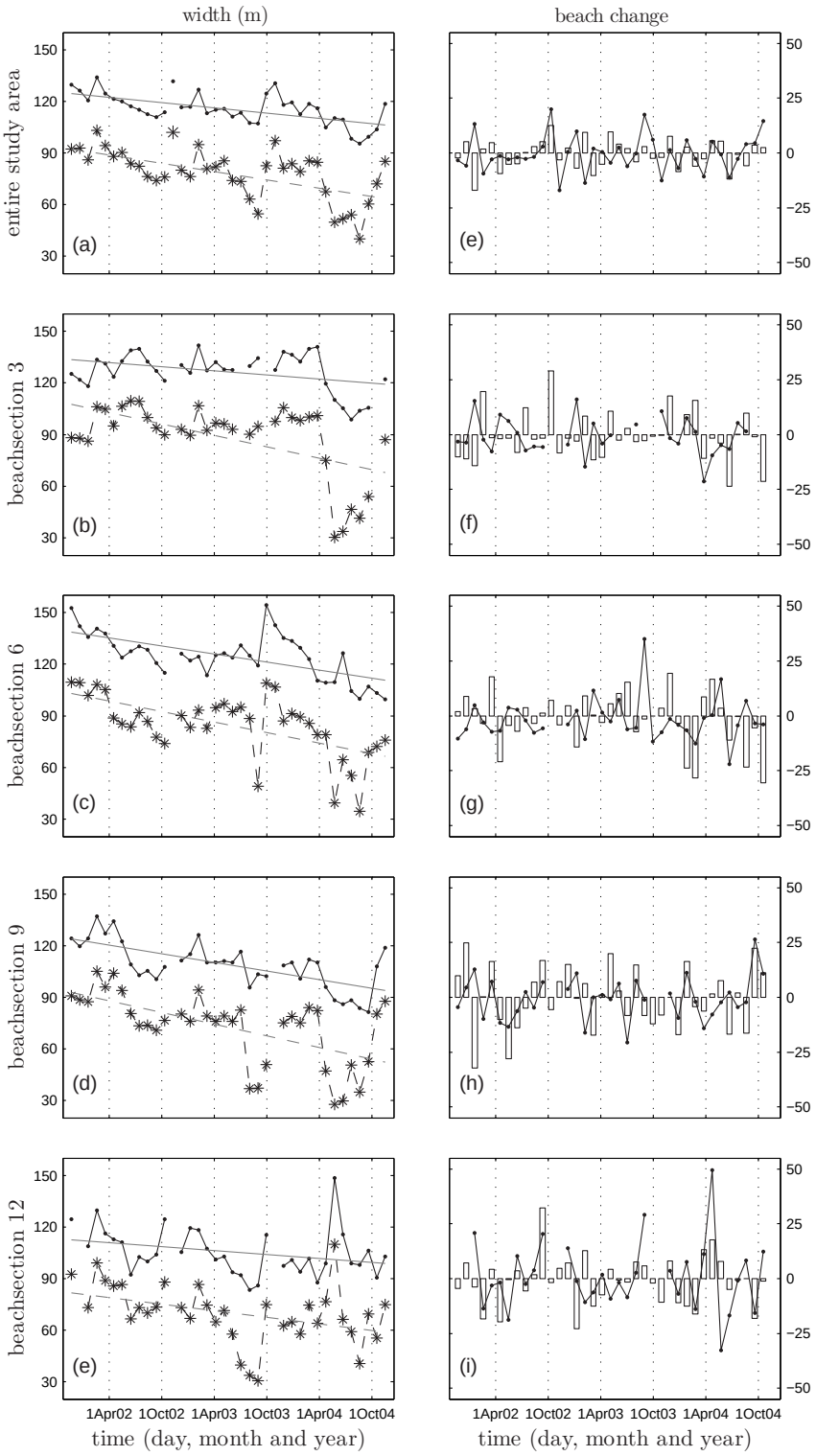

Figure 5.8 The left panels represent the beach and intertidal zone width over time for the whole alongshore beach (a) and for beach section 3, 6, 9, 12 (b to e, respectively). The variation of the beach width ($\Delta W_{\mathrm{b}}(t)$ in m; line) and beach volume ($\Delta V_{\mathrm{b}}(t)$ in m^3/m; bars) is shown in the right panels (f to i).

$\bar{X}_{\mathrm{df}}(t)$ shift. This implies straightening of the dunefoot during storms. In contrast, $\bar{X}_{\mathrm{df}}(t)$ gradually migrated in the seaward direction over a period of several months during summer (April to September) when storms occurred less frequently, indicating the formation of embryonic dunes in front of the primary dunes in the summer months. The inverse pattern of gradual landward and abrupt seaward changes marks the behaviour of $\bar{X}_{\mathrm{MLW}}(t)$ (Figure 5.7c). However, the moments of abrupt changes for $\bar{X}_{\mathrm{df}}(t)$ and $\bar{X}_{\mathrm{MLW}}(t)$ did not occur simultaneously and their behaviour was not correlated ($r^2 = 0.03$, $p > 0.05$).

The alongshore average cross-shore position of MHW, $\bar{X}_{\mathrm{MHW}}(t)$, showed a different pattern during the 3-year period that comprised two states (Figure 5.7b). $\bar{X}_{\mathrm{MHW}}(t)$ was located more landward and showed less alongshore variation during the first state than during the second state, which prevailed during the summer months of 2003 and 2004. Intertidal bars migrated landward (Quartel et al., 2007) above the MHW level as less storms occurred during these months (Figure 5.4). Consequently, $X_{\mathrm{MHW}}(y,t)$ moved seaward where the bar crest height intersected MHW. As this did not happen at the same time along the entire beach, the range in $\bar{X}_{\mathrm{MHW}}(t)$ also increased relative to the range during the first state.

The landward and seaward boundaries of the intertidal zone were defined by the MHW and MLW, respectively. In the behaviour of both $\bar{X}_{\mathrm{MHW}}(t)$ and $\bar{X}_{\mathrm{MLW}}(t)$ related well ($r = -0.85$ and 0.89, respectively, $p < 0.01$) to the behaviour of the alongshore-averaged intertidal zone width $\bar{W}_{\mathrm{iz}}(t)$ (Figure 5.8). However, the behaviour of the alongshore-averaged beach width $\bar{W}_{\mathrm{b}}(t)$ (Figure 5.8) was primarily related to that of the seaward boundary $\bar{X}_{\mathrm{MLW}}(t)$ ($r = 0.98$, $p < 0.01$) and not to the behaviour of the landward boundary $\bar{X}_{\mathrm{df}}(t)$ ($r^2 = 0.00$, $p > 0.05$), propably due to the smaller temporal variability of $\bar{X}_{\mathrm{df}}(t)$ than $\bar{X}_{\mathrm{MLW}}(t)$. The behaviour of $\bar{W}_{\mathrm{iz}}(t)$ and especially $\bar{W}_{\mathrm{b}}(t)$ was marked by large values during winter months and small values during summer months (Figure 5.8). Small $\bar{W}_{\mathrm{iz}}(t)$ was mainly induced by the extreme seaward positions of MHW, when intertidal bars intersected this contour (Figure 5.7b). Small $\bar{W}_{\mathrm{iz}}(t)$ and $\bar{W}_{\mathrm{b}}(t)$ imply relatively steep, reflective beaches in summer, while the relatively large $\bar{W}_{\mathrm{iz}}(t)$ and $\bar{W}_{\mathrm{b}}(t)$ in winter are characteristic of low-sloping, dissipative beaches. This pattern shows the seasonal aspect of the 'storm - post-storm' model (Section 5.1).

The behaviour of $\bar{V}_{\mathrm{b}}(t)$ was generally characterized by a post-winter minimum (between May and July; Figure 5.9). The beach accreted in the following summer and reached a maximum in volume at the beginning of the winter (November). The net gain or loss over the DF or MLW of beach sediment over one season amounted to approximately 19 m^3/m, which was about 10% of the total beach volume. Figure 5.9 is indicative of a cross-shore sediment exchange between the (upper and lower) supratidal zone and the lower intertidal zone. Generally, the volume of both the upper and lower supratidal zone was largest in October/November and smallest around March/April (Figures 5.9b and c). These beach zones lost sand during the winter season and gained sand over the summer. The volume of the lower intertidal zone increased in winter and decreased in summer, the reverse of the supratidal zone behaviour. This suggests a seasonal cross-shore exchange in sediment between the

supratidal and lower intertidal zones. The sediment volume changes of the upper intertidal zone lacked a clear seasonal dependence, which implies that the behaviour of the upper intertidal zone to correspond in turns with that of the supratidal zones and the lower intertidal zone. The amount of sediment for cross-shore exchange was usually around 5% of the total beach sediment, but sometimes reached 10%. This suggests that about 80% of the total sediment volume (≈ 150 m^3/m) was stationary.

The non-uniformity of the beach became visible in the spatial variability of $W_\mathrm{b}(y,t)$ and $V_\mathrm{b}(y,t)$ (Figure 5.8). The changes in $\bar{W}_\mathrm{b}(t)$ ($\Delta\bar{W}_\mathrm{b}(t)$) of the entire study area remained usually around $\pm$10 m and were smaller than the $\Delta\bar{W}_\mathrm{b}(t)$ of the individual beach sections, with values between -30 and +50 m (Section 12; Figure 5.8). These extreme changes occurred during winter months with more frequent and more energetic storm events, while gradual changes took place during summer months. Despite differences in magnitude, the sign of $\Delta\bar{W}_\mathrm{b}(t)$ was the same for all different beach sections. The monthly changes in total sediment volume $\Delta\bar{V}_\mathrm{b}(t)$ were also smaller for the whole beach than for individual beach sections. Opposite changes in beach volumes for individual beach sections occurred simultaneously (Figure 5.8), emphasizing the non-uniform alongshore behaviour of the beach.

The time series of $\bar{W}_\mathrm{b}$, $\bar{W}_\mathrm{iz}(t)$ and $\bar{V}_\mathrm{b}(t)$ show a decreasing trend over the 3-year study period. A best-fit linear line for $\bar{W}_\mathrm{b}(t)$ and $\bar{W}_\mathrm{iz}(t)$ showed a decrease of 18.7 m and 28.9 m, respectively (Figure 5.8). A decline in $\bar{W}_\mathrm{b}(t)$ and $\bar{W}_\mathrm{iz}(t)$ was also found for all individual beach sections. The cumulative change of $\bar{V}_\mathrm{b}(t)$ (Figure 5.8) showed a negative value after 3 years for the total beach and for 12 out of 15 beach sections. A linear trend fit through the beach volumes gave a loss of 5.17 m^3/m over the 3-year period. The reduction of beach width and beach volume suggests degradation of this coast. However, long-term (decades) data reported in Quartel & Grasmeijer (2006) showed that the 3-year change was comparable with the annual variability of this beach and the present degradation was preceded by progradation from 1998 to 2001 (see also Section 1.4).

5.4 Storm events and seasonal beach changes

The seasonal pattern in beach changes may be due to the differences in intensity and frequency of storms during summer and winter (Figure 5.4). The quantification of this relation was made by coupling beach characteristics, expressed as the change in $\bar{W}_\mathrm{b}(t)$ and $\bar{V}_\mathrm{b}(t)$ ($\Delta W_\mathrm{b}(t)$ and $\Delta V_\mathrm{b}(t)$, respectively), between two successive surveys, with wave and water level conditions over the same period. Wright et al. (1985) suggested that the beach changes may be related to wave conditions averaged over a few preceding days, but the amount of days was not clear. The offshore characteristics are thus expressed as an average of the hourly H_rms0 and η_0 during a variable amount of preceding days D by

$$\bar{H}_\mathrm{rms0}(D) = \frac{\sum_{i=0}^{D} H_\mathrm{rms0}(t)}{D} \tag{5.4}$$

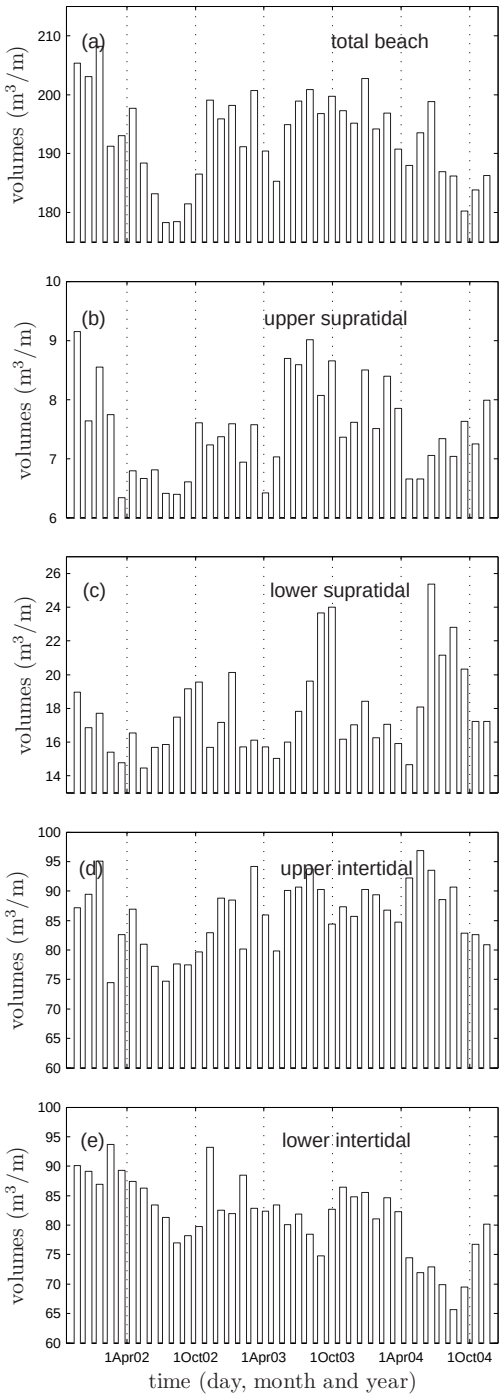

Figure 5.9 Time series of alongshore-averaged beach volumes (m^3/m) of the total beach (a) and the defined individual vertical zones (b to e).

and

$$\bar{\eta}_0(D) = \frac{\sum_{i=0}^{D} \eta_0(t)}{D} \tag{5.5}$$

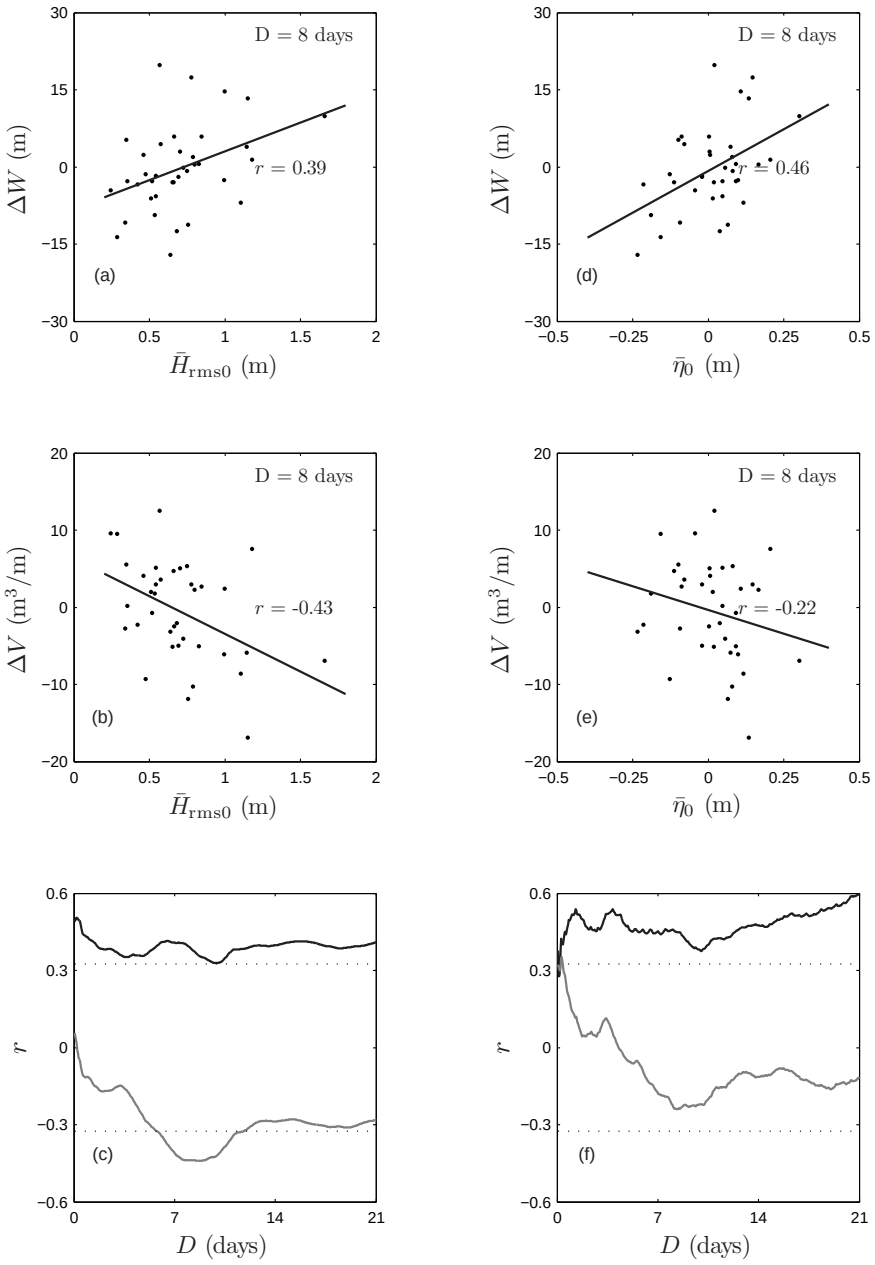

Figure 5.10 The relation of $\bar{H}_{\mathrm{rms0}}$ and $\bar{\eta}_0$ with the changes in beach width ($\Delta W_{\mathrm{b}}(t)$; a and d) and the changes in beach volume ($\Delta V_{\mathrm{b}}(t)$; b and e), where $\bar{H}_{\mathrm{rms0}}$ and $\bar{\eta}_0$ are values over the preceding 8 days. The bottom plots (c and f) show that the relations between the hydrodynamic characteristics and beach changes, $\Delta W_{\mathrm{b}}(t)$ (black) and $\Delta V_{\mathrm{b}}(t)$ (grey), were weak for D varying from 1 hour to 21 days. The critical values of r, r_{cr}, are computed for $\alpha = 0.05$ (dashed line).

where $i = 0$ is the moment of the second survey.

The monthly-averaged H_{rms0} and η_0 were computed as $\bar{H}_{\mathrm{rms0}}(D)$ and $\bar{\eta}_0(D)$ for $D = 21$ days, which was the minimum number of days between two successive surveys. The relation between the monthly-averaged wave characteristics and $\Delta W_{\mathrm{b}}(t)$ was statistically significant at the 95% confidence level (see Jenkins & Watts (1968) for

computational details) and stronger for $\bar{\eta}_{0,D=21}$ than for $\bar{H}_{rms0,D=21}$ ($r = 0.59$ and 0.41, respectively; Figures 5.10c and f). The large r for $\bar{\eta}_{0,D=21}$ indicates the importance of prolonged submergence before beach changes take place (see also Quartel et al., 2007). Smaller D also entailed significant relations between the time-averaged wave characteristics and $\Delta W_b(t)$, but there was not a clear optimum (Figures 5.10c and f) as was suggested by Wright et al. (1985). The relation was constantly positive, which is consistent with the large positive $\Delta W_b(t)$ (i.e. a wider beach) during high-energy wave conditions (the winter season, see Figure 5.4).

The volumetric changes were not significantly related to the monthly variations in offshore conditions, $\bar{H}_{rms0,D=21}$ and $\bar{\eta}_{0,D=21}$ (Figures 5.10c and f). However, a clear optimum in r was found around $D = 8$ days for $\bar{H}_{rms0}(D)$ meaning that the effect of large waves can still be found in $\bar{V}_b$ 8 days after a storm. The relation between the time-averaged offshore characteristics and $\Delta V_b(t)$ generally was inverse (Figures 5.10b and e), which confirms the accretion in summer associated with low-energy offshore conditions (Figure 5.4).

Although the relation of the offshore conditions with $\bar{W}_b(t)$ for all D and with $\bar{V}_b(t)$ around $D = 8$ days was statistically significant (Figure 5.10), the correlation coefficients on the whole were low. Therefore, the time-averaged offshore conditions do not conclusively explain the monthly process-response of the beach. A possible explanation for this poor correlation is the timing of the beach survey relative to a storm event. Due to the monthly survey interval, the period between a storm event and the survey may vary between 1 day and 4 weeks. The beach changes caused by a storm are less distinct with a long period than with a short period between the event and the survey if the recovery of the beach is in the order of a few days to weeks (e.g. Kroon, 1994; Masselink et al., 2006). Timing of the monthly survey with respect to a storm event is therefore of great importance. The optimum at $D = 8$ days already points to the relevance of survey - storm timing.

To examine the role of survey - storm timing further, the Argus-derived cross-shore positions were used to study daily beach behaviour in between a number of selected surveys. Argus images with the shoreline around MLW were available for only a few days between these selected surveys. As a result, the daily behaviour of $\bar{X}_{MLW}(t)$ was difficult to follow. Figures 5.11 and 5.12 represent two time series of the daily behaviour of MHW, MSW and MLW in October and December 2003, respectively. The hydrodynamic conditions consisted mainly of low-energy conditions interrupted by a major storm event (7 October in Figure 5.11d and 15 December in Figure 5.12d), but the period between the storm event and the second survey was longer (20 days) in the time series of October than of December (7 days). Both events led to large landward shifts (O 10^1m) of $\bar{X}_{MHW}(t)$ and $\bar{X}_{MSW}(t)$ (Figures 5.11a, b and 5.12a, b)). The storm of 7 October also led to a seaward shift of $\bar{X}_{MLW}(t)$ (2 to 12 October; Figure 5.11c), but the storm event of 15 December did not seem to affect $\bar{X}_{MLW}(t)$ (12 to 16 December; Figure 5.12c).

Low-energy conditions led to a less consistent response of the contours. Sometimes, $\bar{X}_{MHW}(t)$ barely changed during these conditions (e.g. after 15 October 2003; Figure 5.11a) as η_{ht} did not reach MHW. Whenever low-energy conditions succeeded a storm

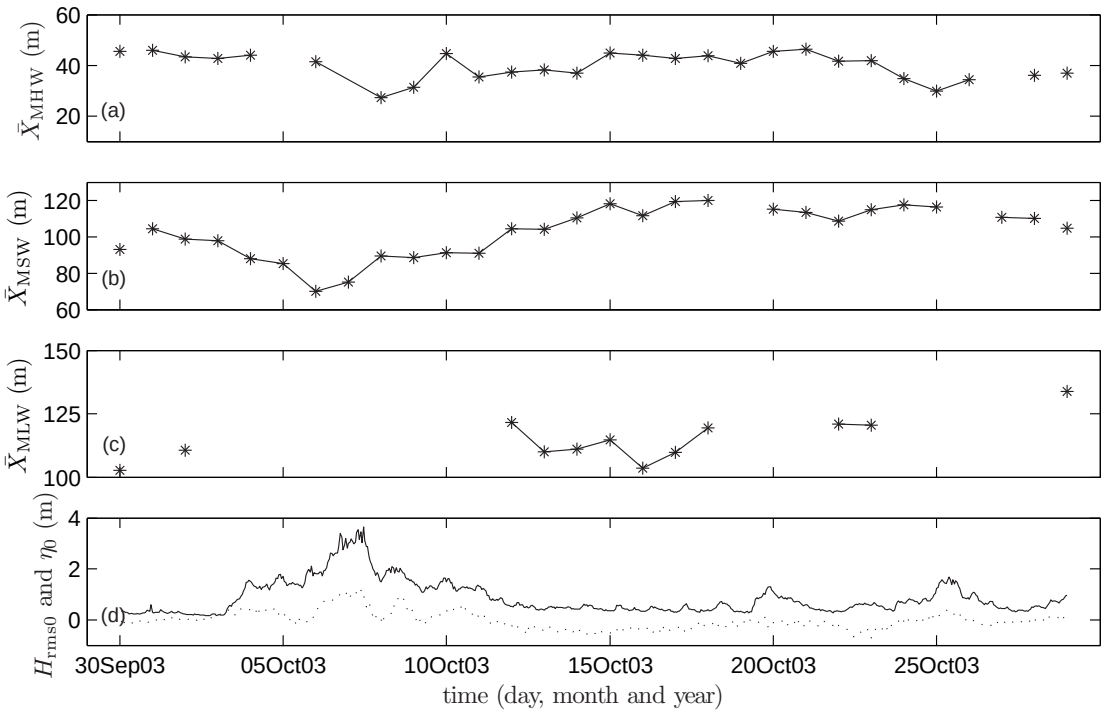

Figure 5.11 Daily $\bar{X}(t)$ time series of the MHW, MSW and MLW (from a to c, respectively) contours in different beach sections for the period from 30 September to 29 October 2003 with the first and the last data points derived from surveys and the remaining data obtained from Argus images. Panel (d) shows the accompanying offshore conditions H_{rms0} (solid) and η_{surge} (dashed).

and η_{ht} did exceed MHW, $\bar{X}_{\mathrm{MHW}}(t)$ either shifted to a more landward position (e.g. 7 October 2003; Figure 5.11a) or regained its pre-storm position within a few days (e.g. 14 December 2003; Figure 5.12a). The latter confirmed the possibility of a quick beach recovery and emphasizes the importance of survey - storm timing to understand the temporal variability in beach width and volume.

The difference in response of $\bar{X}_{\mathrm{MHW}}(t)$ to post-storm low-energy conditions may depend on differences in morphology antecedent to a storm, which varies with the duration between two successive storms (i.e. the storm interval). The storm intervals, and consequently the duration of low-energy conditions, were longer during summer than during winter (Figure 5.4a). The beach morphology at the end of the summer consisted of a narrow, reflective beach profile with a seaward position of MHW ($\bar{X}_{\mathrm{MHW}}(t) \approx 45$m; Figure 5.11a) as a result of a long period of low-energy conditions (Section 5.3a). When the winter season started, the first storm event created a wider, more dissipative beach with a more landward position of MHW ($\bar{X}_{\mathrm{MHW}}(t) \approx 40$m; Figure 5.12a). The beach morphology adapted to the post-storm, low-energy conditions. However, unlike the end of the summer, it did not regain the same morphology before the following storm due to a shorter duration of low-energy conditions. In consequence, the morphology antecedent to storm events varied due to differences in storm interval, which may also have led to variations in monthly beach response.

The daily response of $\bar{X}_{\mathrm{MSW}}(t)$ to low-energy conditions was variable in time. Pe-

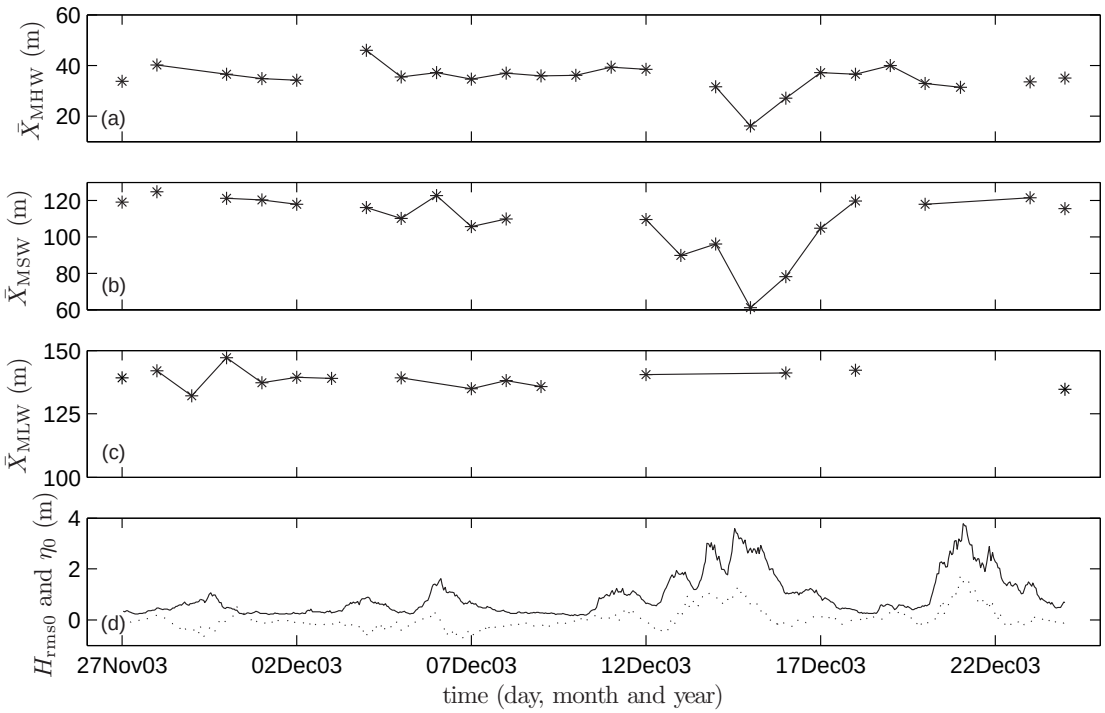

Figure 5.12 Daily $\bar{X}(t)$ time series of the MHW, MSW and MLW (from a to c, respectively) contour in different beach sections for the period from 27 November to 24 December 2003 with the first and the last data points derived from surveys and the remaining data obtained from Argus images. Panel (d) shows the accompanying offshore conditions H_{rms0} (solid) and η_{surge} (dashed).

riods of gradual migration of $\bar{X}_{\mathrm{MSW}}(t)$ occurred in the landward as well as in the seaward directions. The gradual landward migration of $\bar{X}_{\mathrm{MSW}}(t)$ (e.g. 30 November to 5 December; Figure 5.12b) was associated with landward-migrating intertidal bars during consistent low-energy conditions. Periods of gradual seaward migration of $\bar{X}_{\mathrm{MSW}}(t)$ were found during low-energy conditions just after a storm event. $\bar{X}_{\mathrm{MSW}}(t)$ shifted landward during the storm, but subsequently regained its pre-storm position due to this gradual seaward migration (Figures 5.11b and 5.12b). Furthermore, the alongshore (spatial) variations in beach morphology (Figure 5.5) may contribute to variable (in time) $\bar{X}_{\mathrm{MSW}}(t)$ response to low-energy conditions. The alongshore alternation of intertidal rips and bars led to alongshore variable cross-shore position of $X_{\mathrm{MSW}}(y,t)$. The generation or disappearance of these rips will lead to local landward or seaward shifts of $X_{\mathrm{MSW}}(y,t)$. Besides, the response of bars may differ from that of rips, because of differences in local hydrodynamic processes. Additionally, alongshore morphological beach response may be due to the change in orientation of the rips (Figure 5.5), which leads to large variations of $X_{\mathrm{MSW}}(y,t)$ at the rips, in contrast to small variations of $X_{\mathrm{MSW}}(y,t)$ at the bar, thus obviously contributing to variations in $\bar{X}_{\mathrm{MSW}}(t)$ response.

Apart from the response of MHW and MSW to high-energy conditions, there appears to be little consistency in the daily process-response of the beach due to the influence of antecedent morphology and alongshore morphological variability. The

daily inconsistency in combination with the timing of surveys relative to storms may explain why there was no strong relation between offshore conditions and monthly beach changes.

5.5 Discussion

The monthly changes of a sandy, storm-dominated beach for a 3-year period were studied with emphasis on seasonal patterns of accretion and erosion. The alongshore-averaged cross-shore positions of the dunefoot, MHW and MLW contour were retrieved from interpolated beach elevation maps and used in the computation of beach characteristics. At the beginning of winter, the onset of frequent storm events, all three contours straighten, the dunefoot shifts landward and the MLW shifts seaward (Figures 5.4 and 5.7). This results in a flatter beach profile in winter than in summer. The summer steepening results primarily from the gradual landward migration of MLW with seaward shifts of the dunefoot (embryo dunes) being of minor importance.

Another seasonal effect was found in the summer months of 2003 and 2004, viz. the abrupt seaward migration of MHW and the subsequent abrupt decrease in $\bar{W}_{\mathrm{ib}}$. These changes are likely due to intertidal bar welding to the supratidal beach (e.g Hayes & Boothroyd, 1969; Masselink et al., 2006). Bar welding occurred only once a year at the beginning of each summer (Figure 5.7). In summer, wave set-up and swash rarely pushes the water levels past the MHW level, implying that the bar could not migrate up to this contour and weld to the supratidal beach.

Beach width $\bar{W}_{\mathrm{b}}(t)$ and beach volume $\bar{V}_{\mathrm{b}}(t)$ both showed a seasonal trend: $\bar{W}_{\mathrm{b}}$ was larger during winters and smaller during summers, while $\bar{V}_{\mathrm{b}}$ was smaller during winters and larger during summers. This contrasts with swell-dominated beaches, where a large beach width is usually coupled to a large volume of beach sediment and associated with accretion (Aubrey, 1979; Dubois, 1988). The inverse relationship found on this storm-dominated beach calls into question the use of beach width as a proxy for beach volume. In addition, the present monthly changes in $\bar{W}_{\mathrm{b}}(t)$ and $\bar{V}_{\mathrm{b}}(t)$ were weakly related ($r = 0.43$, $p < 0.01$).

Another difference between storm- and swell-dominated beaches is the amount of 'active' sediment. Beach volume changes are in the order of 100 m^3/m during storm conditions (Aubrey, 1979), and 50 m^3/m over a few months (Dubois, 1988) on swell-dominated beaches. The latter appears to be the same amount of sediment stationary on the beach (that is, not participating in the seasonal exchange). In contrast, ~ 150 m^3/m sediment was stationary on the present beach and about 19 m^3/m sediment was gained or lost over a season. This reveals the robust character of microtidal, storm-dominated beaches which are protected by persistent subtidal bar systems.

In spite of the seasonal trends described above, daily to weekly averaged wave characteristics and monthly beach changes did not show a good relationship, in contrast to findings for swell-dominated beaches (e.g. Wright et al., 1985; Dubois, 1988; List & Farris, 1999). A potential reason for this lack in coupling is the timing of the

second survey in relation to the preceding storm event, as $\bar{X}_{MHW}(t)$ and $\bar{X}_{MSW}(t)$ could recover to pre-storm values within a few days, an observation consistent with those of Kroon (1994) and Masselink et al. (2006). Other potential reasons include: (I) alongshore variations and changes in beach morphology and (II) the storm intervals, which influence antecedent morphology. A pre- and post-storm measuring technique would be more appropriate to examine storm effects on beach changes in a storm-dominated environment, whereas the recovery would be monitored best with weekly to monthly measurements.

5.6 Conclusions

The more intense and frequent storm events in winter than in summer result in a seasonal accretion and erosion pattern of a storm-dominated beach at Noordwijk aan Zee, the Netherlands. The seasonal pattern involves a narrow, large-volume beach in summer, and a wide, small-volume beach at the end of the winter. The seasonal variations in beach width are uniform alongshore, unlike the beach volume, which varies alongshore. The seasonal pattern in beach width results from cross-shore sediment exchange between the supratidal and lower-intertidal parts of the beach, with the intermediate upper-intertidal beach functioning as a pivotal point with little internal seasonal variability in sediment volume. Beach width variability between successive surveys was statistically significant related to day- to week-averages of the preceding offshore conditions, but the beach volume variability usually was not. Both correlations were poor though, and an explanation is found in the precise timing of a storm relative to the two survey moments. Furthermore, daily variability determined from the video images shows variable beach response, possibly due to differences in the antecedent morphology and alongshore variations of the beach morphology, both of which may contribute to the monthly variations in the process-response of the beach.

6 Synthesis

6.1 Introduction

The central aim of this study was to understand the contribution of daily morphologic changes to seasonal beach evolution along a microtidal, sea- and storm-dominated coast. Therefore, (I) the day-to-day changes of an intertidal bar system were studied with respect to the daily morphologic response of the bar, trough and rip channels to wave conditions during different seasons and (II) the monthly variation in beach width and beach volume were analyzed to quantify the seasonal variability of the sediment budget of the beach. The field site was the beach of Noordwijk aan Zee, the Netherlands.

The daily beach morphology was obtained from low-tide time-averaged images collected with a shore-based Argus video system (Chapter 1.2.3). In the low-tide images, intertidal bars, troughs and rip channels are distinguishable due to their surface composition. Chapter 2 described the classification algorithm, which was developed to classify the surface composition into water, wet sand and dry sand. Patches of dry sand reflect the intertidal bar, whereas patches of wet sand, generally combined with water, revealed the trough and rip channels. The landward boundary of the patches indicates the cross-shore position of the respective morphologic features. In this way, the low-tide Argus images of a 15 month period were analyzed revealing the daily cross-shore behaviour of the bar system (Chapter 3). The cross-shore changes of the bar and trough boundaries displayed a sawtooth motion with periods of one to four months, comprising gradual landward migration followed by an abrupt seaward shift during intense storms with a duration of at least 30 hours, a large average root-mean-square wave height (> 2 m) and offshore surge level (> 0.5 m). Besides, the width of the trough had to be less than 20 m for bar-trough system to be erased entirely.

The funnel of a intertidal rip channel leads to a local seaward deviation of the landward boundary of the intertidal bar. Intertidal rip channels are indicated as open rip channel when the funnel is clearly connected to the open sea by a channel. When the channel fills up with sediment during falling tide, the rip channel is defined as a filled rip channel. The temporal and spatial variability in the alongshore positions of both open and filled rip channels reflect the daily alongshore behaviour of the bar system (Chapter 4). Rip channels were alongshore unequally distributed (47%

spatial variation) and live shorter (10 days) than the sawtooth motion of the bar and troughs lasts. During the existence of the rip channels, their amount increased with the preceding wave height and they generally migrate in the direction of the alongshore current with rates $O(10^0 - 10^1$ m/day). The intertidal bar line is always coupled to the subtidal bar line implying the influence of the subtidal bar system on the behaviour of the intertidal bar system.

The seasonal changes in the sediment budget of the beach were quantified using monthly elevation measurements (Chapter 5). From these measurements, time-series of monthly cross-shore positions of specific contours (e.g. the mean high-water line), beach width and beach volume were derived. The seasonal pattern in the measurements consists of wide beaches with a small volume at the end of the winter alternating with narrow beaches with a large volume in the summer. The seasonal pattern in beach width results from the cross-shore sediment exchange between the supratidal and the lower-intertidal beach zone.

This chapter will synthesize the results of all daily morphologic changes and their reflection on seasonal variability of a microtidal, storm- and sea-dominated beach. In succession, the daily morphodynamics, the seasonal beach variability and the integration of the daily and seasonal morphodynamics are described. Section 6.3 highlights the general conclusions of the results and ends this chapter with recommendations.

6.2 Temporal upscaling of beach morphodynamics

6.2.1 Daily morphodynamics

Storm impact

Storm events were defined as the period between the moment the offshore wave height exceeded 1.5 m and the moment the offshore wave height remained below 1.5 m for at least 12 hours. Only storms lasting longer than 30 hours with average root-mean-square wave height over 2 m and a surge level over 0.5 m result in morphologic resets of the beach (Chapter 3). During such a reset, the landward boundaries of the bar and trough, and the rip channels disappear along the largest part of the beach.

Simultaneously with these morphologic resets, the cross-shore position of the mean high-water line and the contour of the mean sea level move landward due to erosion of the upper part of the beach (Chapter 5). Whereas these both lines and the intertidal morphologic features respond unambiguously to a reset storm event, the cross-shore position of the mean low-water line responded variable to such storms. The difference in response is determined by the pre-storm morphology, which depends strongly on the period between successive storms (Chapter 5). Also the pre-storm morphology determines the effect of a reset storm event due to width of the trough, which needs to be small (< 20 m wide) for the beach to reset entirely (Chapter 3).

Beach recovery

During the post-storm low wave conditions, the beach starts to recover by the

reappearance of the bar system and the tendency of the mean high-, sea- and low-water line to regain their pre-storm position. A new intertidal bar is generated near the low-water line within a few days (Chapter 3). The amount of rip channels just after the storm averaged 3 over the 1250 m long study site, but increased to 6 or 7 around 10 days after a storm (Chapter 4). Because the bar-trough relief initially is small, the trough drains little water to the sea through some rip channels. After generation, the intertidal bar develops and migrates landward (Chapter 3). Simultaneously, the trough becomes deeper and the importance of drainage increases, which apparently leads to development of more rip channels up onto 10 days after the storm. After 10 days, the amount of rip channels decreased, which could be the result of a higher position on the beach due to continuously landward migration of the bar. The decrease in rip channel number due to calm wave conditions corresponds with the positive relation between the incident wave height and the amount of rip channels (Chapter 4).

The time needed for the contours to reoccupy approximately the same cross-shore position as before the storm varies for each storm (Chapter 5). This variable required time depends on the pre-storm position of the contour (i.e. the antecedent morphology), which depends on the time-interval between two successive storms. The required time is also likely to rely on the differences in the post-storm conditions. For example, if the post-storm conditions consist of offshore-directed wind, the surge level is negative (Chapter 3). Consequently, the sea water level will remain below the mean high-water level during high tide. Thus, shallow-water wave processes will hardly affect the zone around the mean high-water line and the mean high-water line (i.e. accretion) is unlikely to migrate seaward.

During persisting calm weather conditions, the boundary of the bar and trough continues to migrate landward and the rip channels join the cross-shore migration of the bar boundary (Chapters 3 and 4). The cross-shore migration lasts until a specific cross-shore position is reached, which usually is after a little over one month. This specific cross-shore position results in an asymptotic trend and skewed occurrence distribution for the boundary of the trough (Figures 3.7 and 3.10). The specific cross-shore position of the bar boundary did not correspond with the location of the mean high-water line suggesting that the bar does not weld to the supratidal beach. Besides, the sequential behaviour of the bar boundary was always ended by a reset storm event (Chapter 3). Despite the absence of bar welding, which generally results in an increase of the sediment at the upper part of the beach (e.g. Doeglas, 1955; Wijnberg & Kroon, 2002), the increase in sediment still occurs due to landward bar migration and the subsequent vertical bar growth. The processes of vertical bar growth may exceed the processes of cross-shore bar migration when the specific cross-shore position is reached. The (landward) cross-shore migration can be seen as the displacement of sediment from the lower intertidal beach zone to the upper intertidal beach. When the width of the bar is stable, also the vertical growth of a bar comprises an increase in sediment.

The intertidal bar system migrates alongshore by several meters per day on average. The filled rip channels migrate less the open rip channels (2.4 and 4.6 m/day,

respectively; Chapter 4). Besides the filled rip channels are positioned more landward than the open rip channels. The smaller migration rates combined with the more landward position of the filled rip channels with respect to the open rip channels suggests that the upper part of the intertidal beach migrates less alongshore than the lower part of the intertidal beach. The alongshore migration of the open rip channels is in the same direction as the estimated direction of the alongshore current as well as the observed alongshore migration of the subtidal rip channels. Besides, the shape of the intertidal bar line relates well to the subtidal bar line. This both indicates that the daily morphologic changes of the beach during calm wave conditions are to a large extent steered by the inner subtidal bar. Moreover, the intertidal bar is frequently absent at the alongshore locations where the inner subtidal bar is located within a distance of about 25 m from the beach ($y > 500$ m; Chapter 4). Here, the intertidal beach is small in width ($\approx$ 75 m; Chapter 5) and thus steeper (1 : 37) than the remaining stretch of intertidal beach (1 : 50 for $y < 500$ m). Microtidal beaches associated with intertidal bar development comprise beach slopes of 1 : 33 up to 1 : 100 (Wijnberg & Kroon, 2002). Possibly the intertidal beach slope related to a landward-located inner subtidal bar is too steep for an intertidal bar to fully develop.

The monthly changes in beach elevation are non-uniform in the alongshore direction (Chapter 5). The alongshore non-uniform behaviour will also result in the variability of daily morphologic changes during recovery as well as a storm event.

6.2.2 Seasonal variations of the beach

Storm impact

In general, the increase in storm frequency and intensity starts around October and lasts until approximately March (Figure 3.11). The cumulative effect of these storm events leads to seasonal patterns in beach behaviour. The sawtooth motions of the cross-shore position bar and trough boundary are generally shorter (1-2 month) during this season, because the reset storm events more frequently interrupt the development and migration of the bar system. Especially during the winter months of 2001, the landward boundary of the bar and the trough were positioned more seaward (about 10 m) than their overall cross-shore position (Chapter 3). The bars are likely to be smaller during the winter, because frequent storm events restrain vertical bar growth. Intertidal bar systems influence the amount of energy reaching the upper part of the beach around high tide and their volume functions as a sediment buffer. More energy will reach the upper part of the beach when the bar system is in an earlier phase of development. Consequently, the impact of a particular storm event on the supratidal zone will be larger at the end of winter than during summer owing to differences in pre-storm morphology.

The more intense storm events caused dune erosion, which is visible as the landward shift of the dune foot. This adds extra sediment to the beach. This extra sediment did not lead to an increase in the supratidal beach volume, meaning this sediment is directly transported in the seaward direction. Some sand may also be distributed alongshore, because of the alongshore non-uniformity of dune erosion.

Furthermore, the cumulative effect of the frequent occurring storm events even results in a continuing decrease of the supratidal beach volume (Chapter 5). The water only reaches the upper supratidal beach zone during high-energy conditions suggesting the shallow-water wave processes always to be responsible for sediment decrease in the supratidal beach zone. Part of the eroded sediment from the supratidal zone is deposited in the lower intertidal zone, where it led to an increase in sediment. Another part of the sediment is transported into the subtidal zone, which led to a net loss of beach sediment during winter. These net sediment loss include about 10% of the averaged total sediment volume in contrast to the net sediment losses at swell-dominated beaches, which reach about 50% of the averaged total sediment volume. The small net sediment losses and the large amount of stationary sediment (80%) in the present beach reveals the robust character of storm-dominated, microtidal beaches.

The frequent storms during winter did not affect the daily behaviour of the intertidal rip channels. In the literature, an increase in wave height is generally assumed to result in an increase in spacing and thus a decrease in the number of rip channels (e.g. Huntley and Short, 1992). In the Noordwijk data, the number of intertidal rip channels temporarily increased as an indirect result of the increased wave height during a reset storm event (see also Section 6.2.1). In contrast, the number of subtidal rip channels indeed seems to be smaller during winter when the longer-term average wave height increases (Chapter 4). Therefore, an adjustment of the shoreline structure on which the intertidal rip channels are superimposed is plausible after a storm season, because of the coupling between the intertidal and subtidal bar line. Individual storms, though, induce no clear alongshore changes in the pattern of the shoreline or the inner subtidal bar along the sea-dominated, microtidal Dutch coast (Van Enckevort & Ruessink, 2003b; Aagaard et al., 2005). Along swell-dominated coasts as Duck (North Carolina, USA) and Gold Coast (Queensland, Australia), however, individual storms reset the subtidal morphology leading to temporal disappearance of the subtidal bar system (Van Enckevort et al., 2004; Turner et al., 2007). Not only the swell could be responsible for the temporal disappearance, but also the sizes of the bar systems. Possibly, the subtidal bars at swell-dominated coasts are smaller than along storm-dominated coasts leading to a larger morphologic variability of the subtidal bars along swell-dominated coasts. Along the Dutch coast, an outer subtidal bar system protects the inner subtidal bar system and consequently the intertidal beach, which reflects another way in which the subtidal morphology influences the intertidal morphology.

Beach recovery

During the summer (April to September), storms were less frequent and less intense. The periods of the sawtooth motion became longer revealing the asymptotic behaviour of the trough boundary (Chapter 3). The daily landward migration and vertical bar growth moved cumulatively more sand to the upper intertidal beach. Kroon (1994) stated that intertidal bars only migrate landward and grow vertically when the tidal phase goes from neap tide to spring tide. In case of a spring tide to neap tide phase, the intertidal bars hardly migrate landward nor grow vertically and only a minor overall increase of sediment volume appears on the intertidal cross-shore profile. However, in this study, a difference in bar behaviour in response to the tidal

phase was not observed. As mentioned above, shallow-water wave processes never affected the upper supratidal beach zone during lower energetic wave conditions and the lower supratidal beach zone only for short periods. The supply of sediment for recovery of the supratidal zone will therefore mainly depend on landward-directed aeolian transport.

The recovery of the mean high-water line from the storm season happens during the summer months (Chapter 5). This is noteworthy, because this contour tends to regain its pre-storm position on a daily timescale (Section 6.2.1). Apparently, the first step of recovery happens quite fast, but small differences in the pre-and post storm positions remain. The contours only fully recover and regain their pre-storm position after a longer period of consistent low-energetic wave conditions. Welding of the studied intertidal bar system did not induce the landward migration of the mean high-water line (Chapters 3 and 5). However, in the data set used for the quantitative validation of the classification model, a small bar system was located landward of the 'main' intertidal bar system. This bar system was not detected due to the lack of contrast of the wet sand segments of its accompanying trough (Chapter 2). Perhaps these smaller, undetected bar-trough systems migrate to the high water line, merge and subsequently lead to the recovery of the mean high-water line.

The upper inter-tidal zone does neither accrete nor erode on a seasonal scale; it functions as a pivotal point (Chapter 5). However, the monthly changes in the volume of the upper intertidal beach zone were inversely related to the changes in the cross-shore distance of the landward bar boundary ($r = -0.82, p < 0.01$). A decrease in sediment corresponds to a seaward migration of the landward bar boundary, whereas the landward migration of the landward bar boundary leads to the increase in sediment on the upper part of the beach. This indicates that the changes of the upper intertidal beach zone directly result from the cross-shore migration of the intertidal bar, and only indirectly result from the forcing wave conditions. Despite the absence of a linear relation with the preceding wave conditions, the monthly volumetric changes of the supratidal and lower intertidal zone revealed a seasonal pattern indicating forcing of the wave conditions.

6.2.3 Integration of temporal scales

The daily morphologic changes in response to storm conditions and quiescent wave conditions (i.e. recovery) were spatially and temporally variable. This variability was ascribed to five different aspects: (I) different pre-storm morphology, (II) variation in recovery time of different beach zones, (III) duration between two subsequent storms, (IV) coupling with the subtidal morphology and (V) alongshore non-uniformity. These five aspects did not function individually but were mutually related. For instance, alongshore non-uniformity of the beach could result from the coupling with the subtidal morphology. Independent from the large variability of the daily morphologic changes, only a part of the daily changes eventually contribute to seasonal beach evolution.

The daily morphologic changes are not primarily responsible for the sawtooth motion that characterizes the cross-shore behaviour of the landward boundary of the bar and the trough (Chapter 3). The weekly component of the cross-shore position reflects this sawtooth motion best. The daily component of the cross-shore position are fluctuations superimposed on the weekly component and thus of less importance for the longer-term beach development. However, the extreme daily seaward-directed migration rates indicate the abrupt seaward shift of the sawtooth motion and are associated with storms. So with respect to the cross-shore behaviour of the intertidal bar system, the importance of the daily changes during beach recovery is negligible for seasonal beach evolution as opposed to the daily changes due to a storm.

The alongshore position of the intertidal rip channels shows the alongshore behaviour of the bar system. The alongshore behaviour exhibits only daily morphologic changes and no longer-term trend (Chapter 4). This suggests that the seasonal alongshore beach evolution will not depend on the daily morphologic changes with respect to the rip channels. Besides, the rip channels are presumably superimposed on a bar line rhythmicity of a larger spatial scale. Since the spatial and temporal scales of morphologic features correlate positive, larger timescales of beach development are associated to larger spatial scales. This suggests that morphologic changes on larger spatial scales (e.g. the above-mentioned bar line rhythmicity) determine the seasonal beach development and the intertidal rip channels are marginal features whose daily variability do not contribute to seasonal beach evolution.

The cross-shore behaviour of the dunefoot emphasizes the importance of daily changes due to a storm. A storm moves the dunefoot several meters landward and the gradual recovery takes several months before the dunefoot regains its pre-storm position (Chapter 5). The weekly, or even monthly, component of the dunefoots cross-shore position will show the recovery, whereas the daily component is not important and does not contribute to the seasonal evolution. The daily changes of the cross-shore positions of several mean water lines mainly explain the variability of the monthly changes in beach width and volume, in response to comparable wave conditions. But these daily changes are not decisive for the seasonal pattern of the beach width and volume.

All these findings suggest that the majority of the daily morphologic beach changes are noise to the seasonal beach evolution. Further evidence is found in Smit et al. (2007), who could predict coastline evolution for a period of about 9 months with a data-driven model using monthly data of which all short-term variation was removed. However, the effect of daily variations due to reset storm events at locations on the beach, which have a long recovery time (e.g. the dunefoot, upper supratidal beach zone), should not be discarded. For understanding seasonal beach evolution, the daily changes around storm events and the weekly to monthly changes during recovery are essential.

6.3 Conclusion and recommendations

In this thesis, the daily cross-shore and alongshore changes of an intertidal bar system and the monthly variation in beach width and volume were studied over a period of 1.3 and 3 years respectively, to understand the contribution of the daily morphologic changes on the seasonal beach evolution of a microtidal, storm- and sea-dominated beach. The daily morphologic changes in response to storm impact and during recovery are quite variable. The contribution on seasonal beach evolution of the daily morphologic changes during recovery is negligible in contrast to the effect of daily morphologic changes due to a storm. These latter morphologic changes remained visible in time series over a many months mainly because of a long recovery time. During the recovery of the beach, weekly components describe the longer-term evolution best, whereas the daily changes only resemble noise on this weekly signal.

Therefore, the time interval between successive measurements or observations would be one or a few days during storm conditions and week to months during recovery to efficiently study the seasonal evolution of a microtidal, storm-dominated beach. Whether this approach is generic and applicable for other beach types needs to be tested. The emphasis would be on contrasting beach characteristics as storm- versus swell-dominated beaches or microtidal versus macrotidal beaches.

The innovation of image processing endures and, logically, classification techniques are almost always imperfect, so enhancement of the developed classification technique is nessecary. Furthermore, the technical capabilities of the Argus system continue to progress and more recent stations comprise cameras with higher pixel resolution than the cameras of the Argus system used for this study. This could contribute to larger accuracies of the intertidal beach morphology detection. Additionally the oblique Argus images are initially stored in a compressed JPEG format due to the logistics and storage of the large amount of data produced by the cameras. However, the compression affects RGB information of the pixels. A different (non-compressed) image format would be beneficial for distinguishing beach patterns, which are characterized by the RGB values.

This study clearly revealed that the beach is indeed not an individual system, but it interacts with the landward-located dunes and the seaward-located subtidal morphology. Especially the coupling between the intertidal and subtidal bar systems shows the influence of the subtidal morphology on the intertidal beach morphodynamics. Many model studies ignore this coupling and assume the beach to be fixed. Further research on the coupling of the beach with the nearshore and the dunes is thus recommended, especially to improve the understanding of the beach itself.

Summary

Introduction

Sandy beaches are the dynamic interface between the sea and the land, and continuously change their width, volume and appearance in response to the stochastically changing wave conditions. The beach appearance comprises interesting morphologic patterns with characteristic spatial scales. The changes in width, volume and appearance cover a broad range of temporal scales varying from seconds up to decades. Uncertainty exists on how the shorter timescale changes lead to beach evolution on longer time scale. The combination of the continuously changing character with its function as a natural defense attracts the interest of the coastal manager. Coastal managers need to intervene when the beach is vulnerable to storms and would benefit by the predictability of the beach evolution on longer timescales starting at seasonal. Seasons are distinguishable by the alternation of storm events and fair weather conditions, which acts on a shorter timescale (i.e. days).

The central aim of this study was to understand the contribution of daily morphologic changes to seasonal beach evolution along a microtidal, storm-dominated coast. Therefore, (I) the day-to-day changes of an intertidal bar system were studied with respect to the daily morphologic response of the bar, trough and rip channels to wave conditions during different seasons and (II) the monthly variation in beach width and beach volume were analyzed to quantify the seasonal variability of the sediment budget. The study site was the beach of Noordwijk aan Zee, the Netherlands. The daily morphodynamics of the beach was acquired from daily Argus images taken around low tide. The seasonal variability of the beach width and beach volume was obtained from monthly elevation surveys of the beach at Noordwijk.

Extraction of daily morphology of video-images

Beach morphology was quantified from daily, time-averaged images collected by a shore-based Argus video system. In low-tide Argus images, the intertidal bar, trough and rip channels were distinguishable owing to their surface composition. A semi-automatic object-oriented algorithm was developed to classify the surface composition into water, wet sand and dry sand, and was subsequently tested on 13 low-tide Argus images. In a classified image, patches of dry sand reflected the intertidal bar, whereas patches of wet sand, generally combined with water, revealed the trough and rip channels.

The algorithm comprised several steps starting with segmentation, which was em-

ployed because of the strong relation between the visual observations and object-oriented image analysis. Segmentation subdivided the Argus images in small homogeneous areas called objects. A random selection of the objects was manually labelled and used with their accompanying variables in a maximum likelihood classification. The maximum likelihood classification created a classification model for each day, which was implemented on all objects resulting in a classified image. One classified image was compared to an in-situ classification for quantitative validation, which ensued a correct classification of 43.4% of the wet sand objects, and of 90.1% and 92.8% of the water and dry sand classes, respectively. Therefore, the algorithm extracts the intertidal bar more accurately than the intertidal trough and rip channels.

Daily cross-shore morphodynamics

The classification algorithm was applied to all daily low-tide images collected for a 15-month period in 2001 and 2002. The landward boundary of the dry sand patches provided the landward boundary of the bar, while the landward boundary of the combined wet sand and water classes yielded the landward boundary of the trough. The time series of alongshore-averaged cross-shore position of the two boundaries revealed the daily to seasonal cross-shore behaviour of the intertidal bar and trough.

The bar and trough boundaries behaved differently in time: the alongshore-averaged cross-shore boundary position of the bar was more dynamic than the landward boundary of the trough. Both the alongshore-averaged cross-shore positions of the boundaries described a sawtooth motion with a period between 1 and 4 months, comprising gradual landward migration followed by abrupt seaward shifts. The abrupt seaward shift represented a morphological reset during which pre-existing morphology was erased, while the gradual landward migration represented the recovery of the intertidal bar and trough. Only storm events that lasted at least 30 hours with an average offshore root-mean-square wave height over 2 m and an offshore surge level exceeding 0.5 m resulted in a reset. Also, the width of the trough had to be less than 20 m for bar-trough system to be erased entirely. The time series of the boundary positions exhibited the largest variability on the daily and weekly time scale, while variability on the seasonal scale was essentially absent. The weekly component of the boundary positions described the sawtooth motion and rapid seaward migration during a reset highlights the importance of the daily timescale.

Daily alongshore morphodynamics

In the alongshore direction, rip channels intercept the intertidal bar and function as a drainage channel for the landward located trough. Some rip channels filled up during falling tide and were only visible in an image by their funnel, but the majority of funnels remained in open connection with the sea. The presence of the funnel of both type of rip channels led to local seaward deviation in the landward bar boundary, which was used to derive the location of both type of rip channels. Other characteristics such as the spacing and the alongshore migration rate were derived from these locations. Filled rip channels were, on average, located about 10 m more landward and migrated slower (2.4 vs 4.6 m/day) than the open rip channels. The

time- and alongshore average spacing of the intertidal rip channels equalled half the spacing of the subtidal rip channels, but the intertidal rips were not spaced regularly ($CV \approx 0.47$).

The intertidal rip channels disappeared simultaneously with the intertidal bar and trough in response to reset storm events. During the recovery of the intertidal rip channels, they tended to reappear around the pre-storm alongshore location. On a daily scale, the amount and the alongshore migration of open intertidal rip channels were correlated to the preceding wave heights ($r = 0.26$ and $r = 0.22$, respectively, $p < 0.01$) and the alongshore component of the offshore wave power ($r = 0.34$ and $r = 0.18$, respectively, $p < 0.01$). The alongshore variability in the intertidal bar boundary and the subtidal bar line were generally coupled, usually with a non-zero phase difference. This phase difference gradually changed in time and varied between in-phase (0°) and out-of-phase (180°). The results indicate that the temporal and spatial variability in intertidal rip channel characteristics cannot be understood solely from offshore wave parameters; instead, morphological coupling appears to be the rule rather than the exception.

Seasonal beach variability

The seasonal variability of the beach width and beach volume was obtained from monthly elevation surveys of the beach at Noordwijk. The more intense and frequent storm events in winter than in summer resulted in a seasonal change from a wide beach with a small volume at the end of winter, to a narrow, large-volume beach in summer. The seasonal pattern in beach width resulted from the cross-shore sediment exchange between the supratidal and lower-intertidal part of the beach. In contrast to this coupling between beach behaviour and wave-characteristics on a seasonal scale, beach variability between successive surveys was unrelated to day- to week-averages of the preceding offshore wave conditions. This lack of correlation was partly due to the precise timing of a storm relative to the two survey moments. Due to the monthly survey interval, the period between a storm event and the survey could vary between 1 day and 4 weeks. The beach changes caused by a storm are less distinct with a long period than with a short period between the event and the survey if the recovery is in the order of a few days to weeks. Therefore, additional daily cross-shore positions of contours obtained from Argus video images were used to examine the impact of storms and the daily beach recovery in response to fair weather conditions. The daily variability disclosed differing antecedent morphology to storms and alongshore variations in beach morphology to contribute to spatially and temporally variable beach response.

Temporal upscaling of beach morphodynamics

The daily morphologic changes in response to storm impact and during recovery are quite variable and partly contribute to the seasonal patterns. This variable response resulted from differing pre-storm morphology, variation in recovery time for lower and higher parts of the beach, the duration between two subsequent storm events, the coupling with the subtidal morphology and the alongshore non-uniformity

of the beach. The development of the beach during its recovery took place on weekly scales with day-to-day variability primarily being noise to this weekly signal. Thus during recovery, the daily variations were of no additional value for the longer-term development. On the other hand, some daily morphologic changes due to major storm events remained visible in the time series for extended periods, because of a relatively long recovery time. Therefore, daily morphologic changes do not control the seasonal beach evolution, but they can disorder the trend of seasonal beach evolution.

For future work, this suggests that a time interval between successive observations of one to a few days during storm conditions and week to months during fair weather conditions would be efficient enough to study the seasonal evolution of a microtidal, storm-dominated beach. Besides, the beach clearly does not function as an individual system, thus further research on the coupling of the beach with the nearshore and the dunes is recommended to improve the understanding of beach development.

Samenvatting

Strandwacht

De invloed van dagelijkse morfodynamiek op seizoensgebonden strandontwikkeling

Introductie

Een zandstrand vormt een dynamische zone tussen land en zee die continu verandert in breedte, volume en uiterlijk (morfologie) als reactie op de varirende golfcondities en het getij. De veranderingen van de strandbreedte, de hoeveelheid zand (het volume) en de morfologie gebeuren over tijdsperiodes van seconden tot decennia. Er bestaat nog onzekerheid over hoe de korte termijn (seconden tot een dag) veranderingen leiden tot de lange termijn (seizoenen tot jaren) strandontwikkeling. De kust kan in een korte tijd grote veranderingen ondergaan, maar heeft ook een belangrijke functie bij het verdedigen van de kust. Daarom willen kustbeheerders weten wanneer het strand te zwak is om het achterliggende land te beschermen tegen een storm en zijn ze genteresseerd in het voorspellen van de lange termijn strandontwikkeling. Stormen komen juist voor over een tijdsperiode van enkele dagen (= korte termijn), maar het aantal en sterkte van de stormen varieert over de seizoenen (= lange termijn).

Het doel van dit proefschrift is om vast te stellen wat de bijdrage van de dagelijkse morfologische veranderingen is op de seizoensgebonden ontwikkeling van het strand aan een microgetijde (waterstandsverschil tussen eb en vloed is 1.8 m), stormgedomineerde kust. Daarvoor zijn (I) de dag-tot-dag veranderingen van een intergetijde zandbanksysteem die tussen de eb- en de vloedlijn ligt, en (II) de maandelijks veranderingen in strandbreedte en -volume bestudeerd. Het zandbanksysteem bestaat uit een zandbank die in kustlangse richting wordt doorbroken door geulen die muien worden genoemd, en in kustdwarse richting een landwaarts gelegen geul heeft die trog of zwin wordt genoemd. De morfologie van dit intergetijde zandbanksysteem verandert dagelijks door golfcondities, welke variren met de seizoenen. Het kwantificeren van de maandelijkse veranderingen in strandbreedte en -volume laat de seizoensgebonden variaties in de zandhoeveelheid van het strand zien. De studie is uitgevoerd op het strand van Noordwijk aan Zee (Nederland), waar de dagelijkse veranderingen in de strandmorfologie overdag rond eb werden vastgelegd met behulp van videobeelden afkomstig van het zogeheten Argus videosysteem. De seizoensgebonden variaties van de strandbreedte en -volume werden verkregen uit maandelijkse hoogtemetingen van ditzelfde strand over een kustlangse afstand van 1,5 km.

Detectie van strandvormen in videobeelden

De gebruikte videobeelden zijn een tijdsgemiddeld beeld over 10 minuten, genomen tijdens laagwater. In deze Argus-beelden zijn de het intergetijde zandbank, trog en muien zichtbaar door de samenstelling van het grondoppervlak, zoals vochtgehalte en sedimenttype. Een semi-automatische rekenmethode is ontwikkeld om de samenstelling van het grondoppervlak te classificeren als water, nat zand of droog zand. Vervolgens is deze rekenmethode getest op 13 Argus-beelden. In de geclassificeerde beelden zijn de intergetijde bank zichtbaar als vlakken van droog zand en de intergetijde trog en muien als vlakken van nat zand en water.

De rekenmethode bestaat uit een aantal stappen beginnende met segmentatie. Met segmentatie worden de Argus-beelden opgedeeld in kleine homogene vlakken die objecten worden genoemd. Segmentatie is toegepast vanwege de sterke overeenkomst met de visuele waarneming van de mens. Een willekeurige selectie van de objecten wordt handmatig geclassificeerd en daarna, samen met bijbehorende variabelen zoals kleurwaarde en kustdwarse positie, gebruikt als invoer voor een maximum likelihood classificatiemethode. De classificatiemethode creëert een model die vervolgens alle objecten in één van de drie klasse verdeeld waardoor een geclassificeerd beeld ontstaat. De resultaten van de rekenmethode zijn voor éénn beeld vergeleken met een handmatige classificatie op het strand zelf. Hieruit bleek dat 43,4% van de nat zand objecten, 90,1% van de water objecten en 92,8% van de droog zand objecten correct worden geclassificeerd. Dit betekent dat de intergetijde bank beter opgespoord kan worden dan de intergetijde trog en muien.

Dagelijkse kustdwarse verschuivingen van strandvormen

De landwaartse grens van de intergetijde bank wordt gekenmerkt door een overgang in landwaartse richting van droog zand naar nat zand. De landwaartse grens van de trog wordt gekenmerkt door een overgang in landwaartse richting van nat zand of water naar droog zand. Alle kustdwarse posities van deze grenzen worden langs het gemeten stuk strand gemiddeld, zodat per dag n kustdwarse positie van de landwaartse grenzen van de bank en de trog verkregen wordt. Dit is gedaan voor alle beschikbare beelden uit een periode van 15 maanden in 2001 en 2002.

De landwaartse grenzen van de bank en trog laten verschillend gedrag zien: de kustdwarse positie van de grens van de bank is dynamischer dan de grens van de trog. De kustdwarse posities van beide grenzen vertonen een zaagtand beweging met een periode varirend tussen 1 en 4 maanden. De zaagtand beweging bestaat uit een geleidelijke, landwaartse migratie gevolgd door een abrupte zeewaartse verschuiving. De abrupte zeewaartse verschuiving stelt een morfologische 'reset' voor, waarbij de voorafgaande strandmorfologie weggevaagd is door een storm. Alleen bepaalde stormen leiden tot deze 'reset'. De storm moet én meer dan 30 uur duren én een gemiddelde golfhoogte boven de 2 m hebben én een waterstandsverhoging van meer dan 0,5 m hebben. Daarnaast moet ook de breedte van de trog van de strandmorfologie voor de storm minder dan 20 m zijn. De geleidelijke landwaartse verschuiving laat het herstel van de intergetijde bank en trog zien. De grenzen blijken te veranderen op tijdschalen van dagen en weken. Er zijn geen veranderingen bekeken over seizoenen.

De zaagtand beweging wordt voornamelijk bepaald door de wekelijkse veranderingen van de grenzen, maar de abrupte zeewaartse verschuiving gedurende een morfologische 'reset' laten het belang van de dagelijkse tijdschaal zien.

Dagelijkse kustlangse verschuivingen van strandvormen

In de kustlangse richting wordt de intergetijde bank doorbroken door muien, welke functioneren als afwatering voor de landwaarts gelegen trog. Kleine uitwijkingen in zeewaartse richting van de landwaartse grens van de bank laten de ligging van de muien zien. Als het laag water wordt, worden sommige muien opgevuld met sediment (opgevulde mui), maar het merendeel van de muien houden een open verbinding met de zee (open mui). Per Argus-beeld wordt o.a. de ligging van de muien bepaald en uit opeenvolgende beelden wordt de kustlangse migratie snelheid afgeleid van de muien. De opgevulde muien liggen gemiddeld 10 m landwaarts en bewegen langzamer (2,4 tegen 4,6 m/dag) dan de open muien. De intergetijde muien verdwijnen tegelijkertijd met de intergetijde bank en trog gedurende een storm die een morfologische 'reset' veroorzaakt. Tijdens het herstel neigen de intergetijde muien dezelfde kustlangse positie in te nemen als voor de storm. Bezien over dagen is er een zwak verband tussen het aantal open muien en de voorafgaande golfhoogtes. Het verband met de kustlangse component van de inkomende golf energie is iets sterker.

Verder zeewaarts van het strand liggen ook zandbanken die altijd onder water liggen. Dit zijn subgetijde banken en deze worden in kustdwarse richting ook onderbroken door muien. De gemiddelde afstand tussen twee intergetijde muien is ongeveer de helft van de afstand tussen twee subgetijde muien. Echter de afstand tussen twee intergetijde muien varieerde sterker. De wijze waarop de posities van de intergetijde muien zich verhouden tot de posities van de subgetijde muien, verandert door de tijd heen, maar de posities van de intergetijde muien blijken wel gekoppeld te zijn met de posities van de subgetijde muien. De aanwezigheid van een koppeling tussen de intergetijde en subgetijde muien is belangrijk, omdat de veranderingen van de intergetijde morfologie dus niet alleen worden beïnvloedt door de golven maar ook de subgetijde morfologie.

Seizoensgebonden variabiliteit van het strand

De seizoensvariaties in strandbreedte en strandvolume zijn gekwantificeerd met maandelijkse hoogtemetingen van het strand van Noordwijk. De stormen in de winter zijn vaak intensiever en komen vaker voor dan in de zomer. Daardoor ontstaat er een breed strand met een klein sedimentvolume aan het eind van de winter en een smal strand met een groot sedimentvolume in de zomer. Dit seizoensgebonden patroon in strandbreedte komt door een kustdwarse uitwisseling van sediment tussen het gedeelte van het strand boven de vloedlijn (supragetijde) en het onderste intergetijde gedeelte van het strand. Ondanks bovengenoemde relatie tussen het verschil in stormfrequentie en intensiteit tussen seizoenen en de algehele vorm van het strand, is er geen verband gevonden tussen de maandelijkse veranderingen op het strand en de voorafgaande golfcondities. De afwezigheid van deze relatie is deels het gevolg van de tijdsduur tussen het moment van de storm en het moment van de hoogtemetingen. Doordat de

hoogtemetingen op een vast moment in de maand zijn uitgevoerd, kan deze tijdsduur variren tussen 1 dag en 4 weken. De veranderingen op het strand veroorzaakt door een storm, zijn minder duidelijk zichtbaar als er een lange tijdsduur tussen de storm en de hoogtemetingen zit, omdat het herstel van het strand slechts enkele dagen duurt. Daarom zijn er aanvullend dagelijkse kustdwarse posities van de gemiddelde vloedlijn, het zeeniveau en eblijn afgeleid uit de Argus-beelden. Deze hoogtelijnen zijn bestudeerd op de impact van stormen en het dagelijkse herstel van het strand tijdens rustige golfcondities. De dagelijkse variabiliteit laat zien dat de reactie van het strand afhankelijk is van zowel de morfologie voorafgaand aan de storm als de kustlangse variaties in de strandmorfologie.

Temporele opschaling van strandmorfodynamiek

De dagelijkse morfologische veranderingen als gevolg van stormen en tijdens het herstel zijn erg variabel en leveren maar ten dele een bijdrage aan seizoensgebonden patronen. De variabiliteit van de dagelijkse veranderingen is het gevolg van variatie in de strandmorfologie voor een storm, verschil in herstellend vermogen van het onderste en het bovenste deel van het strand, de tijdsduur tussen twee opeenvolgende stormen, de koppeling met de subgetijde morfologie en de kustlangse variaties van de strandmorfologie. Het herstel van het strand gebeurt op een wekelijkse tijdschaal waarbij de dagelijkse variatie voornamelijk ruis is op dit wekelijkse signaal. Dus tijdens het herstel zijn de dagelijkse morfologische veranderingen niet van belang voor de seizoensgebonden ontwikkeling van het strand. Echter, sommige dagelijkse veranderingen die door stormen veroorzaakt worden, blijven voor een langere tijd zichtbaar in de tijdseries, omdat hier een langere herstelperiode voor nodig is. Dus, de dagelijkse morfologische veranderingen controleren de seizoensgebonden strandontwikkeling niet, maar ze kunnen wel de trend van de seizoensgebonden strandontwikkeling verstoren.

Voor de toekomst suggereert dit dat een tijdsinterval tussen opeenvolgende metingen van enkele dagen tijdens storm condities en enkele weken tot maanden tijdens rustig weer condities goed genoeg is voor het bestuderen van de seizoensgebonden ontwikkeling van een microgetijde, stormgedomineerd strand. Bovendien functioneert het strand duidelijk niet als een individueel systeem, en is toekomstig onderzoek over de (morfologische) koppeling van het strand en het subgetijde gebied noodzakelijk.

Bibliography

Aagaard, T., J. Nielsen, N. Nielsen & B. Greenwood (1997), Suspended sediment transport and morphological evolution on a intertidal beach. In: Proceedings of Coastal Dynamics '97, Plymouth, U.K., ASCE, pp. 824–833.

Aagaard, T., A. Kroon, S. Andersen, R. M. Sørensen, S. Quartel & N. Vinther (2005), Intertidal beach change during storm conditions; Egmond, The Netherlands. Marine Geology 218, pp. 65–80.

Aagaard, T., M. Hughes & R. S. Andersen (2006), Hydrodynamics and sediment fluxes across an onshore migrating intertidal bar. Journal of Coastal Research 22, pp. 247–259.

Aarninkhof, S. G. J. & J. A. Roelvink (1999), Argus-based monitoring of intertidal beach morphodynamics. In: Proceedings of Coastal Sediments '99, Long Island, New York, ASCE, pp. 2429–2444.

Aarninkhof, S. G. J., I. L. Turner, T. D. T. Dronkers, M. Caljouw & L. Nipius (2003), A video-based technique for mapping intertidal beach bathymetry. Coastal Engineering 49, pp. 275–289.

Allen, J. R. (1981), Beach erosion as a function of variations in the sediment budget, Sandy Hook, New Jersey, U.S.A. Earth Surface Processes and Landforms 6, pp. 139–150.

Anthony, E. J., F. Levoy & O. Monfort (2004), Morphodynamics of intertidal bars on a megatidal beach, Merlimont, northern France. Marine Geology 208, pp. 73–100.

Anthony, E. J., F. Levoy, O. Monfort & C. Degryse-Kulkarni (2005), Short-term intertidal bar mobility on a ridge-and-runnel beach, Merlimont, northern France. Earth Surface Processes and Landforms 30, pp. 81–93.

Aubrey, D. G. (1979), Seasonal patterns in onshore/offshore sediment movement. Journal of Geophysical Research 84, pp. 6347–6354.

Battjes, J. & J. P. F. M. Janssen (1978), Energy loss and set-up due to breaking of random waves. In: Proc. 16th Int. Conf. on Coast. Eng., 1978, Hamburg, Germany, pp. 569–587.

Blaschke, T., C. Burnett & A. Pekkarinen (2004), Image segmentation methods for object-based analysis and classification. In: S. M. D. Jong & F. D. V. der Meer, eds., Remote sensing image analysis: including the spatial domain, Kluwer Academic Publishers, Dordrecht, 1st edn., pp. 211–236.

Bowen, A. J. & D. L. Inman (1969), Rip Currents. 2. Laboratory and field observations. Journal of Geophysical Research 74, pp. 5479–5490.

Burrough, P. A. & R. A. McDonnell (1998), Principles of Geographical Information Systems. Oxford University Press.

Calvete, D., G. Coco, A. Falqués & N. Dodd (2007), (Un)predictability in rip channel systems. Geophysical Research Letters 34, pp. 1–5.

Castelle, B. & P. Bonneton (2004), Nearshore waves and currents over crescentic bars. Journal of Coastal Research SI 39, pp. 310–315.
Cowell, P. J., P. S. Roy & R. A. Jones (1995), Simulation of large-scale coastal change using a morphological behaviour model. Marine Geology 126, pp. 45–61.
Davis, R. A., Jr. & W. T. Fox (1972), Coastal processes and nearshore sand bars. Journal of Sedimentary Petrology 42, pp. 401–412.
Davis, R. A., Jr., W. T. Fox, M. O. Hayes & J. C. Boothroyd (1972), Comparison of ridge and runnel systems in tidal and non-tidal environments. Journal of Sedimentary Petrology 42, pp. 413–421.
De Vriend, H. J. (1991), Mathematical modelling an large-scale coastal behaviour. J. Hydr. Res. 29, pp. 727–740.
De Vriend, H. J. (1997), Prediction of aggregated-scale coastal evolution. In: Proceedings of Coastal Dynamics '97, Plymouth, U.K., pp. 644–653.
Deigaard, R., N. Drønen, J. Fredsøe, J. H. Jensen & M. P. Jørgensen (1999), A morphological stability analysis for a long straight barred coast. Coastal Engineering 36, pp. 171–195.
Deronde, B., P. Kempeneers & R. M. Forster (2006), Imaging spectroscopy as a tool to study sediment characteristics on a tidal sandbank in the Wester-Schelde. Estuarine, Coastal and Shelf Science 69, pp. 580–590.
Descartes (1637), Discours de la méthode.
Doeglas, D. J. (1955), The origin and destruction of beach ridges. Leidse Geologische Mededelingen 20, pp. 34–47.
Dubois, R. N. (1988), Seasonal changes in beach topography and beach volume in Delaware. Marine Geology 81, pp. 79–96.
eCognition (2002), User Guide. Munich: Definiens Imaging GmbH.
Fenster, M. S. & R. Dolan (1993), Historical shoreline trends along the outer Banks, North Carolina: Processes and responses. Journal of Coastal Research 9, pp. 172–188.
Greenwood, B. & R. G. D. Davidson-Arnott (1975), Marine bars and nearshore sedimentary processes, Kouchibouguac Bay, New Brunswick, Canada. In: J. Hails & A. Carr, eds., Nearshore sediment dynamics and sedimentation, vol. 16, London, England: John Wiley, pp. 123–150.
Guillén, J., M. J. F. Stive & M. Capobianco (1999), Shoreline evolution of the holland coast on a decadal scale. Earth Surface Processes and Landforms 24, pp. 517–536.
Haas, K. A., I. A. Svendsen, M. C. Haller & Q. Zhao (2003), Quasi-three-dimensional modeling of rip currents systems. Journal of Geophysical Research 108, p. 3217. Doi:10.1029/2002JC001355, 2003.
Hamm, L., M. Capobianco, H. H. Dette, A. Lechuga, R. Spanhoff & M. J. F. Stive (2002), A summary of european experience with shore nourishment. Coastal Engineering 47, pp. 237–264.
Harper, J. R. (1980), Seasonal changes in beach morphology along the B.C. Coast. In: Canadian Coastal Conference 1980, pp. 136–150.
Hay, G. J., K. O. Niemann & G. F. McLean (1996), An object-specific image-texture analysis of H-resolution forest imagery. Remote Sensing of Environment 55, pp. 1–19.
Hayes, M. O. & J. C. Boothroyd (1969), Storms as modifying agents in coastal environment. In: M. O. Hayes, ed., Coastal Environments: NE Massachusetts, University of Massachusetts, Amherst: Department of Geology, pp. 290–315.
Holland, K. T., R. A. Holman, T. C. Lippmann, J. Stanley & N. G. Plant (1997), Practical use of video imagery in nearshore oceanographic field studies. Journal of Oceanic Engineering 22, pp. 81–92.

Holman, R. A. & A. H. Sallenger, Jr. (1986), High-energy nearshore processes. Eos 67, pp. 1369–1371.

Holman, R. A. & J. Stanley (2007), The history and technical capabilities of Argus. Coastal Engineering 54, pp. 477–491.

Holman, R. A., A. H. Sallenger, Jr., T. C. Lippmann & J. W. Haines (1993), The application of video image processing to the study of nearshore processes. Oceanography 6, pp. 78–85.

Holman, R. A., G. Symonds, E. B. Thornton & R. Ranasinghe (2006), Rip spacing and persistence on an embayed beach. Journal of Geophysical Research 111, pp. C01006, doi:10.1029/2005JC002965.

Hom-ma, M. & C. Sonu (1962), Rhythmic pattern of longshore bars related to sediment characteristics. In: Proc. 8th Int. Conf. on Coast. Eng., 1962, Mexico City, Mexico, ASCE, New York, pp. 248–278.

Houser, C. & B. Greenwood (2007), Onshore migration of a swash bar during a storm. Journal of Coastal Research 23, pp. 1–14.

Huntley, D. A. & A. D. Short (1992), On the spacing between observed rip currents. Coastal Engineering 17, pp. 211–225.

Jenkins, G. M. & D. G. Watts (1968), Spectral analysis and its applications. San Fransisco: Holden-Day.

Jiménez, J., A. Osorio, I. Marino-Tapia, M. Davidson, R. Medina, A. Kroon, R. Archetti, P. Ciavola & S. G. J. Aarninkhof (2007), Beach recreation planning using video-derived coastal state indicators. Coastal Engineering 54, pp. 507–521.

Kingston, K. S. (2003), Applications of complex adaptive systems approaches to coastal systems. PhD-thesis, Institute of Marine Studies, Faculty of Science, University of Plymouth.

Komar, P. D. (1998), Beach processes and sedimention. New Jersey: Prentice Hall.

Kroon, A. (1994), Sediment transport and morphodynamics of the beach and nearshore zone near Egmond, The Netherlands. PhD-thesis, KNAG/Faculteit der Ruimtelijke Wetenschappen, Universiteit Utrecht.

Kroon, A. & A. G. De Boer (2001), Horizontal flow circulation on a mixed energy beach. In: Proceedings of Coastal Dynamics '01, Lund, Sweden, pp. 548–557.

Kroon, A. & G. Masselink (2002), Morphodynamics of intertidal bar morphology on a macrotidal beach under low-energy wave conditions, North Lincolnshire, England. Marine Geology 190, pp. 591–608.

Kroon, A., A. C. de Kruif, S. Quartel & C. M. Reintjes (2003), Influence of storms on the sequential behavior of bars and rips. In: Proceedings of Coastal Sediments '03, Clearwater, Florida, ASCE. (on CD).

Lafon, V., H. Dupuis, R. Butel, B. Castelle, D. Michel, H. Howa & D. De Melo Apoluceno (2005), Morphodynamics of nearshore rhythmic sandbars in mixed-energy environment (SW France): 2. Physical foring analysis. Estuarine, Coastal and Shelf Science 65, pp. 449–462.

Lillesand, T. M. & R. W. Kiefer (1994), Remote sensing and image interpretation. New York: John Wiley & Sons, Inc., 3rd edn.

Lippmann, T. C. & R. A. Holman (1990), The spatial and temporal variability of sand bar morphology. Journal of Geophysical Research 95, pp. 11,575–11,590.

List, J. H. & A. S. Farris (1999), Large-scale shoreline response to storms and fair weather. In: Proceedings of Coastal Sediments '99, Long Island, New York, pp. 1324–1338.

MacMahan, J. H., E. B. Thornton & A. J. H. M. Reniers (2006), Rip current review.

Coastal Engineering 53, pp. 191–208.
Masselink, G. & A. D. Short (1993), The effect of tide range on beach morpodynamics and morphology: a conceptual beach model. Journal of Coastal Research 9, pp. 785–800.
Masselink, G., A. Kroon & R. G. D. Davidson-Arnott (2006), Morphodynamics of intertidal bars in wave-dominated coastal settings - a review. Geomorphology 73, pp. 33–49.
McGrew, Jr., J. C. & C. B. Monroe (1993), An introduction to statistical problem solving in geography. Dubuque, Iowa: Wm. C. Brown Publishers, 1st edn.
Morton, R. A., J. C. Gibeaut & J. G. Paine (1995), Meso-scale transfer of sand during and after storms: implications for prediction of shoreline movement. Marine Geology 126, pp. 161–179.
Mulrennan, M. E. (1992), Ridge and runnel beach morphodynamics: an example from the Central East Coast of Ireland. Journal of Coastal Research 8, pp. 906–918.
Nagao, M. & T. Matsuyama (1979), Edge Preserving Smoothing. Computer Graphics and Image Processing 9, pp. 394–407.
Nordstrom, K. F. (1980), Cyclic and seasonal beach response: a comparison of oceanside and bayside beaches. Physical Geography 1, pp. 177–196.
Ojeda, E., B. G. Ruessink & J. Guillen (in prep), Morphodynamic response a two-barred beach to a shoreface nourishment .
Owens, E. H. & D. H. Frobel (1977), Ridge and runnel systems in the Magdalen Islands, Quebec. Journal of Sedimentary Petrology 47, pp. 191–198.
Plant, N. G., R. A. Holman, M. H. Freilich & W. A. Birkemeier (1999), A simple model for internannual sandbar behavior. Journal of Geophysical Research 104, pp. 15755–15776.
Plant, N. G., K. T. Holland & J. A. Puleo (2002), Analysis of the scale of errors in nearshore bathymetric data. Marine Geology 191, pp. 71–86.
Plant, N. G., S. G. J. Aarninkhof, I. L. Turner & K. Kingston (2007), The performance of shoreline detection models applied to video imagery. Journal of Coastal Research 23, pp. 658–670.
Quartel, S. & B. Grasmeijer (2006), Dynamiek van het strand bij Noordwijk aan Zee en Egmond aan Zee en het effect van suppleties. Tech. Rep. CR-2006-01, IMAU, Faculty of Geosciences, Utrecht University. (in Dutch).
Quartel, S. & B. Grasmeijer (2007), Dynamiek van het strand bij Noordwijk aan Zee en Egmond aan Zee en het effect van suppleties. Tech. Rep. CR-2007-01, IMAU, Faculty of Geosciences, Utrecht University. (in Dutch).
Quartel, S., E. A. Addink & B. G. Ruessink (2006), Object-oriented extraction of beach morphology from video images. International Journal of Applied Earth Observations and Geoinformation 8, pp. 256–269.
Quartel, S., B. G. Ruessink & A. Kroon (2007), Daily to seasonal cross-shore behavior of quasi-persistent intertidal beach morphology. Earth Surface Processes and Landforms 32, pp. 1293–1307. DOI: 10.1002/esp.1477.
Ranasinghe, R., G. Symonds & R. Holman (1999), Quantitative characterisation of rip dynamics via video imaging. In: Proceedings of Coastal Sediments '99, Long Island, New York, ASCE, pp. 987–1002.
Reniers, A. J. H. M., J. A. Roelvink & E. B. Thornton (2004), Morphodynamic modeling of an embayed beach under wave group forcing. Journal of Geophysical Research 109. Doi:10.1029/2002JC001586.
Ruessink, B. G., I. M. J. van Enckevort, K. S. Kingston & M. A. Davidson (2000), Analysis of observed two- and three-dimensional nearshore bar behaviour. Marine Geology

169, pp. 161–183.
Ruessink, B. G., G. Coco, R. Ranasinghe & I. Turner (2007), Coupled and non-coupled behavior of three-dimensional morphological patterns in double sandbar system. Journal of Geophysical Research 112.
Shepard, F. P. (1950), Beach cycles in southern California. Technical Memo 20, Beach Erosion Board, U.S. Army Corps of Engineering, Washington, D.C.
Short, A. D. (1985), Rip-current type, spacing and persistence, Narrabeen Beach, Australia. Marine Geology 65, pp. 47–71.
Short, A. D. & R. W. Brander (1999), Regional variations in rip density. Journal of Coastal Research 15, pp. 813–822.
Short, A. D. & C. L. Hogan (1994), Rip currents and beach hazards: their impact on public safety and implications for coastal management. Journal of Coastal Research SI12, p. 197209.
Smit, M. W. J., S. G. J. Aarninkhof, K. M. Wijnberg, M. González, K. S. Kingston, H. N. Southgate, B. G. Ruessink, R. A. Holman, E. Siegle, M. Davidson & R. Medina (2007), The role of video imagery in predicting daily to monthly coastal evolution. Coastal Engineering 54, pp. 539–553. Doi:10.1016/j.coastaleng.2007.01.009.
Sonu, C. J. (1973), Three-dimensional beach changes. Journal of Geology 81, pp. 42–64.
Stive, M. J. F., S. G. J. Aarninkhof, L. Hamm, H. Hanson, M. Larson, K. M. Wijnberg, R. J. Nicholls & M. Capobianco (2002), Variability of shore and shoreline evolution. Coastal Engineering 47, pp. 211–235.
Swales, A. (2002), Geostatistical estimation of short-term changes in beach morphology and sand budget. Journal of Coastal Research 18, pp. 338–351.
Turner, I. L., V. M. Leyden, G. Symonds, J. McGrath, A. Jackson, T. Jancar, S. G. J. Aarninkhof & I. E. Elshoff (2000), Predicted and observed coastline changes at the gold coast artificial reef. In: Proceedings 27th International Conference on Coastal Engineering, Sydney, ASCE, pp. 1836–1847.
Turner, I. L., D. Whyte, B. G. Ruessink & R. Ranasinghe (2007), Observations of rip spacing, persistence and mobility at a long, straight coastline. Marine Geology 236, pp. 209–221.
Van Bemmelen, C. E. (1988), De korrelgrootte-samenstelling van het strandzand langs de Nederlandse Noordzee-kust. Tech. Rep. 1988-01, Rijksuniversiteit Utrecht, Vakgroep Fysische Geografie Report Geopro. (in Dutch).
Van der Sande, C. J., S. M. de Jong & A. P. J. de Roo (2003), A segmentation and classification approach of IKONOS-2 imagery for land cover mapping to assist flood risk and flood damage assessment. International Journal of Applied Earth Observations and Geoinformation 4, pp. 217–229.
Van Enckevort, I. M. J. (2001), Daily to yearly nearshore bar behaviour. PhD-thesis, KNAG/Faculteit der Ruimtelijke Wetenschappen, Universiteit Utrecht.
Van Enckevort, I. M. J. & B. G. Ruessink (2001), Effect of hydrodynamics and bathymetry on video estimates of nearshore sandbar position. Journal of Geophysical Research 106, pp. 16969–16980.
Van Enckevort, I. M. J. & B. G. Ruessink (2003a), Video observations of nearshore bar behaviour. Part 1: alongshore uniform variability. Continental Shelf Research 23, pp. 501–512.
Van Enckevort, I. M. J. & B. G. Ruessink (2003b), Video observations of nearshore bar behaviour. Part 2: alongshore non-uniform variability. Continental Shelf Research 23, pp. 513–532.

Van Enckevort, I. M. J., B. G. Ruessink, G. Coco, K. Suzuki, I. L. Turner, N. G. Plant & R. A. Holman (2004), Observations of nearshore crescentic sandbars. Journal of Geophysical Research 109.

Van Houwelingen, S., G. Masselink & J. Bullard (2006), Characteristics and dynamics of multiple intertidal bars, north Lincolnshire, England. Earth Surface Processes and Landforms 31, pp. 428–443.

Wijnberg, K. M. (1995), Morphologic behaviour of a barred coast over a period of decades. Phd-thesis, KNAG/Faculteit der Ruimtelijke Wetenschappen, Universiteit Utrecht.

Wijnberg, K. M. & A. Kroon (2002), Barred beaches. Geomorphology 48, pp. 103–120.

Wijnberg, K. M. & J. H. J. Terwindt (1995), Extracting decadal morphological behaviour from high-resolution, long-term bathymetric surveys along the holland coast using eigenfunction analysis. Marine Geology 126, pp. 301–330.

Winant, C. D., D. L. Inman & C. E. Nordstrom (1975), Description of seasonal beach changes using empirical eigenfunctions. Journal of Geophysical Research 80, pp. 1979–1986.

Wright, L. D. & A. D. Short (1984), Morphodynamic variability of surf zones and beaches: a synthesis. Marine Geology 56, pp. 93–118.

Wright, L. D., A. D. Short & M. O. Green (1985), Short-term changes in the morphodynamic states of beaches and surf zones: an empirical predictive model. Marine Geology 62, pp. 339–364.

Yates, M. G., A. R. Jones, S. McGrorty & J. D. Goss-Custard (1993), The use of satellite imagery to determine the distribution of intertidal surface sediments of the Wash England. Estuarine, Coastal and Shelf Science 36, pp. 333–344.

Dankwoord

'Zand op je boterham, zand in je haar. Bah, wat voelt dat naar.
Zand in je oren, van achteren en van voren. Zand, zand, zand!'
Radio Lawaaipapegaai, 1977

Veel mensen zullen zeggen dat ze 'iets' met het strand hebben. Ik heb dat ook, en wel met het Hollandse strand. Naast de jeugdherinneringen aan menige strandvakantie is er een hele reeks van nieuwe herinneringen bijgekomen, verzameld in de afgelopen 6 jaar tijdens mijn promotieonderzoek. In die tijd heb ik een ware relatie met het strand opgebouwd: gevoelens van intens geluk werden afgewisseld door enorme frustraties. Eenmaal eraan begonnen, liet dit onderzoek me niet meer los. Dat kwam niet door de wetenschappelijke onderzoeksvragen, maar meer door de persoonlijke onderzoeksvragen die ontstonden over mijn kunnen, mijn willen, en wat vind ik belangrijk? Ik heb (uiteraard) nog niet alle antwoorden, maar zeker is wel: het voelt toch best lekker dat het nu af is.

Nu is het dan belangrijk dat alle mensen, die op hun manier een bijdrage hebben geleverd aan dit onderzoek, worden bedankt. Daarbij wil ik beginnen bij Gerben Ruessink. Gerben, de structuur en voortgang van mijn onderzoek heb ik aan jou te danken. Je dwong me tot het afleveren van resultaten door het stellen van deadlines, waar ik me niet altijd aan hield, maar die ik zeker wel nodig had. Zelfs bij versie 38 van hoofdstuk 5 bleef je de voortgang zien. Door het enthousiasme waarmee Elisabeth Addink objecten in de Argus-beelden begon de beeldanalyse echt. Onze (inhoudelijke) gesprekken, Elisabeth, gaan altijd gepaard met gezelligheid en werden daarom zelfs tijdens het bodybalancen voortgezet. De basis van het onderzoek ligt bij Aart Kroon. Hé Aart, jij schreef een voorstel met een onderwerp wat je na aan het hart ligt en waarmee je me aan de slag liet gaan. Je eeuwige optimisme kon ik een poosje moeilijk plaatsen, maar ervaar ik nu als stimulans. Uiteraard hoort de duur van een promotie onderzoek wel wat korter te zijn dan 6 jaar. Piet Hoekstra, je hulp bij het verlengen van mijn verblijf op de uni gaf me vertrouwen goed bezig te zijn met het onderzoek.

De dagelijkse activiteiten op de Uithof bestonden gewoon uit computerwerk: dit is prima te doen dankzij de uitstekende sociale en technische ondersteuning van ons departement. 's Ochtends kon ik altijd eerst even wakker worden bij Irene Esser tijdens het uitwisselen van zeer belangrijke (non-)info. Dank aan Bart Grasmeijer met wie ik ruim 5 jaar de kamer deelde waar we liters koffie en rode wijn, en kilo's italiaanse bollen en ontbijtkoeken hebben weggewerkt. Hulp in technische zaken van

meetinstrumenten tot crashende computerschijven werd altijd geboden door Marcel van Maarseveen (hoe zit dat nou met dat post-processen?), Bas van Dam, Chris Roosendaal, Theo Tiemissen, Hassan Aarab en Henk Markies. Menno Straatsma, Kim Cohen, Ton Hoitink en Maarten Kleinhans dwongen me wel eens tot een echte wetenschappelijke discussie. De werksfeer was goed dankzij de aanwezigheid van alle FG-medewerkers, maar specifiek wil ik noemen (oud-)kustencollega's Bas, Nicholas, Pieter, Miriam, Frans, Leo, Michel, Irene, en (oud-)FG-collega's Hanneke, Gilles, Reinder, Sanneke, Arien, Wiebe, Wim, Steven, Hans, Raymond en Daniel.

Bijeenkomsten voor Coastview en Argus waren altijd een welkome afwisseling voor de dagelijkse activiteiten. Door deze bijeenkomsten ben ik bijna over mijn presentatie-fobie heen en heb ik het belang van borrels geleerd. Bedankt Aart Kroon, Stefan Aarninkhof, Mark van Koningsveld (en barman Giovanni), Arno de Kruif, Mark Davidson, Ruud Spanhoff, Anna Cohen, Robin Morellissen, Marije Smit, Rob Holman en Howard Southgate.

Geen fysisch geografisch onderzoek gaat zonder de ontberingen van een veldwerk. Tijdens mijn maandelijkse uitstapjes naar het strand van Noordwijk en Egmond hebben velen mij vergezeld. Absoluut op nummer 1 staat Hester: je ging elke keer maar mee, ondanks dat het weer het je voeten niet makkelijk hebben gemaakt. Zeker ook wil ik voor hun inspanningen bedanken: Aart, Kim, Ton, Bas, Maarten, Bart, Marcel, Chris, Raymond & Hans, Hanneke, Tamara, Marije, Jacoline (nee, tegen zoveel zon valt niet op te smeren). Tijdens mijn Noordwijk-dagen was er altijd goede verzorging van Maaike: 's ochtends ff een Senseo-tje, een bezoekje op het strand met Ole, en 's avonds aanschuiven voor het eten. Na 2.5 jaar werd deze fysieke inspanning van het veldwerk overgenomen door Youri en Jolanthe, die uiteraard op sublieme wijze de metingen hebben uitgevoerd.

Gelukkig had ik ook een 'gewoon leven' naast mijn promotieonderzoek. Gezelligheid tijdens etentjes, borrels, vakanties, sauna bezoekjes en/of fietsen met: Hester, Tamara, Hanneke, Linda, Jacoline & Sjoerd, Anneke, Eeske & Robert, Fab, Gijs, Ingrid, Ivan, Jaap, Katrien & Denis, Kim, Marije & Jaap, Michiel & Maaike, Monique, Peter, Petra, Simon & Myrthe en Ton.

Paps & mams, Maaike & Arieke, Barend, Diede, Evi, Maarten, Milou, Ole en Jan & Toke. Voor jullie ging mijn onderzoek over swash, satellieten, Teletubbies en landingsbanen. Bedankt voor jullie interesse in mijn bezigheden, relativerende opmerkingen tijdens mijn dipjes en vooral gewoon voor de afleiding. De steun van mijn zussen, Maaike & Arieke, in mijn dagelijks leven is voor mij zo belangrijk dat ik heel blij ben met hun steun als paranimfen tijdens de verdediging.

Lieve Pim. 'In dienst van de wetenschap' ben je er op alle mogelijke manieren voor mij geweest in de afgelopen 6 jaar. Daarbij heb je me geleerd hoe belangrijk het is om je gevoel te volgen. Zonder jou en zonder Boris was dit echt nooit afgekomen!

Publications

Peer-reviewed

Quartel, S., A. Kroon & B.G. Ruessink (in review). Seasonal accretion and erosion patterns of a microtidal sandy beach. Submitted to Marine Geology.

Quartel, S., B.G. Ruessink & A. Kroon (2007). Daily to seasonal cross-shore behaviour of quasi-persistent intertidal beach morphology. Earth Surface Processes and Landforms, 32, 1293-1307.

Quartel, S., A. Kroon, P.G.E.F. Augustinus, P. van Santen & N.H. Tri (2007). Wave attenuation in coastal mangroves in the Red River Delta, Vietnam. Special issue of Red River Delta Research Program in Journal of Asian Earth Sciences, 29(4), 576-584.

Van Santen, P., P.G.E.F. Augustinus, B.M. Janssen-Stelder, S. Quartel & N.H. Tri (2007). Sedimentation in an estuarine mangrove system. Special issue of Red River Delta Research Program in Journal of Asian Earth Sciences, 29(4), 566-575.

Quartel, S., E.A. Addink & B.G. Ruessink (2006). Object-oriented extraction of beach morphology from video images. International Journal of Applied Earth Observation and Geoinformation, 8, 256-269.

Aagaard, T., A. Kroon, S. Andersen, R.M. Sørensen, S. Quartel & N. Vinther (2005). Intertidal beach change during storm conditions; Egmond, the Netherlands. Marine Geology, 218, 65-80.

To be submitted

Quartel, S. (in prep). Temporal and spatial behaviour of rip channels in a multiple-barred coastal system.

Conference abstracts and papers

Kroon, A., S. Quartel & T. Aagaard (2007). Impact of a major storm on sediment exchanges between the dunes, beach and nearshore. Proceedings of Coastal Sediments '07, New Orleans (USA), ASCE, 951-962 (also on CD-ROM).

Quartel, S. & E.A. Addink (2006). Intertidal beach morphodynamics from Argus video images. Proceedings of the 25^{th} EARSeL Symposium 2005, Porto (Portugal), 819-827.

Kroon, A., S. Quartel & S.G.J. Aarninkhof (2004). Spatial and temporal variability of water line positions on a sandy beach, EOS Trans. AGU, 84 (52), Ocean Science Meeting Abstract OS22J-03.

Quartel, S. & A. Kroon (2004). Seasonal volumetric beach changes at a sandy beach in Noordwijk, The Netherlands. EOS Trans. AGU, 84 (52), Ocean Science Meeting Abstract OS32F-09.

Kroon, A., A.C. de Kruif, S. Quartel & C.M. Reintjes (2003). Influence of storms on the sequential behavior of bars and rips. Proceedings of Coastal Sediments '03, St. Petersburg (USA), ASCE (on CD-ROM).

Reports

Quartel, S. & B.T. Grasmeijer (2006 & 2007). Dynamiek van het strand bij Noordwijk aan Zee en Egmond aan Zee en het effect van suppleties. Rapport: CR-2006-01 & CR-2007-01, Faculteit Geowetenschappen, Universiteit Utrecht (in Dutch).

Dankers, P.J.T. & S. Quartel (2001). Swash on a steep, coarse sanded beach (Teignmouth, Devon, UK). M.Sc. Thesis, Department of Physical Geography, Utrecht University.

Cohen, K.M., S. Quartel & H.J.A. Berendsen (1998). Zanddikte op oeverwallen van de Waal (km 900-910) een jaar na het hoogwater van 1997. Netherlands Centre for Geo-ecological Research, ICG report 98/14 (in Dutch).

Curriculum Vitae

Susanne Quartel was born on May 30^{st} 1977 in Apeldoorn, The Netherlands. In 1995 she graduated from high school (VWO) at the Christelijk Lyceum Apeldoorn and subsequently started the study Physical Geography at the Utrecht University. Her main interests were in coastal and fluvial morphodynamics. Therefore, she did an internship on the wave attenuation in mangrove forests of the Red River Delta, Vietnam. Her master thesis described the sediment transport in the swash zone of steep, coarse sandy beach (Teignmouth, UK) and her MSc was received in 2001.

Daily to seasonal beach morphodynamics became the topic of her PhD research, which started in September 2001 at the same university. During this research, she discovered the hugh amount of possibilities of applying remote sensing in coastal research. Besides the participation in the EU-project Coastview showed her the importance of applied science. After 6 years, all results of her PhD research have been written down and can be found in this book.

At this moment she is working as a post-doc, still at the Physical Geography Department of the Utrecht University, on a research that focusses on the temporal and spatial variations of the beach.

Susanne Quartel werd geboren op 30 mei 1977 in Apeldoorn. In 1995 behaalde zij haar VWO-diploma aan het Christelijk Lyceum Apeldoorn en begon ze met de studie Fysische Geografie aan de Universiteit Utrecht. Haar interesse lag bij de morfodynamiek van kusten en rivieren. Daarom heeft ze een stage-onderzoek gedaan over golfdemping in de mangrovebossen van de Rode Rivier, Vietnam. Haar afstudeeronderzoek beschrijft het sediment transport in de swash-zone op steile, grof-zandige stranden (Teignmouth, UK) en zij studeerde in 2001 af.

De morfodynamiek van het strand op een tijdschaal van dagen tot seizoenen werd het onderwerp van haar promotieonderzoek en daar begon ze in september 2001 aan dezelfde universiteit mee. Tijdens dit promotie onderzoek, ontdekte ze de vele mogelijkheden van remote sensing technieken binnen het kustonderzoek. Daarnaast zorgde de participatie in het EU-project Coastview voor meer interesse in toegepast onderzoek. Na 6 jaar zijn alle resultaten van haar promotie-onderzoek opgeschreven en kunnen in dit boek worden teruggevonden.

Momenteel is zij nogsteeds werkzaam aan bij het departement Fysische Geografie van de Universiteit van Utrecht. Hier doet zij een post-doc onderzoek en houdt zich bezig met de temporele en ruimtelijke variatie in strandbreedte.